The role of the Mackenzie River in the carbon biogeochemistry of the Beaufort Sea coastal waters (Arctic Ocean)

Clément Bertin

LA ROCHELLE UNIVERSITY

DOCTORAL SCHOOL - 618 EUCLIDE

LIENSs Laboratory - LIttoral ENvironnement et Sociétés, UMRi 7266

PhD THESIS presented by:

Clément BERTIN

Defended on March 14, 2023

For the degree of Doctor of Philosophy in Earth and Fluid Envelopes

THE ROLE OF THE MACKENZIE RIVER IN THE CARBON BIOGEOCHEMISTRY OF THE BEAUFORT SEA COASTAL WATERS (ARCTIC OCEAN)

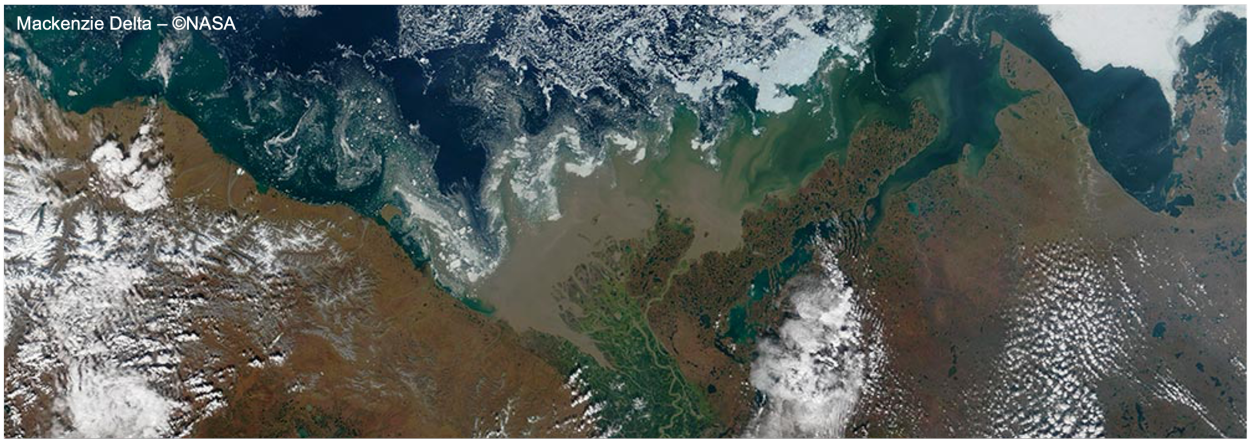

COMMITTEE MEMBERS:

Laurent BOPP	Research Director, École Normale Supérieure, France, Reviewer
Marc SIMARD	Senior Researcher, NASA-JPL Caltech, USA, Reviewer
Mélanie BECKER	Research Director, La Rochelle Université, France
Catherine JEANDEL	Research Director, Université Toulouse 3, France
Hugues LANTUIT	Professor, University of Potsdam, Germany
Stephanie DUTKIEWICZ	Senior Researcher, MIT, USA, Invited
Dustin CARROLL	Research Affiliate, San José State University, USA, Invited
Vincent LE FOUEST	Associate Professor, La Rochelle Université, France, PhD supervisor

LA ROCHELLE UNIVERSITÉ

ÉCOLE DOCTORALE - 618 EUCLIDE

Laboratoire LIENSs - LIttoral ENvironnement et Sociétés, UMRi 7266

THÈSE présentée par :

Clément BERTIN

Soutenue le 14 Mars 2023

pour obtenir le grade de Docteur en Terre et Enveloppes Fluides

LE RÔLE DU FLEUVE MACKENZIE DANS LA BIOGÉOCHIMIE DU CARBONE DES EAUX CÔTIÈRES DE LA MER DE BEAUFORT (OCÉAN ARCTIQUE)

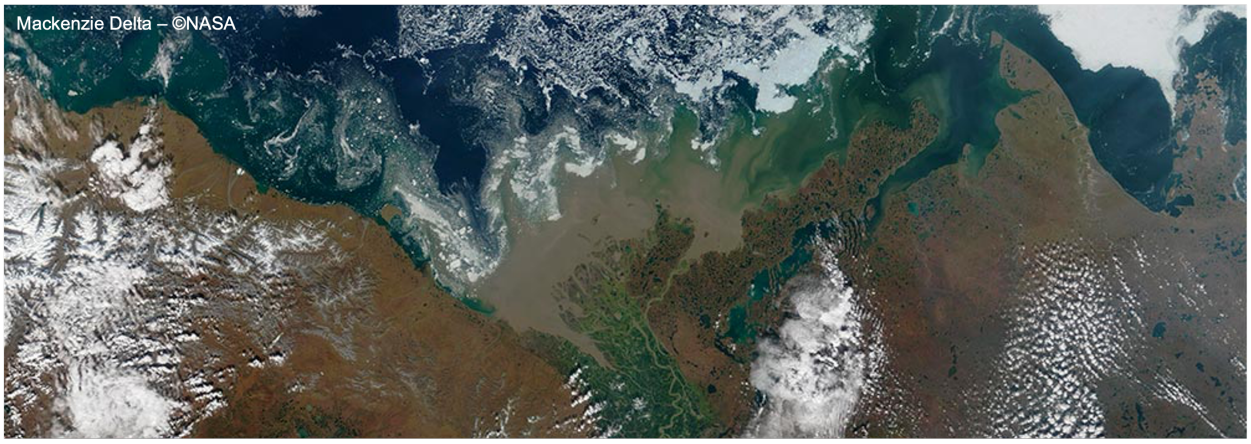

JURY :

Laurent BOPP	Directeur de recherche, École Normale Supérieure, Rapporteur
Marc SIMARD	Chercheur Senior, NASA-JPL Caltech, USA, Rapporteur
Mélanie BECKER	Directrice de recherche, La Rochelle Université, France
Catherine JEANDEL	Directrice de recherche, Université Toulouse 3, France
Hugues LANTUIT	Professeur, University of Potsdam, Allemagne
Stephanie DUTKIEWICZ	Chercheuse Senior, MIT, USA, Invitée
Dustin CARROLL	Chargé de recherche, San José State University, USA, Invité
Vincent LE FOUEST	Maître de conférences, La Rochelle Université, Directeur de thèse

“C’est assez curieux de se dire que les hasards,
les rencontres forgent une destinée.”
Édouard Baer (Otis)

ACKNOWLEDGMENTS / REMERCIEMENTS

First of all, I would like to thank the PhD thesis committee members, who have kindly accepted to read and evaluate my work: Laurent BOPP, Marc SIMARD, Mélanie BECKER, Catherine JEANDEL, Hugues LANTUIT, Stephanie DUTKIEWICZ and Dustin CARROLL.

I would like to thank Vincent LE FOUEST, who offered me the opportunity to work on this PhD thesis. Thank you for guiding me so well to pass through the numerous obstacles I have had to face. I am especially grateful for your patience and advice when it was necessary to take a step back or to think of new possibilities after turnarounds.

I am very grateful to all the researchers I met and worked with all along these 3.5 years. I would especially like to thank Dimitris MENEMENLIS and Dustin CARROLL for their precious advice and these meetings shared between serious work and jokes. I hope I could continue to collaborate with you in the future. Thank you Dimitris for welcoming me twice at JPL and for picking me up at the badging office every morning, which I must admit was very time consuming. Thank you to Hong ZHANG for his precious technical support on ECCO-Darwin model and computer science related topics. I am also grateful to Stephanie DUTKIEWICZ for hosting me at MIT and for sharing her knowledge, guiding through the complexity of biogeochemical modeling; as a trained physicist it was not easy every day, Vincent can testify. Thank you Atsushi MATSUOKA for hosting me at Takuvik laboratory and for helping me on DOC issues all along these 3.5 years. I would also like to thank Marcel BABIN and Antoine MANGIN for providing me their feedbacks and guidance all along the thesis, I really appreciated that. Thank you Fabien JOUX and Eva ORTEGA-RETUERTA for hosting me at Banyuls-sur-Mer and sharing your knowledge on bacteria. These few days were hard for my brain, but very rewarding. I would also like to thank the members of NASA IDS project for the constructive discussions, especially Charles MILLER, Dustin CARROLL, Dimitris MENEMENLIS, Stephanie DUTKIEWICZ, Manfredi MANIZZA, Melissa SCHWAB and Atsushi MATSUOKA. Finally, thanks to Dimitri KALENITCHENKO, Giuliana PANIERI for allowing me to participate to the fabulous AKMA mission offshore Svalbard.

I would like to thank all the agencies and projects that contributed to fund this PhD thesis: The European Union's Horizon 2020 Research and Innovation Program through Nunataryuk project, the Centre National de la Recherche Scientifique (CNRS) through the LEFE program and the NASA Earth Science Division's Interdisciplinary Science (IDS) program. I am also very rewarding for the La Rochelle University for the PhD fellowship, and to the Euclide Doctoral School (Paco BUSTAMANTE) and LUDI for their additional financial support related to the COVID situation.

Il est temps de passer en français pour remercier mes collègues, mes amis et ma famille. Tout d'abord je voudrais remercier l'ensemble de collègues du LIENSs pour leur accueil tout au long de ces trois années et demie. Tout particulièrement j'aimerais remercier mes camarades du Bureau 122, aka les Supers Nanas : Belle, Bulle et Rebelle, respectivement Fanny, Margot et Ophélia. Comme on dit, toutes les bonnes choses ont une fin, les membres du quatuor intrépide des docs de l'environnement (alias docs 122) finissent par voguer vers d'autres horizons. À toutes ces discussions, confessions mais aussi débats sur le doctorat ou la politique. Je remercie également mes amis du groupe de Mammifères, dont la liste s'est agrandie au fur et à mesure des années (ils se reconnaitront), pour ces après-midis et soirées détendues ou plus alcoolisées et pour ces moments de rires qui resteront gravés dans ma mémoire. Un remerciement spécial pour la Juls qui a accepté de faire le joli schéma récapitulatif de cette thèse. Merci également à Axelle ma seule et unique

stagiaire que j'ai pris plaisir à encadrer et qui vole maintenant de ses propres ailes vers trois folles années de doctorat. Et pour finir comment oublier mon Émilien ! Merci mon tchiot père, pour ton grain. . . de folie. Hâte de raconter Strasbourg encore une fois comme depuis 4 ans.

Merci à mes coéquipiers de La Rochelle Volleyball, avec qui j'ai joué pendant ces 3 années. Merci pour ces moments de victoire, de défaite, d'entrainement et de fête. Merci pour toutes ces soirées (dédicace à la Chonch-house) et tous ces beachs (et toutes les bitchs) qui m'ont permis d'avoir la tête hors du boulot.

Je voudrais ensuite remercier mes parents, pas seulement pour ces 3 dernières années mais pour l'ensemble des années d'études qui m'ont mené jusqu'au doctorat. Ils ont, chacun à leur manière, su m'aider, me motiver et rester compréhensifs toutes ces années, même dans les années compliquées. Je remercie également ma sœur Fanny qui me soutient malgré la distance de ces dernières années. Merci à mes grands-parents qui m'ont toujours encouragé même s'ils ne comprennent pas toujours la teneur de mes travaux. J'ai une pensée toute particulière pour ma grand-mère Françoise, qui m'a vu débuter cette thèse et à qui j'aurais aimé montrer le résultat. Je voudrais également remercier ma cousine Maylis qui a relu et corrigé quelques pages de ce manuscrit grâce à son anglais parfait.

Pour finir j'aimerais remercier Océane (alias Chonchon) qui m'a soutenu au quotidien, parfois supporté dans les moments difficiles de la thèse mais aussi de blessure (RIP la hernie discale) et de maladie (RIP la mononucléose).

PUBLICATIONS LIST

- **Bertin, C.**, Carroll, D., Menemenlis, D., Dutkiewicz, S., Zang, H., Matsuoka, A., Manizza, M., Babin, M., Miller, C.E., Mangin, A., & Le Fouest, V. (In Prep). Paving the way to an improved representation of tDOC and physical plume: a sensitivity analysis.
- **Bertin, C.**, Carroll, D., Menemenlis, D., Dutkiewicz, S., Zang, H., Matsuoka, A., Tank S., Manizza, M., Babin, M., Miller, C.E., Mangin, A., & Le Fouest, V. (2023). Biogeochemical river runoff drives intense coastal Arctic Ocean CO_2 outgassing. Geophysical Research Letters, 50, e2022GL102377. doi:10.1029/2022GL102377
- **Bertin, C.**, Matsuoka, A., Mangin, A., Babin, M., & Le Fouest, V. (2022). Merging satellite and in situ data to assess the flux of terrestrial dissolved organic carbon from the Mackenzie river to the coastal Beaufort Sea. Frontiers in Earth Science, 10. doi: 10.3389/feart.2022.694062
- Panieri, G., Bünz, S., Savini, A., Jensen, A., Løfquist, B., Runar, Olsen B.R., Willis, C., Argentino, C., **Bertin, C.**, Oddone, D., ..., Dyrved, Holm V. (2022). CAGE22-2 Scientific Cruise Report: AKMA 2/Ocean Senses CAGE22-2 Scientific Cruise Report: AKMA 2/Ocean Senses. doi:10.7557/cage.6755

CONFERENCES LIST

- **Bertin, C.**, Carroll, D., Menemenlis, D., Dutkiewicz, S., Zang, H., Miller, C.E., Matsuoka, M., Babin, M., Mangin, A., & Le Fouest, V. (2022). Quantifying the impact of terrestrial dissolved organic carbon runoff on Beaufort Sea coastal air-sea CO_2 fluxes over seasonal to interannual timescales [Oral presentation-Poster]. Arctic Frontiers, May 8- 11, 2022, Tromsø, Norway.
- **Bertin, C.**, Carroll, D., Menemenlis, D., Dutkiewicz, S., Zang, H., Matsuoka, M., Babin, M., Mangin, A., & Le Fouest, V. (2021). Terrestrial DOC removal by marine heterotrophic bacteria in the oligotrophic Beaufort Sea, western Arctic Ocean: a model study [Oral presentation]. Aquatic Science Meeting, June 22-27, 2021, Online.
- Gaffet, A., **Bertin, C.**, Carroll, D., Menemenlis, D., Dutkiewicz, S., Zang, H., Matsuoka, M., Babin, M., Mangin, A., & Le Fouest, V. (2021). Comparison of a regional ocean biogeochemistry model to observations in the highly-dynamic Mackenzie shelf region (Beaufort Sea) [Poster]. Aquatic Science Meeting, June 22-27, 2021, Online.
- **Bertin, C.**, Menemenlis, D., Caroll, D., Zhang, H., Decharme, B., & Le Fouest, V. (2021). Impact of River Forcing on Simulated Ocean-Sea Ice Coupling in the Arctic Mackenzie Shelf (South-Eastern Beaufort Sea) [Oral presentation]. Arctic Science Summit Week, Online, March 19-26, 2021, Lisbon, Portugal.
- **Bertin, C.**, Matsuoka, A., Mangin, A., Babin, M. & Le Fouest, V. (2020). Merging remotely-sensed and in situ data to assess the riverine flux of dissolved organic carbon form the Mackenzie river to the Beaufort Sea [Poster]. Arctic Change, December 7-10, 2020, Online.
- **Bertin, C.**, Matsuoka, A., Mangin, A., Babin, M. & Le Fouest, V. (2020). Plus-value de l'apport de mesures satellites pour l'estimation du flux de DOC du fleuve Mackenzie vers l'océan Arctique [Oral presentation]. 16ième journées scientifiques du Comité National Français des Recherches Arctiques et Antarctiques, September 22-23, 2020, La Rochelle, France.

AWARDS

- Arctic Frontier 2022 outstanding poster award organized by the Association of Polar Early Career Scientists (APECS)

OUTREACH

- Participation to the Ocean-Senses workshop aimed at creating educational content to make student feel the ocean floor through the 5 senses. AKMA Expedition, Svalbard, May 2022.
- Participation to the local (La Rochelle University) phase of Ma Thèse en 180 Secondes (MT180; french version of Three Minutes Thesis, 3MT). March 19, 2021, La Rochelle, France.
- Recording of a podcast for the program "*LIttoral, ENvironnement & Sociétés*", presented by Gaëlle de Christen (radio RCF, Link). December 10, 2020, La Rochelle, France.
- Organization of a conference on the risks of permafrost thaw due to global warming for the "*Fête de la Science*" festival. February 25, 2020, La Rochelle, France.
- Creation of Instagram and Facebook accounts aimed at sharing the daily life of PhD students to the broad audience (2020).

CONTENTS

List of Figures

List of Tables

CHAPTER

1 GENERAL INTRODUCTION

1.1 The coastal Arctic Ocean

1.1.1 Surface circulation and biogeochemistry of Arctic Ocean

The Arctic Ocean (AO) is the smallest and shallowest ocean on Earth, containing only 1 % of the global ocean volume. Part of the *Arctic Mediterranean* (Østerhus et al., 2019; Timmermans & Labe, 2021), the AO is surrounded by land masses extending far into the ocean through wide continental shelves (50 % of the AO Sverdrup et al., 1942; Carmack et al., 2006). Characterized by a succession of multiple seas, the AO connects with the Pacific and Atlantic oceans by three shallow and one deep channels (Fig. 1.1). On the Pacific side, Bering Strait (BS) is the only gateway between the AO and the Pacific Ocean through which 1.0 $\pm$ 0.1 Sv of Pacific waters is transported into the AO. On the Atlantic side, the largest inflow to the AO comes from the Barents Sea Opening (BSO; 3.8 $\pm$ 0.5 Sv). In contrast, Fram Strait (FS) and Davis Strait (DS) are the main exits for surface waters flowing out the AO (-1.8 Sv and -3.1 Sv, respectively Torres-Valdés et al., 2013; MacGilchrist et al., 2014; Vetrov & Romankevich, 2019). By just taking into account

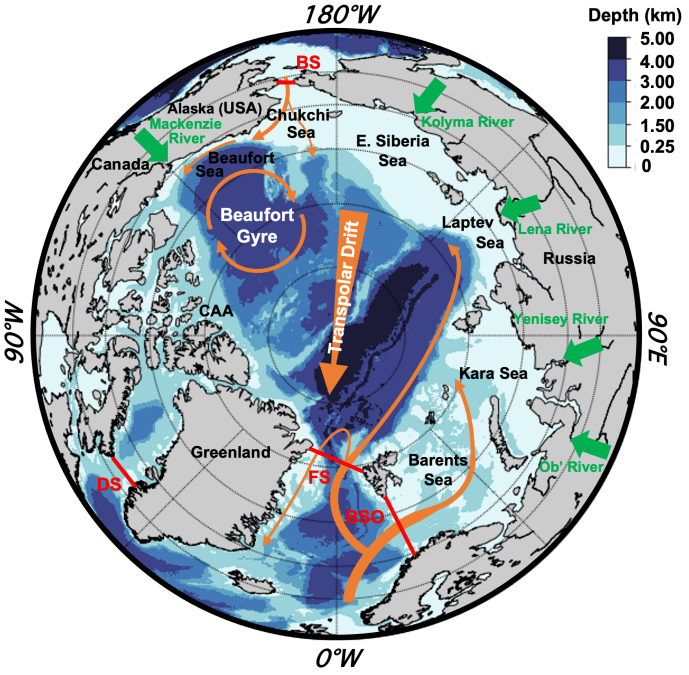

Figure 1.1: Map of the Arctic Ocean and its gateways (red lines) in Bering Strait (BS), Fram Strait (FS), Davis Strait (DS), and in the Barents Sea Opening (BSO). The Chukchi, Beaufort, Canadian Arctic Archipelago (CAA), Barents, Kara, Laptev, and East Siberian seas are also indicated. A conceptual representation of the major surface circulation patterns is shown (orange arrows; adapted from Juranek (2022)) with the five major pan-Arctic rivers overlaid (green arrows).

these inflows and outflows, the AO would experience a deficit of water. The budget is balanced by the freshwater input from the Pan-Arctic rivers (0.1 Sv Vetrov & Romankevich, 2019), which reflects their contribution at the global scale. Arctic rivers represent about 10 % of the global freshwater discharge into the World ocean (Opsahl et al., 1999). The Arctic rivers and Atlantic and Pacific waters convey large amounts of dissolved inorganic nitrogen (DIN; nitrate, nitrite and ammonium), phosphorus and silica (Si) into the AO. The BSO is the main gateway for DIN and phosphate contributing to 78 % (30.1 TgN yr^{-1}; Juranek, 2022) and 62 % (2.34 TgP yr^{-1}; Torres-Valdés et al., 2013) of the AO inputs, respectively. In terms of Si, BS accounts for 47 % of the total input into the AO (18.5 TgSi yr^{-1}; Torres-Valdés et al., 2013). Arctic rivers exports 0.32 TgN yr^{-1}, 0.06 TgP yr^{-1} and 8.8 TgSi yr^{-1}, of DIN, Phosphates and Si, respectively (Terhaar et al., 2021a). Rivers contributing the most to the terrestrial input of freshwater and dissolved nutrients are along the Siberian (Kara, Laptev and East Siberia Seas) and Beaufort Sea shelves (Fig. 1.1).

Within the AO, two major wind-driven circulation patterns drive the transport of nutrients. On the first hand, the transpolar drift redistributes the nutrients supply from the Eastern to central AO (Charette et al., 2020). On the other hand, the Beaufort Gyre traps the surface freshwater promoting the persistence of sea-ice in the western AO (Timmermans & Labe, 2021). With shelves accounting for 62 % of the total AO continental plateau (Carmack et al., 2006), the Eastern AO receives more external nutrients than the Western part defined as an oligotrophic system. The Eastern AO is seasonally free of sea-ice and DIN-rich (up to 20 mmolN m^{-3} in the Barents Sea; Juranek, 2022), which is favorable to phytoplankton growth, but with a limited supply of Silicates (Tuerena et al., 2022). Arrigo and van Dijken (2015) estimated that 55 % (283 TgC yr^{-1}) of the total AO net primary production (NPP) occurs on Eastern shelves. In contrast, oligotrophic conditions and persistent sea-ice cover that prevail in the Western AO are not favorable to phytoplantkton growth. While DIN-limited, high Si concentrations from the Pacific waters promote the development of diatoms. The contribution of riverine nutrients on NPP remains highly uncertain (Le Fouest et al., 2013) although Terhaar et al. (2021a) suggested that one third of the Arctic NPP could be sustained by riverine nutrients and coastal erosion. Overall, the AO is assumed as a net sink of atmospheric carbon dioxide (CO_2) estimated to (118-180 TgC yr^{-1}; Arrigo et al., 2010; Yasunaka et al., 2018; Manizza et al., 2019) mainly driven by the Eastern AO. At the global scale, the AO is an important component of the climate system regulation, contributing to about 10 % of the global carbon sequestration (Landschützer et al., 2016; Watson et al., 2020). In response to the global warming, the decline of sea-ice cover observed between 1998 to 2012 translated into more

NPP (Ardyna & Arrigo, 2020) showing the potential of AO to absorb more anthropogenic CO_2. Since 2012, sea-ice cover stabilized while NPP doubled suggesting that factors governing the NPP changed. In addition, changes in the Arctic freshwater cycle might exacerbate regional disparities in terms of carbon ingassing (Brown et al., 2020). However, other riverine biogeochemical tracers as dissolved organic carbon (DOC) and dissolved inorganic carbon (DIC) have a counteracting effect and can hamper the AO sink capacity.

In the ocean, DIC plays the central role acting as a transient carbon form between organic matter and CO_2. Defined as the sum of $[CO_2^*]$ (combined concentrations of aqueous carbon dioxide (CO_2(aq)) and carbonic acid (H_2CO_3)), bicarbonate $[HCO_3^-]$ and carbonate $[CO_3^{2-}]$ ions, DIC modulates seawater properties such as pH, partial pressure of CO_2 (pCO_2) and alkalinity. An increase in surface seawater DIC concentration results into a rise of the pCO_2 that can in turn lead to the release of CO_2 to the atmosphere if seawater pCO_2 exceeds the atmospheric pCO_2. The AO is a source of DIC for the Atlantic Ocean exporting 775 TgC yr^{-1} (MacGilchrist et al., 2014). Pan-Arctic rivers are reported to supply 57 TgC yr^{-1} of terrestrial DIC (tDIC; Tank et al., 2012). Another substantial source of DIC results from the degradation of organic matter, mostly present in the water column in a dissolved form, in which DOC is the mass-predominant component (Lønborg et al., 2020). In the AO, the Atlantic and Pacific oceans contribute together to 117 TgC yr^{-1} (Vetrov & Romankevich, 2019) of the DOC supply while rivers convey 27.6 TgC yr^{-1} (Holmes et al., 2012; Terhaar et al., 2021a). An additional 14 TgC yr^{-1} of carbon mostly under particulate form (POC) is released by coastal erosion, increasing the potential of CO_2 outgassing by Arctic shelves (Irrgang et al., 2022). Then, 26 % of the total external supply of DOC would originate from land.

1.1.2 tDOC in the Arctic land-ocean aquatic continuum (LOAC)

The pan-arctic drainage basin covers 16.8 millions km^2 (Holmes et al., 2013), which is similar to the AO surface area. The AO is naturally strongly influenced by the land-ocean aquatic continuum (LOAC). The five largest rivers flowing into the AO (Mackenzie, Kolyma, Lena, Yenisey and Ob') drain vast watersheds accounting for a surface area of $\sim$10.3 millions km^2 (Fig. 1.2.a. Vörösmarty et al., 2000; Lammers et al., 2001; Holmes et al., 2013). Three of them situated in the Eurasian side (Lena, Yenisey and Kolyma) are ranked in the ten World's largest watersheds. Pan-Arctic rivers flow across a wide diversity of landscapes characterized by a surface vegetation transitioning South to North from boreal forests (taiga) dominated by coniferous evergreen trees

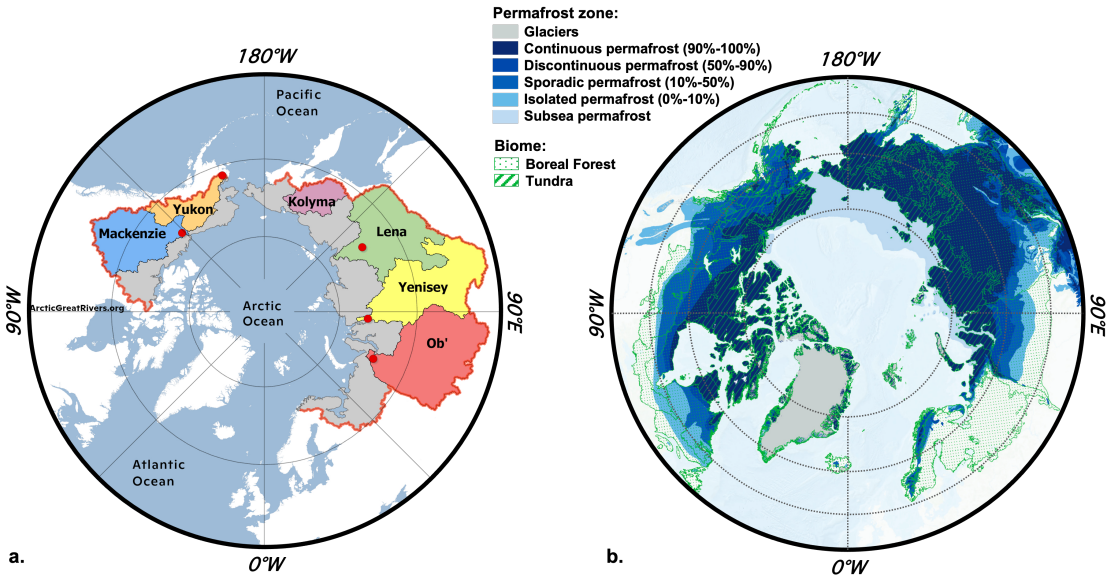

Figure 1.2: Map of the Arctic region showing (a) the 6 main Arctic watersheds and location of the Arctic Great River Observatory (ArcticGRO) gauging stations (red dots; source: ArcticGRO) and (b) permafrost types and terrestrial biomes (Adapted from Schuur et al., 2022).

(gymnosperm) to tundra composed by lichens, mosses, shrubs or sedge (Fig. 1.2.b. Olson et al., 2001; Bartsch et al., 2016; Raynolds et al., 2019). The Ob' and Yenisey catchments drain the World's largest peatland (Martens et al., 2022). The carbon stored in Arctic vegetation is estimated between 60 and 70 PgC, representing about 15 % of the global land vegetation inventory (McGuire et al., 2009). Underneath the surface, Arctic ground soils are dominated by a vast area of 17.8 million km^2 of permafrost (Box 1.1) that is sporadic (0-10 %) in southern regions and continuous (90-100 %) farther North (Schuur et al., 2022). The organic carbon stock locked in frozen form is estimated to 1,500$\pm$100 PgC of which 70 % is contained in the near-surface (0-3m) (Tarnocai et al., 2009; Hugelius et al., 2014). Permafrost strongly contributes to the organic carbon transported to the AO with 61 % of terrestrial organic carbon (particulate and dissolved) originating from near-surface soils (Martens et al., 2022). Since the 1980's, the accelerated permafrost thaw turned Arctic watersheds into a potential massive source of organic carbon to the AO (Slater & Lawrence, 2013; Schuur et al., 2015, 2022). Along with soils carbon (including permafrost), vascular plants decomposition and carbon derived from bacterial degradation in streams and rivers are two other major sources of riverine tDOC, contributing to 16-87 % (Amon et al., 2012) and 21-42 %, respectively (Kaiser et al., 2017). Recent studies suggest that coastal erosion adds to this supply (Bruhn et al., 2021; Bristol et al., 2021; Irrgang et al., 2022). It is particularly pronounced along the Laptev to Beaufort Sea coastline (up to 3 m yr^{-1} locally; Lantz et al., 2015) with a

carbon release estimated to 13-14 TgC yr^{-1} (Fritz et al., 2017; Martens et al., 2022; Irrgang et al., 2022). The particulate organic carbon (POC) largely dominates the coastal erosion organic carbon flux with a DOC:POC ratio of 1:900 (Tanski et al., 2016). In the Beaufort Sea, coastal erosion already releases more terrestrial POC than all rivers combined, and is projected to at least double in pace by 2100 (Nielsen et al., 2022).

In the environment, dissolved organic matter can take more than 60,000 molecular forms with their own chemical behavior (Riedel & Dittmar, 2014; Zark et al., 2017). The "intrinsic recalcitrance" paradigm consists in dividing the DOC pool into five compartments, depending on the molecule lifetime under a specific form (turnorver rate τ; Lønborg et al., 2020; Dittmar et al., 2021). DOC separates into labile (DOC_l; τ=hours to days), semi-labile (DOC_{sl}; τ=weeks to months), semi-refractory (DOC_{sr}; τ=decades),refractory (DOC_r; τ=thousand years) and ultra-refractory (DOC_{ur}; τ=ten thousand years) pools. In Arctic rivers, tDOC exported towards the AO originates from soils or plants and mostly fuels the oceanic DOC_{sl} pool (6 PgC; Lønborg et al., 2020; Dittmar et al., 2021). Depending on its origin, the DOC_{sl} turnover rates vary from 2 weeks to several months (Spencer et al., 2015; Wickland et al., 2012; Mann et al., 2022). In the water, heterotrophic organisms recycle DOC into DIC or more complex DOC forms. tDOC derived from heterotrophic bacteria mostly fuels the oceanic DOC_{sr} pool already made of 14Pg of reprocessed DOC. On Arctic shelves, DOC_{sr} turnover rates are estimated to range between 7 and 10 years (Hansell et al., 2004; Manizza et al., 2009). However, given the Arctic landscape diversity and climate variability, tDOC mobilized by river exhibits huge spatial and seasonal disparities in its molecular composition. By comparing carbohydrates, amino acids (bacterial biomarker) and plant phenols (plant protein biomarker) concentrations in riverine tDOC, Kaiser et al. (2017) suggest that the lability of tDOC transported by Siberian rivers is strongly linked to the seasonal flow regime with a peak of increased lability occurring during the freshet. This is in line with studies of Mann et al. (2012) and Mann et al. (2015), but contrasts with Wickland et al. (2012) that report a seasonal peak of tDOC bioavailability in winter based on DOC:DIN ratios. On the North American side, in the Mackenzie River, no peak of tDOC bioavailability is observed during freshet period (Wickland et al., 2012; Kaiser et al., 2017). This difference between the Siberian and North American sides relies on higher microbial removal due to numerous and large lakes and other water bodies present in the Mackenzie catchment, which increases water residence times in the river (Kaiser et al., 2017). However, the increasing amounts of highly labile tDOC released from deep permafrost could modify the bioavailability properties of tDOC exported by the rivers

to the AO (Schwab et al., 2020; Mann et al., 2022). Because of the high connectivity between discharge and tDOC export in Siberian Rivers, the increase of river discharge observed since the past 40 decades (1980-2020) might exacerbate the DOC concentration imbalance between the Eastern and Western basins (Ahmed et al., 2020; Feng et al., 2021). Our growing knowledge on changes ongoing in the Arctic LOAC and the associated spatial and temporal disparities around the Arctic support the idea of an absence of "average" AO state, to which are associated important physical and biogeochemical constraints on the coastal carbon cycle.

Box 1.1. THE PERMAFROST

Permafrost is frozen ground soil that remains at temperatures under 0°C for at least two consecutive years. This frozen ground is constituted of rocks and soils in which a fraction of the entire volume of pore water is ice. Permafrost stores organic matter originating from remains of animals, plant and microbes buried several hundreds to thousands years ago. The 17.8 millions km^2 occupied by permafrost represent a quarter of the Northern Hemisphere's land area (Schuur et al., 2015, 2022) and account for 33 % of the global soil carbon stock. Frozen permafrost lies between a top active layer subject to change of water state associated to seasonal variations of air temperature and a deeper unfrozen layer influenced by the warmer Earth's crust. In the unfrozen soil, there are no seasonal variations of temperature under the zero annual amplitude zone (ZAA). Unfrozen soil features called taliks can intrude into frozen permafrost under three differents forms: i) closed taliks completely surrounded by permafrost, ii) through taliks that breach through permafrost under deep lakes and iii) open taliks underneath thermokarst lakes (Fig. 1.3). Because the Arctic warms three to four times faster than anywhere on Earth (Rantanen et al., 2022),the seasonal variations of the soils temperature has increased since the 1980's resulting in permafrost thaw and a thicker active layer (Åkerman & Johansson, 2008). According to the Representative Concentration Pathway (RCP) scenarios set by the United Nations (UN) Intergovernmental Panel on Climate Change (IPCC), permafrost might lose 15 % (RCP4.5) to 99 % (RCP8.5) of its total surface area (Slater & Lawrence, 2013; Arzhanov et al., 2013) potentially leading to a massive release of organic carbon to the AO.

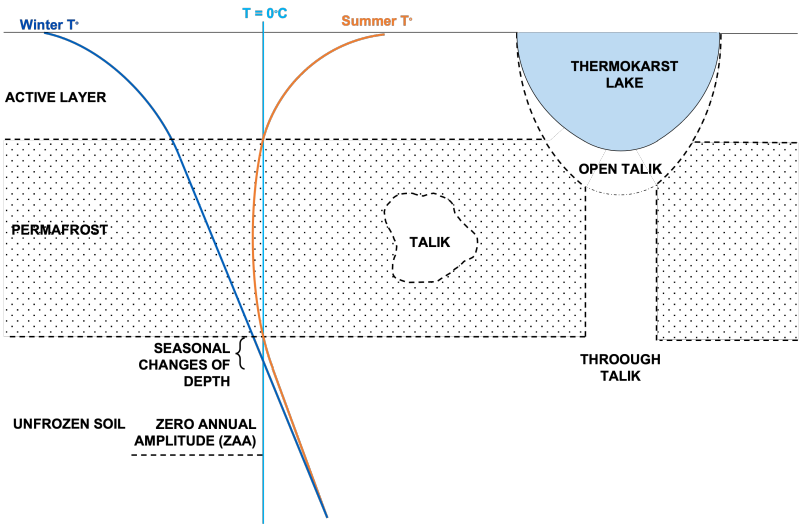

Figure 1.3: Schematic description of permafrost-dominated Arctic soil showing seasonal variations of temperature and the principal geological features (Adapted from Dobinski, 2011).

1.1.3 The study site: the Southeastern Beaufort Sea

The Southeastern Beaufort Sea (SBS) encompasses coastal waters of the westernmost Canadian Arctic. Situated to the West of the Amundsen Gulf, which delimits the end of the Canadian Archipelago (Fig. 1.4a.), it receives at its northern boundary water masses coming from the oligotrophic Beaufort Gyre. On its western side, the SBS connects with the Alaskan Beaufort Sea that brings Si-rich waters from the Pacific Ocean on its plateau (Fig. 1.4b. Macdonald et al., 1987; Pickart, 2004). Closer to the coast, the second largest Arctic delta, the Mackenzie Delta (Burn & Kokelj, 2009), delivers 306 km^3 of riverine freshwater (Dittmar & Kattner, 2003; Holmes et al., 2012; Mulligan & Perrie, 2019). The Mackenzie River drains 1.7 million km^2 mainly covered by boreal forest in the South and tundra plains in the North covering the delta (1 % ; Raynolds et al., 2019). This wide watershed is underlain by 82 % of isolated to continuous permafrost (Vörösmarty et al., 2000; Holmes et al., 2013). The drainage basin splits into two different topographic types, a mountainous western area and a rather flat eastern area with multiple large lakes (Rosenberg & Barton, 2013). As a consequence, the organic matter composition conveyed towards the SBS may differ as it is more degraded along it path through the different eastern lakes (Macdonald & Yu, 2006). Within the delta itself, the soil organic carbon content of deltaic alluvium provides an additional source of carbon to the SBS (34–41 PgC (Tarnocai et al., 2009; Hugelius et al., 2014)). Freshwater reaches the SBS through a complex river network made of thermokarst lakes

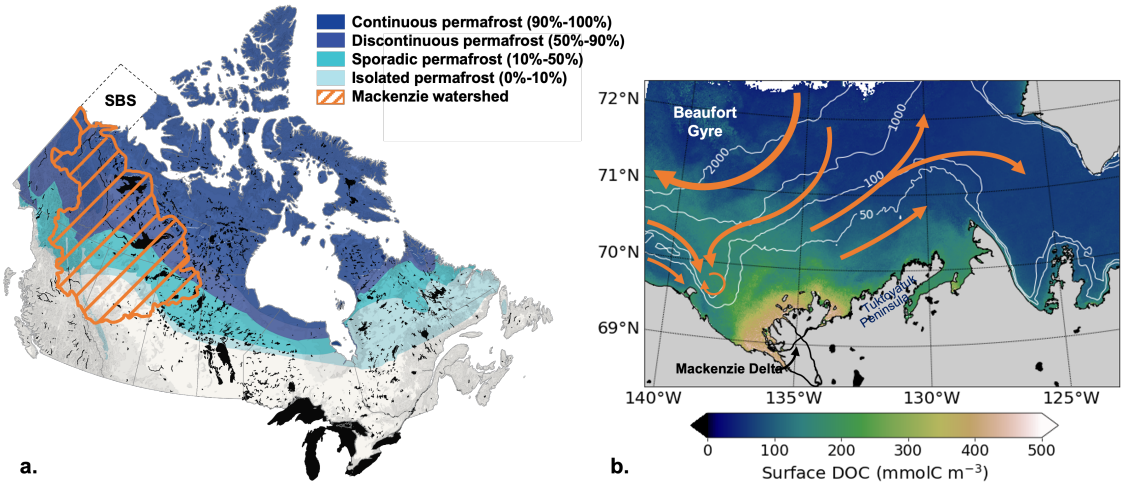

Figure 1.4: a) Map of Canada showing the permafrost types with Mackenzie River catchment (orange hatches) overlaid and the Southern Beaufort Sea (SBS) domain (black dashed lines), and b) mean summer surface concentration of remotely sensed dissolved organic matter in 2012 (Aqua-MODIS sensor) with principal observed sea surface currents (orange arrows).

and channels (Tank et al., 2011; Nill et al., 2019) of which the main branches end up into three major outlets: Shallow Bay (western delta), Beluga Bay (central delta) and Kugmallit Bay (eastern delta) (Morley, 2012).

The Mackenzie River plume induces a large seasonal variability of the physical and biogeochemical characteristics of the SBS. The SBS is sea ice-covered over 8-9 months generally from mid-October to June (Macdonald & Yu, 2006). During this period, a 2 m thick landfast ice pack accumulates in the vicinity of the Mackenzie Delta forming a bottleneck that prevents the river to flow out into the sea. The westward motion of the ice pack combined with intermittent winds moving the ice either northward or southward lead to an open-water area offshore, over the shelf, and promotes the formation of a rubble ice block called "Stamukhi" (Carmack & Macdonald, 2002). The "Stamukhi" acts as a barrier that blocks the propagation of riverine freshwater, managing to spread in the estuary under the landfast ice (Fig. 1.5). At the freshet (end of May), with acceler-

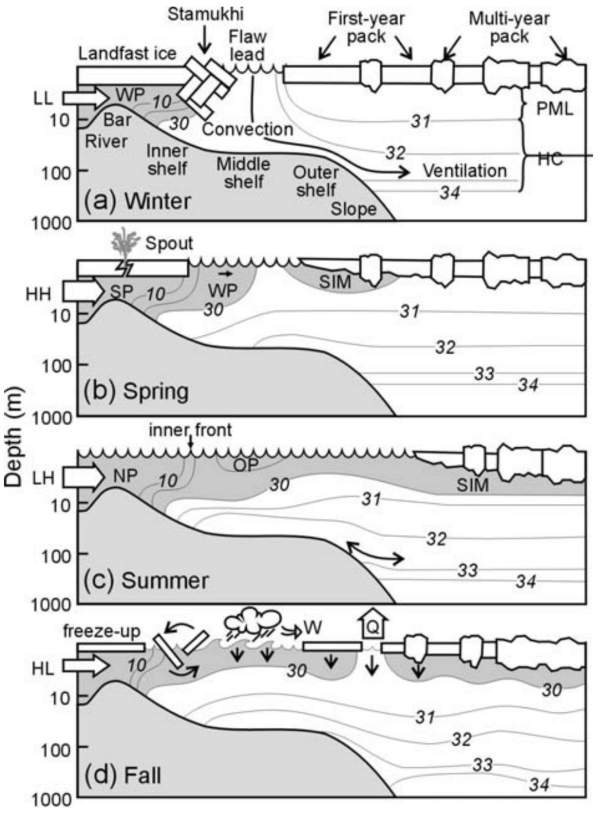

Figure 1.5: Seasonal pattern of the sea ice-Mackenzie riverine plume interaction along the SBS shelf. The salinity isolines are shown (full lines). Abbreviations: HH = higher high river discharge; LH = lower high river discharge; LL = lower low river discharge; HL = higher lower river discharge; NP = new plume water; OP = old plume water; Q = surface heat flux; SIM = sea ice melt; SP = spring inflow; W = wind; WP = winter inflow. (source: Macdonald & Yu, 2006)

ating discharge, the plume reattained in the estuary by the "Stamukhi" starts to melt the landfast ice close to the shore (Searcy et al., 1996; Matsuoka et al., 2016). In June, the thick barrier finally melts allowing the release of warmer freshwater from the Mackenzie River offshore (Mulligan et al., 2010; Nghiem et al., 2014; Mulligan & Perrie, 2019). From July to mid-September, the whole SBS is free of sea ice and the continuous river outflow feeds a large and 3 m-thick riverine plume (Carmack & Macdonald, 2002; Mulligan & Perrie, 2019). Westerlies confine the riverine plume along the Tuktoyaktuk Peninsula (Fig. 1.4) and promote coastal downwelling along the Peninsula (Macdonald & Yu, 2006; Lin et al., 2021). In contrast, the riverine plume is pushed westward when easterlies prevail and then spreads offshore with the effect of the Coriolis force inducing a strong vertical stratification in the SBS. Such conditions are favorable to the coastal upwelling of DIC and nutrient-rich waters to the surface (Mol et al., 2018; Mulligan & Perrie, 2019). Later in fall, the river outflow weakens and wind storms mix freshwater within the top 10-20 m of the water column setting the conditions for sea-ice formation (Macdonald & Yu, 2006). The decrease in air temperature promotes heat transfer from ocean to atmosphere and sea ice forms as the ocean cools down.

The summer season is characterized by a marked seasonal peak of primary production and air-sea CO_2 fluxes (Carmack et al., 2004; Forest et al., 2014). In the SBS, the riverine Mackenzie plume conveys biogeochemichal tracers within nutrient-poor oceanic waters. As a result, it is suggested that 3.1 to 8.9 % of the SBS NPP could be sustained by the riverine supply of dissolved nutrients (Le Fouest et al., 2013; Terhaar et al., 2021a). In the SBS, this terrestrial supply could support a net oceanic ingassing of CO_2 between -9.1 to -1.5 TgC yr^{-1} (Arrigo et al., 2010; Evans et al., 2015; Manizza et al., 2019; Ouyang et al., 2021). However, the counterbalancing (i.e. outgassing) contribution of riverine tDIC (7.6 TgC yr^{-1} Tank et al., 2012) and tDOC (1.04–1.76 TgC yr^{-1} Macdonald et al., 1989; Dittmar & Kattner, 2003; Raymond et al., 2007; Holmes et al., 2012; Le Fouest et al., 2013) to the net CO_2 flux is poorly understood so that whether the coastal SBS acts as a sink or a source of carbon to the atmosphere remains to be determined. Several field campaigns were conducted in the 2000's to investigate the carbon cycle in the river-influenced SBS plateau. Mucci et al. (2010) first suggested the area to be an overall CO_2 sink in summer (-2.3 $\pm$ 3.5 mmol m^{-2} d^{-1}). This was later confirmed by the study of Forest et al. (2014) that estimated an ocean ingassing of -2.0 ± 3.3 mmol m^{-2} d^{-1}. Both studies report sharp spatial variations in the air-sea CO_2 fluxes characterized by a strong gradient across the Mackenzie shelf. Forest et al. (2014) observed a CO_2 outgassing of up to 45 $\pm$ 30 mg m^{-2} d^{-1} in the inner shelf shifting to

strong ingassing of -43 $\pm$ 5 mg m^{-2} d^{-1} in the outer shelf and weakening offshore to reach -8 $\pm$ 2 mg m^{-2} d^{-1}. Such a gradient is mostly attributed to the presence of the Mackenzie riverine plume that would promote heterotrophic conditions (i.e. respiration) through a more pronounced stratification associated with high tDOC and low nitrate concentrations (Mucci et al., 2010; Forest et al., 2014). During easterlies conditions, coastal upwellings (Lin et al., 2021), bringing deep nutrient-rich waters on the plateau may promote NPP and reverse this CO_2 outgassing pattern. Furthermore, the sea surface supersaturation in pCO_2, in winter, was linked to the confinement of the riverine plume in the inner shelf and to under-ice respiration (Else et al., 2012). Such conditions may be responsible for CO_2 outgassing in early spring when sea-ice breaks up. While pivotal for identifying the mechanisms at stake in modulating the air-sea CO_2 fluxes in the SBS, insights on carbon cycle provided by synoptic field surveys are limited over a wider spatial and time frame. The CO_2 flux assessment based on remote sensing data (Yasunaka et al., 2018; Landschützer et al., 2016) is a powerful tools to fill in this gap but, even though coastal areas start to be included in large datasets (Landschützer et al., 2020), such data do not fulfill the needs required for the Mackenzie Delta area.

1.2 Context and objectives of the PhD thesis

1.2.1 A difficult quantification of land-to-sea carbon fluxes

Land-to-sea fluxes of carbon in the Arctic are altered in both their concentration and composition in response to global warming. Tank et al. (2016) report a 39.3 % increase of the tDOC flux to the SBS over the past four decades, with significant differences according to the season. As a consequence of permafrost thaw, the quality of tDOC flowing onto arctic shelves might change in the future and to which the ecosystem response is very uncertain (Schwab et al., 2020; Mann et al., 2022). In addition, the synoptic variability ($\sim$4 days) in tDOC quantities and quality exported to the ocean (Juhls et al., 2020) highlight a pressing need for a high-frequency monitoring.

An assessment of the high-frequency land-to-sea flux of carbon can be performed using watershed models (Kicklighter et al., 2013; McGuire et al., 2016; Bowring et al., 2020; Rawlins et al., 2021). Arctic watershed models are high-value predictive tool, but they are still limited in their ability to resolve the complex mechanistic processes at stake in tDOC mobilization and transformation, which precludes an accurate flux assessment (Kicklighter et al., 2013; Liao et al., 2019). Another approach relies on the chemodynamic relationship between river discharge and

transported matter (Musolff et al., 2015). Such relationship can explain up to 74 % of the tDOC variability in pan-arctic rivers (Raymond et al., 2007; Holmes et al., 2012; Griffin et al., 2018). To be robust, the non-linear fitting of the chemodynamic relationships (Runkel et al., 2004) requires large observational datasets. However, the remoteness of the Arctic seas makes this task very challenging in both space and time.

Since the 2000s, the PARTNERS/ArcticGRO monitoring program (AGRO) provides high-quality multi-parametric *in situ* measurements in the six major pan-arctic rivers (including the Yukon in the Pacific Ocean; Holmes et al., 2021). Combined with the monitoring efforts from the Water Survey of Canada, the Arctic and Antarctic Research Institute, and the United States Geological Survey, it has led to the establishment and operation of a gauging stations network able to provide high frequency river discharge measurements (see Fig. 1.2; Shiklomanov et al., 2021). Nevertheless, only a few tDOC samples are collected yearly (Holmes et al., 2012), which strongly hampers a robust assessment of tDOC fluxes at the coast. In addition, measurements are often several hundreds kilometers upstream the river mouth that precludes any removal and/or enrichment of tDOC within the estuary or delta to be accounted for in the exported flux (Kipp et al., 2020). The first objective of this PhD thesis consists in improving our ability to estimate interannual riverine tDOC fluxes into the coastal AO by using recent satellite-derived tDOC concentration estimates (Matsuoka et al., 2017).

1.2.2 Uncertainties in the role played by Arctic rivers in coastal air-sea CO_2 fluxes: disentangling physical and biogeochemical contributions

Improving our ability to constrain the land-to sea interface in regional arctic models is thus required, because the AO is an important contributor of the global atmospheric CO_2 sequestration (118 to 180 TgC yr^{-1}; Arrigo et al., 2010; Yasunaka et al., 2018; Manizza et al., 2019). Nevertheless, carbon source and sinks on shelves, which occupy about half of the AO surface area (e.g., Carmack et al., 2006), are still not well understood (Forest et al., 2014; Roobaert et al., 2019). In particular, the role of pan-arctic rivers as conveyors of large amounts of freshwater, inorganic nutrients and organic matter to the sea remains highly uncertain (Dittmar & Kattner, 2003; Holmes et al., 2012; Tank et al., 2012; Le Fouest et al., 2013; Juhls et al., 2020). While riverine carbon supply can promote CO_2 outgassing through complex heterotrophic (Kirchman et al., 2009) and light-induced (Belanger et al., 2006) processes, inorganic nutrients support NPP and then CO_2 up-

take. At pan-arctic scale, less than 15 % of NPP could be supported by riverine nitrogen (Le Fouest et al., 2013; Terhaar et al., 2021a) suggesting that the CO_2 outgassing capacity of river-influenced shelves may be underestimated.

With an Arctic warming three to four time greater than the global average (Rantanen et al., 2022), the river discharge increase (Ahmed et al., 2020; Feng et al., 2021) is concomitant with an earlier spring flow (Brown et al., 2020). Combined with the accelerated permafrost thaw that alters the quality and quantity of tDOC exported seaward with a high seasonal to interannual variability (Schuur et al., 2015; Schwab et al., 2020) we might expect in the future marked changes in air-sea CO_2 fluxes induced by large arctic rivers. Thus, we face a pressing need to gain a better understanding on how the coastal AO could respond to such changes in riverine inputs. In this context, the second objective of this PhD thesis is to disentangle the effects of land-to-sea fluxes of freshwater and terrestrial dissolved inorganic and organic matter on NPP and air-sea CO_2 fluxes from the synoptic to the interannual timescale.

1.2.3 Uncertainties on riverine tDOC inputs and simulated plumes in models

On AO shelves, riverine carbon fluxes are estimated to induce an outgassing of ~ 2 TgC yr^{-1} to the atmosphere (Lena and Mackenzie; Lacroix et al., 2020). However, such an estimate is yet largely uncertain given the complexity of tDOC degradation along the land-ocean aquatic continuum. Riverine tDOC transported to the AO undergoes three major removal processes. First, the biotic degradation by marine heterotrophic bacteria (Lønborg & Álvarez-Salgado, 2012; Herlemann et al., 2014) and abiotic photochemical reactions (Miller & Zepp, 1995; Moran et al., 2000; Belanger et al., 2006) transform tDOC into DIC or other DOC forms with a wide range of lability (Lønborg et al., 2020). Second, the abiotic flocculation of tDOC driven by sharp salinity gradients within the land-to-sea transition (Sholkovitz, 1976) can remove tDOC from surface waters through the sedimentation of flocculates. While bacterial activity and light-driven processes are often considered as prevailing processes (Anderson et al., 2019; Clark et al., 2022), flocculation could be responsible for the removal of more than 50 % of surface tDOC in the Mackenzie Delta (Kipp et al., 2020).

Once in the ocean, the efficiency of the bacterial tDOC degradation strongly depends on the tDOC quality, which varies strongly according to the AO region (Amon et al., 2012; Kaiser et al., 2017). tDOC quality is related to the origin (vascular plants or soils), watershed characteristics

(water residence time and enrichment/removal processes) and climatic conditions (increased DOC lability with more permafrost thaw Schwab et al., 2020; Mann et al., 2022). As a consequence, arctic models may be sensitive to tDOC quality, which may highly constrain the simulated CO_2 fluxes within coastal waters. To the uncertainty underlying the biogeochemical setting of the model adds a realistic physical setting of the plume. As the plume physics and biogeochemistry are tightly related, the last objective of the thesis is to investigate the sensitivity of regional arctic models to the representation of the physical and biogeochemical plume through the prism of observations available for the Mackenzie shelf.

CHAPTER 2

THE OCEAN-SEA ICE-BIOGEOCHEMICAL MODELING FRAMEWORK

It is now timely to gain a better understanding on riverine tDOC contribution to air-sea CO_2 fluxes onto Arctic shelves. In the following PhD thesis, this task will be principally performed using a numerical ocean-sea ice-biogeochemical model (Box 2.1). In the era of "digital twins", models and observations are intrinsically related and feed each others. While observations aim to provide information as close as possible to the reality of the field, they can suffer strong limitations in covering large time and spatial scales. This is particularly true for polar regions, where the remoteness, clouds and sea ice cover make high-frequency measurements very difficult. Models are useful in getting rid of such limitations, providing extensive datasets through large areas and long period of time (up to several decades), as well as across a wide range of environmental conditions. However, their capability in predicting the physics and biogeochemistry can be hampered by the conceptual and/or mathematical description of the simulated processes, which strongly rely on our current knowledge. In this section, I will present the ECCO-Darwin model (Brix et al., 2015) used to simulate the effect of the Mackenzie River freshwater and biogeochemical inputs on the SBS air-sea CO_2 fluxes.

2.1 The ECCO-Darwin model

The consortium for Estimating the Circulation and Climate of the Ocean (ECCO) was established in 1999 with the aim to combine ocean observation and general circulation modeling in order to best estimate the time-evolving state of the global ocean. Therefore, they combined the Massachusetts Institute of Technology general circulation model (MITgcm; Marshall et al., 1997) with the widest dataset of ocean observations available from the World Ocean Circulation Experiment (WOCE) program. As a result of ECCO consortium efforts, the first global ocean circulation model corrected by data assimilation method (Box 2.2) was published in 2002 (Stammer et al., 2002), followed by multiple publications in a wide range of scientific applications. After several years, the ECCO phase II started with the aim to improve the ocean state description rendering the model eddy-permitting and by coupling it with a sea-ice model (Menemenlis, Hill, et al., 2005). The ECCO2 version evolved toward a cube-sphere grid projection (Adcroft & Campin, 2004), which refined the horizontal resolution from 1° to an average 18 km and removed polar singularities. The model was coupled with the J. Zhang et al. (1998) sea ice model, latter replaced by Losch et al. (2010) description. The use of Green's Function approach enhanced the ocean state estimate by better calibrating several empirical ocean and sea ice model parameters as well as initial and

boundary conditions (Menemenlis, Fukumori, & Lee, 2005).

An ocean-biogeochemical model was finally developed combining the ECCO2 model with the Darwin ecosystem model (Follows et al., 2006; Follows & Dutkiewicz, 2011) and its biogeochemical parameterization (Dutkiewicz et al., 2009). Based on an ecosystem parameterization distributed into plankton phenotypes with flexible parameters, ECCO-Darwin highly contributed to better describing the different biogeography in the world's ocean (Dutkiewicz et al., 2013). The addition of Green's Functions to calibrate biogeochemical variables such as nutrients, pH, pCO_2, air-sea CO_2 or DIC considerably improved the ocean-biogeochemical state estimate (Brix et al., 2015; Carroll et al., 2020, 2022).

ECCO-Darwin simulates cycling of carbon, nitrogen, phosphorus, silica, iron, and oxygen as they transition between inorganic, living, and dead organic pools. The simulated carbon cycle considers both soft-tissue and carbonate pumps (Follows et al., 2006). In the ocean, dissolved organic matter mostly plays a role on air-sea CO_2 fluxes through the degradation of DOC into DIC. In ECCO-Darwin, the mass fluxes between DIC and other biogeochemical state variables are simulated as follows:

$$\frac{dDIC}{dt} - \nabla \cdot (K \nabla DIC) = \Phi_{CO_2} + S_{bio}^{DIC}, \tag{2.1}$$

where the terms on left hand side respectively represent the advective transport of DIC and the mixing by eddy diffusion processes (see Box 2.1). On the right hand side Φ_{CO_2} and S_{bio}^{DIC} are the terms that constrain air-sea CO_2 fluxes (see Eq. 2.2 and biological consumption and production of DIC (se Eq. 2.6), respectively.

The air-sea CO_2 flux is determined by the difference between the partial pressure of CO_2 in the sea water (pCO_2^{sw}) and the atmosphere (pCO_2^{atm}), according to the following equation:

$$\Phi_{CO_2} = K_w . K_0 . \left(f^{sw} . pCO_2^{sw} - f^{atm} pCO_2^{atm} \right). \tag{2.2}$$

The intensity of the CO_2 gas transfer is modulated by K_0 and K_w terms calculated as follows:

$$\begin{cases} \ln\left(K_0\right) = A_1 + A_2 \frac{100}{T} + A_3 \frac{T}{100} + S\left(B_1 + B_2 \frac{T}{100} + B_3 \left(\frac{T}{100}\right)^2\right), \\ K_w = \left(1 - SI_{frac}\right) .0.337 . u^2 . \left(\frac{Sc}{660}\right)^{-1/2}, \end{cases} \tag{2.3}$$

where K_0 is the solubility of CO_2 in sea water (Weiss, 1974) that depends on the salinity (S) and the temperature (T; °K) of seawater (see Tab. 2.1 for A_i and B_i values), and K_w is the gas transfer velocity (Wanninkhof, 1992) that depends on the wind velocity (u) and the following Schmidt number (Sc):

$$Sc = 2073.1 - 125.63.T + 3.6276.T^2 - 0.043219.T^3. \tag{2.4}$$

In polar regions, the gas transfer velocity is weighted by the sea-ice fraction SI_{frac}, so that no exchange is possible when the ocean is 100% covered with sea-ice. In equation 2.2, both pCO_2 terms are weighted by two fugacity correction terms (f^{sw} and f^{atm}) that consider the properties of CO_2 as a non-ideal gas (Weiss, 1974). In ECCO-Darwin, while fugacity correction term in sea-water (f^{sw}) is calculated independently (Weiss, 1974), the fugacity correction in the atmosphere (f^{atm}) is computed with the solubility (Weiss & Price, 1980):

$$\begin{cases} f^{sw} = \exp\left(P.\frac{B(T).2\delta_{CO_2-air}}{RT}\right), \\ \ln\left(K_0.f^{atm}\right) = A_1 + A_2\frac{100}{T} + A_3\frac{T}{100} + A_4\left(\frac{T}{100}\right)^2 + S\left(B_1 + B_2\frac{T}{100} + B_3\left(\frac{T}{100}\right)^2\right), \end{cases} \tag{2.5}$$

The production of DIC through organic matter degradation is described in the biological term S_{bio}^{DIC}, calculated as follows:

$$S_{bio}^{DIC} = -U^{DIC}.(1 + r_{PIC:POC}) + R_{DOC} + R_{POC} + \lambda_C^{diss} PIC + R_j^C, \tag{2.6}$$

where U^{DIC} is the uptake of DIC in the ecosystem, R_{DOC} and R_{DOC} are respectively the bacterial degradation of dissolved and particular organic carbon, λ_C^{diss} is the dissolution rate of particular inorganic carbon and R_j^C the production of DIC through the ecosystem respiration.

Constant	$\ln(K_0)$	$\ln(K_0.f^{atm})$
A_1	-60.2409	-162.8301
A_2	93.4517	218.2968
A_3	23.3585	90.9241
A_4	0	-1.47696
B_1	0.023517	0.025695
B_2	-0.023656	-0.025225
B_3	0.0047036	0.0049867

Table 2.1: Constants to calculate the CO_2 solubility coefficient K_0 (Weiss, 1974) and fugacity correction term $K_0.f^{atm}$ in moist air at a total pressure of 1 atm (Weiss & Price, 1980).

Box 2.1. BIOGEOCHEMICAL MODELING

Biogeochemical models describe mass fluxes between different biological and/or biogeochemical compartments (namely state variables) of a system. State variables are expressed as a concentration or a biomass and linked through mass fluxes constrained into time and space by mathematical relationships. The relationships linking different state variables are initially designed by a conceptual model, which is a representation of how the studied system would work to the best of our knowledge. This conceptual model is then translated into a set of differential equations with numerical constants that describe the nature of the fluxes of matter and the magnitude of these fluxes. This is the quantitative model. The constants can be quantified *in situ* or in laboratory under specific conditions. The quantitative model is then resolved numerically. Time is discretized, i.e. divided into a set of equal periods. Then, starting from known initial conditions (i.e. biomass or concentration) for each state variable, the model simulates an estimate of the future biomass or concentration values at each time step by resolving numerically the set of differential equations.

A model that simulates the temporal evolution of a number of state variables without any information on the spatial domain is called a zero dimension (0D) model. As for time, space can be divided into different segments (1D), areas (2D) or volumes (3D). A biogeochemical model can be coupled with the advective and/or diffusive transport equations resulting into the following system of partial differential equations:

$$\frac{\partial C}{\partial t} + u\frac{\partial C}{\partial x} + v\frac{\partial C}{\partial y} + w\frac{\partial C}{\partial z} = \frac{\partial}{\partial x}\left(K_x\frac{\partial C}{\partial x}\right) + \frac{\partial}{\partial y}\left(K_y\frac{\partial C}{\partial y}\right) + \frac{\partial}{\partial z}\left(K_z\frac{\partial C}{\partial z}\right) + S_C \quad (2.7)$$

$$\iff \frac{dC}{dt} = \nabla.(K\nabla C) + S_C,$$

where C is the state variable, t is time, and x, y and z are the spatial coordinates. u, v, w and K_x, K_y, K_z are respectively the current velocities and the eddy diffusion coefficients in the x, y, and z directions. S_C represents the sources and sinks of the simulated mass due to the biogeochemical interactions between state variables. A model is called Eulerian when it simulates the biomass and/or concentration of each state variables at every point of the discretized spatial domain defined by the numerical grid. ECCO-Darwin used in this PhD thesis is a 3D Eulerian model.

Box 2.2. DATA ASSIMILATION (adapted from Wunsch et al. (2009))

Models represent the time-space evolution of several state variables of the ocean through mathematical equations. Even though the mathematical description of the ocean is a good estimator of the time-space evolution of a state variable, it is known to drift from the real state observation. Data assimilation is a method that corrects the model drift based on the real ocean state observation.

To introduce the data assimilation method, we consider an observation of a specific state variable y_i at a fixed time t_i, latitude λ_i, longitude ϕ_i and depth d_i. Then, $\tilde{y}_i$ is the value calculated by a model (for example ECCO) at the equivalent time and location. As the model calculate an approximation, its estimate of the state variable differs from the observation ($\tilde{y}_i \neq y_i$). To measure the misfit between the model and the observation, the ECCO model uses the following equation:

$$\delta_i^2 = \frac{(\tilde{y}_i - y_i)^2}{\sigma_i^2}, \tag{2.8}$$

where σ_i^2 is the expected misfit, i.e. the estimated variance of the noise in y_i plus the estimated square of the model error. If the model perfectly matched the observation, the difference would fall within the standard deviations of the expected misfit ($\delta_i^2 = 1$). However, δ_i^2 is greater than 1 in practice. Then, the aim of data assimilation consists in minimizing the following cost function summed over time, space and state variables:

$$J = \sum_i \delta_i^2 = \sum_i \frac{(\tilde{y}_i - y_i)^2}{\sigma_i^2}. \tag{2.9}$$

Minimizing the cost function J is equivalent to solving a basic least square problem with some technical difficulties summarized in Wunsch et al. (2009). The ECCO consortium selected two potential methods able to resolve such a problem in the model: Kalman filtering followed by Rauch–Tung–Striebel (RTS) smother (Fukumori, 2002) or a Lagrangian multipliers method also called adjoint method (Wunsch & Heimbach, 2007). The latter has widely been generalized in recent versions of the ECCO model.

In terms of mass, DOC is the largest component of the oceanic dissolved organic matter pool (Lønborg et al., 2020). In ECCO-Darwin, the dynamics of the DOC scalar is represented by the following mass transfer equation:

$$S_{bio}^{DOC} = M^{DOC} + G^{DOC} - R_{DOC}, \tag{2.10}$$

where M^{DOC} and G^{DOC} are source terms related to plankton mortality and grazing, respectively, and R_{DOC} is the degradation term. In ECCO-Darwin, heterotrophic bacteria are not explicitly represented. Then, DOC degradation is described following a constant turnover rate λ_{DOC}, which relates to the lifetime ($\tau_{DOC} = 1/\lambda_{DOC}$) of DOC (Eq. 2.11). The efficiency of the DOC degradation depends on a temperature remineralization function prescribed by the Arrhenius function ($f^{remin}(T)$, where T is seawater temperature).

$$R_{DOC} = \lambda_{DOC}.f^{remin}(T).DOC. \tag{2.11}$$

2.2 The regional configuration of the Southeastern Beaufort Sea (ED-SBS)

2.2.1 Baseline configuration

In the following PhD thesis, we use the ECCO-Darwin Southeastern Beaufort Sea (ED-SBS) configuration, which is a regional section of the SBS extracted from the global ECCO-Darwin configuration of Carroll et al. (2020). ED-SBS includes latitudes between 67.2°N–75.1°N and longitudes between 146.7°W–119.7°W delimited over the ECCOvr4 curvilinear grid (Fig. 2.1). The horizontal grid spacing is on average ∼12 km wide and the vertical discretization comprises 44 evenly spaced levels, ranging from 10 m at the surface to 307 m near the bottom of the ocean. Energy sink through mesoscale activity is implicitly parameterized using Redi (1982) and Gent and Mcwilliams (1990) diffusivity schemes. The model integration spans from January 1992 to December 2019 with 1200s time step. Initial, surface and boundary conditions for physical and biogeochemical state variables are constrained according to the global ocean state estimate of Carroll et al. (2020). ED-SBS physical and biogeochemical models are coupled online with no feedback of the biogeochemistry on physical parameters. The model explicitly simulates cycling of carbon, nitrogen, phosphorus, silica, iron, and oxygen as they transition between inorganic, living, and dead organic pools. Carbon cycle considers both soft tissue and carbonate pumps. Mass

fluxes of 31 biogeochemical state variables (Table A.1) are simulated, including seven plankton functional types (PFTs): diatoms, large eukaryotes, *Synechococcus*, low- and high-light adapted *Prochlorococcus* and small and large zooplankton.

2.2.2 Arctic-specific configuration

In order to consistently represent the ecosystem dynamics of the SBS, ED-SBS baseline configuration has been adapted to the Arctic specificity. In the SBS, phytoplankton carbon biomass is mostly represented by diatoms and dinoflagellates (eukaryotes; Coupel et al., 2015). In contrast, *Synechococcus* and low- and high-light adapted *Prochlorococcus* are not representative of the SBS phytoplankton communities and were then removed from the state variables, reducing to 4 the number of simulated PFTs. Furthermore, mortality and grazing were set to zero when total phytoplankton biomass falls below 0.05 mmolC m^{-3} to represent the observed phytoplankton biomass that persists under ice in winter (Randelhoff et al., 2020; Hoppe, 2022) .

In the SBS configuration, the Mackenzie River supply in freshwater and biogeochemical tracers was refined to better match with observations. In the global configuration, a climatology of the Mackenzie River discharge Fekete et al. (2002) was spread over a group of grid cells located offshore. The climatology was replaced by daily gauge measurements from the Water Survey

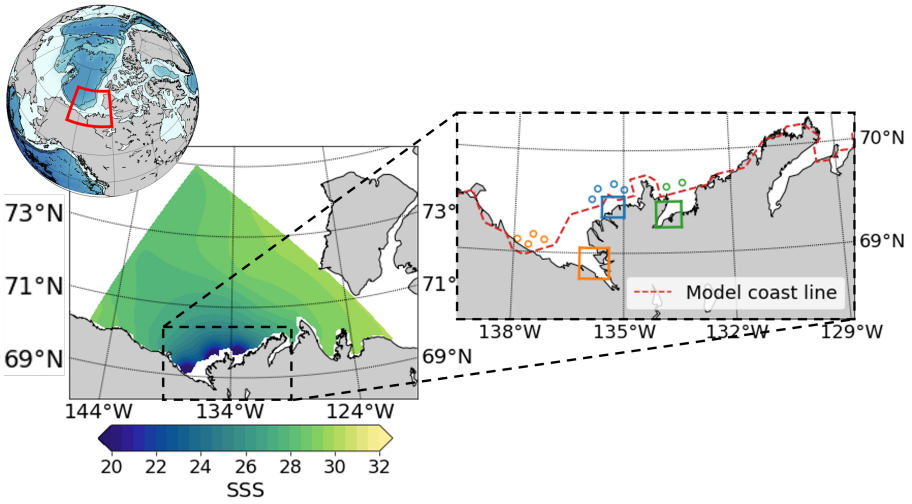

Figure 2.1: 2000–2019 mean sea surface salinity (SSS) over the full ED-SBS numerical domain (left panel) with model region in a global context (top left inset). The colored circles (right panel) are the grid cells at which river forcing is applied: Shallow Bay (orange), Beluga Bay (blue), and Kugmallit Bay (green). The red dashed line represents the coastline of the numerical domain.

of Canada (dataset included in the Arctic Great River Observatory; Shiklomanov et al., 2021). The Mackenzie River discharge measured at the Tsiigehtchic station ∼200 km upstream the delta mouth was redistributed nearshore over model grid cells the closest to the three major delta outlets and according to their relative contribution: Shallow Bay (29.8%), Beluga Bay (37.6%), and Kugmallit Bay (32.6%) (Fig. 2.1, Morley, 2012; Bertin et al., 2022). Daily river temperature data from the Tokuda et al. (2019) dataset and a biogeochemical runoff were also used to constrain the model over the same grid cells used for the river discharge. Terrestrial dissolved organic nitrogen (tDON), phosphorus (tDOP) and inorganic silica (tDSi) forcings were set according to the GlobalNEWS2 annual climatology (Mayorga et al., 2010). The daily terrestrial DIC (tDIC) runoff was estimated according to Tank et al. (2012) (see Bertin et al., 2022) and associated with terrestrial alkalinity (tAlk) estimated using a tAlk:tDIC ratio of 0.93 (Tank et al., 2012). The daily tDOC load was estimated according to a non-linear fitting method fully detailed in Chapter 3 (Bertin et al., 2022).

The ED-SBS baseline configuration extracted from the global ECCO-Darwin model only considers a single pool of autochthonous DOC (i.e. produced by the marine ecosystem, see Eq. 2.10). tDOC being mostly semi-labile (DOC_{sl}) and semi-refractory (DOC_{sr}) in the SBS, the ECCO-Darwin DOC state variable was split into two distinct state variables within ED-SBS as follows:

$$\begin{cases} S_{bio}^{DOC_{sl}} = M^{DOC_{sl}} + G^{DOC_{sl}} - \lambda_{DOC_{sl}}.f^{remin}(T).DOC_{sl} + R_{sl:sr}.tDOC, \\ S_{bio}^{DOC_{sr}} = -\lambda_{DOC_{sr}}.f^{remin}(T).DOC_{sr} + (1 - R_{sl:sr}).tDOC. \end{cases} \tag{2.12}$$

The state variable DOC_{sl} keeps the original mass fluxes of autochtonous DOC described in ECCO-Darwin, i.e. ecosystem mortality ($M^{DOC_{sl}}$), grazing ($G^{DOC_{sl}}$) and remineralization (Eq. 2.10). The allochtonous tDOC forcing from the Mackenzie runoff enters in ED-SBS according to a DOC_{sl}:DOC_{sr} ratio ($R_{sl:sr}$). According to recent data (F. Joux, unpublished data; see Lizotte et al., 2022), $R_{sl:sr}$ was set to 0.5. Hence, the total mass of tDOC flows equally in DOC_{sl} and DOC_{sr}. Depending on its origin, DOC_{sl} can exhibit very different lifetimes (2 weeks to 3 months; Spencer et al., 2015; Holmes et al., 2008). A remineralization rate $\lambda_{DOC_{sl}}$ of 1 month^{-1} was chosen. In contrast, DOC_{sr} represents more refractory molecules originating directly from the river according to $R_{sl:sr}$. DOC_{sr} remineralization rate $\lambda_{DOC_{sr}}$ was set to 10 years^{-1} (Manizza et al., 2009).

CHAPTER

3

MERGING SATELLITE AND IN SITU DATA TO ASSESS THE FLUX OF TERRESTRIAL DISSOLVED ORGANIC CARBON FROM THE MACKENZIE RIVER TO THE COASTAL BEAUFORT SEA

Abstract

In response to global warming, the Arctic is undergoing rapid and unprecedented changes that alter the land-to-sea forcing in large Arctic rivers. Improving our knowledge of terrestrial dissolved organic carbon (tDOC) flux to the coastal Arctic Ocean (AO) is thus critical and timely as these changes strongly alter the biogeochemical cycles on AO shelves. In this study, we merged riverine *in situ* tDOC concentrations with satellite ocean-color estimates retrieved at the land-marine interface of the Mackenzie Delta to make a first assessment of the tDOC export from its main outlets to the shelf. We combined tDOC and river discharge data to develop a regression model that simulated tDOC concentrations and fluxes from daily to interannual (2003-2017) time scales. We then compared the simulated satellite-derived estimates to those simulated by the model constrained by *in situ* tDOC data only. As the satellite tDOC estimates reflect the delta effect in terms of tDOC enrichment and removal, our results inform us of how much tDOC can potentially leave the delta to reach the ocean (1.44 $\pm$0.14 TgC yr^{-1}). The chemodynamic relationships and the model suggest contrasting patterns between Shallow Bay and the two easternmost delta outlets, which can be explained by the variability in their geomorphological settings. At the seasonal scale and for all outlets, the satellite-derived tDOC export departs from the estimate based on *in situ* tDOC data only. During the river freshet in May, the satellite-derived tDOC export is, on average, $\sim$15% (Shallow Bay) to $\sim$20% (Beluga Bay) lower than the *in situ*-derived estimate. This difference was the highest (-60%) in 2005 and exceeds 30% over most of the last decade, and can be explained by qualitative and quantitative differences between the tDOC$_{in\ situ}$ and tDOC$_{sat}$ datasets in a period when the freshet is highly variable. In contrast, in summer and fall, the satellite-derived tDOC export is higher than the *in situ*-derived estimate. The temporal difference between the satellite and *in situ*-derived export estimates suggests that predicting seasonal tDOC concentrations and fluxes from remote Arctic deltas to the coastal AO remains a challenge for assessing their impact on already changing carbon fluxes.

3.1 Introduction

In response to climate change, the Arctic is undergoing unprecedented changes in both its watersheds and coastal ocean. Since the 1970s in the Arctic, the surface air temperature has increased by 2.7 °C (Box et al., 2019) resulting into an increase of the sea surface temperature in

summer (Timmermans & Labe, 2021). These changes alter the land-to-sea forcing with important regional and basin-wide implications for sea ice formation, ocean stratification and heat flux, underwater light regime, nutrients delivery, and marine ecosystems (Searcy et al., 1996; Mulligan et al., 2010; Brown et al., 2020; Juhls et al., 2020). Arctic rivers' discharge and permafrost are key components of this coupling. Northern permafrost contains 1,460-1,600 Gt of organic carbon in the form of frozen organic matter, nearly twice as much as carbon than is currently in the atmosphere (Tarnocai et al., 2009; Schuur et al., 2015). Most of this carbon is stored in the Arctic, where permafrost covers 65% of Russian (Tumel, 2002) and 50% of Canadian lands (Vincent et al., 2017). This carbon pool represents about half the world's soil carbon (Hugelius et al., 2014).

Riverine freshwater inputs to the Arctic Ocean (AO) are the largest of any ocean per basin volume (Opsahl et al., 1999). The Arctic hydrological cycle has intensified resulting in a steady increase in the liquid flow of pan-Arctic rivers over the past 30 years (Box et al., 2019). Because of rapid permafrost thaw, the export flux of terrigenous dissolved organic carbon (tDOC) to the coastal AO tends to increase (Fritz et al., 2017) and reaches rates of change as high as 39% in the Mackenzie River system during the 1978-2012 period (Tank et al., 2016). In addition, the land-to-sea flux of terrestrial organic carbon mobilized through coastline erosion has nearly doubled between 1955 and 2018 (Bristol et al., 2021). Once in the coastal AO, a fraction of this riverine and eroded tDOC pool can be degraded and further mineralized into inorganic carbon (Lønborg et al., 2020, and reference therein) that in turn likely unbalances the delicate air-sea gas exchanges on shelves (Manizza et al., 2013; Spencer et al., 2015; Tanski et al., 2016, 2021).

In this context, there is a growing need to quantify land-to-sea fluxes of tDOC and to investigate the coastal ecosystem response at the seasonal scale, where the physical-biogeochemical interactions play a role on AO shelves. Such an effort has been considerably reinforced since the 2000s with the PARTNERS/ArcticGRO (AGRO) pan-Arctic monitoring program (Holmes et al., 2021; Shiklomanov et al., 2021), which provides high-quality *in situ* measurements of tDOC concentrations. Watershed models also improved considerably to become high-value predictive tools (McGuire et al., 2016) but still require improvements in their ability to resolve the complex mechanistic processes behind tDOC mobilization and transformation within Arctic watersheds (Kicklighter et al., 2013; Liao et al., 2019). Field observations thus remain essential to further understand the coastal ecosystem responses.

The remoteness of Arctic rivers imposes that *in situ*-based tDOC fluxes are estimated up to hundreds of kilometers upstream from their main outlets and based on only a few measurements per year (∼4 on average; Holmes et al., 2021). This strongly hampers a robust assessment of the estimated tDOC export from the land-marine transition to the coastal AO waters and, most importantly, precludes any effect of the delta on concentrations (enrichment/removal) (see Kipp et al., 2020). Using radiometric satellite data, Griffin et al. (2018) more than doubled the number of available data during the open water season and highlighted the strong variability of tDOC estimates that can be observed within Arctic rivers systems. Juhls et al. (2020) highlighted the synoptic (∼4 days) variability of tDOC concentrations within the Lena Delta and point out the growing need to assess tDOC concentrations within the land-ocean interface. The high-frequency sampling improved the yearly assessment of tDOC export to Laptev Sea and highlighted the strong seasonality of tDOC quality (Juhls et al., 2020).

In the present study, we investigate the value of merging *in situ* tDOC concentrations with radiometric satellite tDOC estimates retrieved within nearshore waters at the three main outlets of the Mackenzie Delta in the assessment of the seasonal to interannual flux of tDOC to the shelf. The paper is organized as follows. First, we provide an overview of the Mackenzie watershed and delta. Second, we describe the approach used to simulate tDOC concentrations and fluxes within the Mackenzie Shelf. Then, we compare the simulated tDOC concentrations and fluxes with and without the inclusion of satellite tDOC concentration estimates. Finally, we discuss the potential of coastal satellite tDOC data in assessing the seasonal to interannual flux of tDOC to the AO with perspectives for future developments.

3.2 Material & Methods

We estimated daily tDOC concentrations ($tDOC_{est}$) and fluxes from the Mackenzie River to the shelf (Fig. 3.1) using the USGS load estimator (LOADEST) model (Runkel et al., 2004). This modeling approach was successfully applied in Arctic rivers to simulate tDOC fluxes from sparse *in situ* data (Holmes et al., 2012; Tank et al., 2016; Shrestha et al., 2019). The tDOC data nomenclature further used in the paper and the data treatment and procedure to simulate the daily tDOC fluxes and concentrations are given in Fig. 3.2.

3.2.1 Study Area

The Mackenzie Delta is located in the westernmost Canadian Arctic in the southeastern Beaufort Sea (Fig. 3.1). It is the second largest delta in the AO (Burn & Kokelj, 2009), whose waters spread into the most riverine of all pan-Arctic shelves with respect to its size and residence time (Macdonald et al., 1988). The Mackenzie River drains a 1.68 million km^2 wide area and brings, on average, 306 km^3 of fresh water into the AO each year (Mulligan & Perrie, 2019). Permafrost underlies 82% of this massive watershed (Holmes et al., 2013) and the soil organic carbon content of Mackenzie deltaic alluvium is estimated to 34-41 PgC (Tarnocai et al., 2009; Hugelius et al., 2014). Riverine freshwater reaches the coastal ocean through a complex river network made of channels of different sizes of which the main ones end up into three major outlets: Shallow Bay, Beluga Bay and Kugmallit Bay (Morley, 2012). The three coastal bays are shallow but differ by their geology upstream and their ocean geomorphological settings downstream on the shelf. On

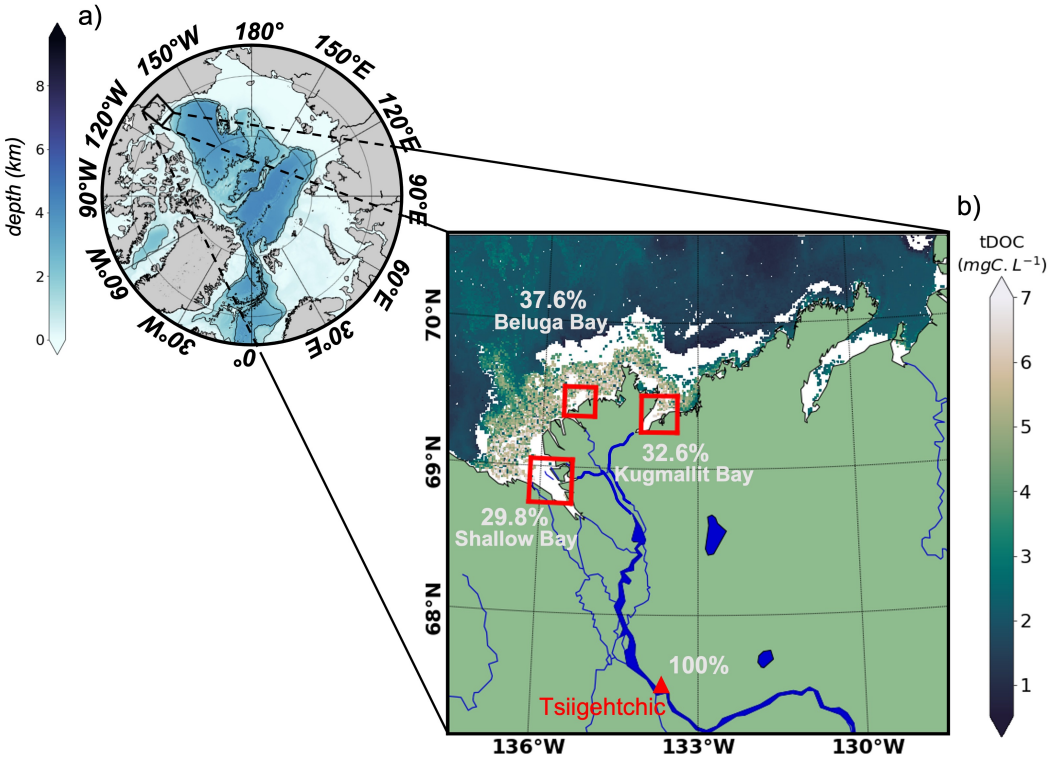

Figure 3.1: Polar stereographic map of (a) the Arctic Ocean bathymetry with the northeastern Beaufort Sea delimited in black and (b) the Mackenzie Delta area with the *in situ* (ArcticGRO/PARTNERS, red triangle) and satellite (red squares) sampling locations overlaid. For each outlet of the Mackenzie Delta, the weights applied to the total river discharge measured at the Tsiigehtchic station are given. An AMODIS satellite scene of tDOC concentration (August 28, 2007) is overlaid.

the West, a flat topography and numerous lakes and channels surround Shallow Bay (Nill et al., 2019). The bay is supplied by three main river channels and its plateau rapidly ends up as a deep canyon. By contrast, Beluga Bay extends far into the coastal ocean. The low-lying grounds of this northernmost part of the delta are mainly inundated tundra composed of sedge and lakes grading into marshes (Harper, 1990; Burn & Kokelj, 2009). The easternmost part of the delta, Kugmallit Bay, which is characterized by rolling hills and termorkarst lakes is highly subject to environmental changes (Nill et al., 2019). The Mackenzie River outflow into the ocean is modulated by the presence of a persistent ice barrier (stamukha; Carmack et al., 2004) close to the shelf, whose break-up results into pulses of freshwater discharge (Doxaran et al., 2015; Matsuoka et al., 2016).

3.2.2 The *In Situ* and Satellite-Derived Data: tDOC Concentration and River Discharge

We used *in situ* tDOC ($tDOC_{in\ situ}$) concentrations and freshwater discharge data (2003–2017) from the water quality datasets provided by the Arctic Great River Observatory (ArcticGRO; Holmes et al., 2021; Shiklomanov et al., 2021). Data encompassed the PARTNERS (2003–2007), ArcticGRO I (2009–2012), II (2012–2016) and III (2017–2020) campaigns. Data were sampled at the Tsiigehtchic station (67.45°N,133.74°W) about 200 km upstream of the Mackenzie Delta

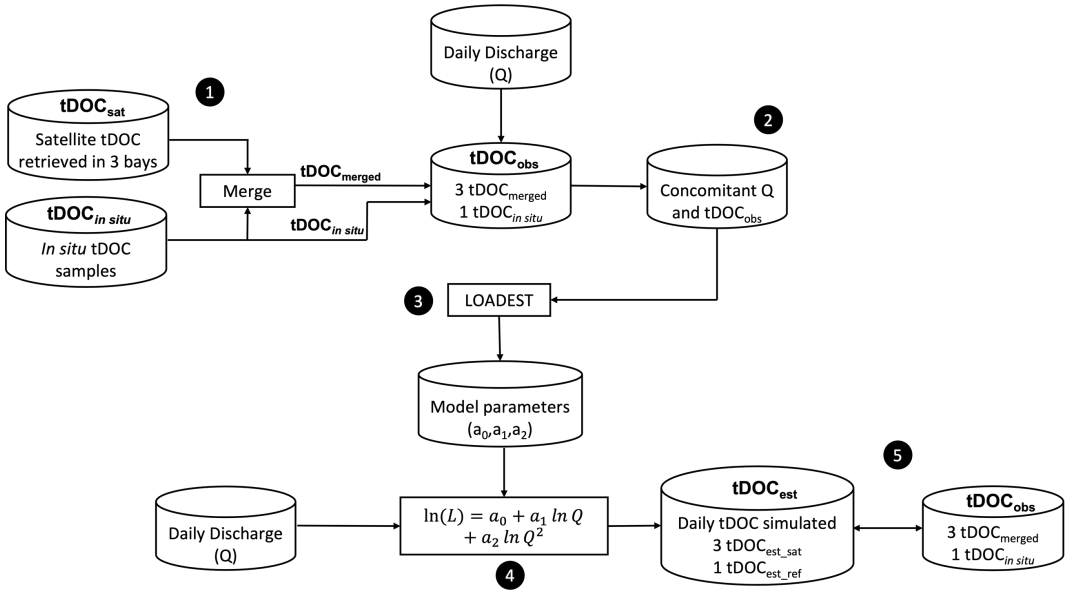

Figure 3.2: Schematic representation of the procedure used to generate the simulated tDOC flux and concentrations with the LOADEST model. Numbers 1 to 5 refer to the main steps fully detailed in the Materials and Methods section.

(Fig. 3.1). River discharge was measured daily over the whole period (2003–2017), whereas the sampling frequency of tDOC concentrations was year-dependent (0 to 7 measurements per year).

Satellite-derived tDOC ($tDOC_{dat}$) concentration estimates were determined for the same time period as *in situ* data (2003–2017) from radiometric spectral reflectance data retrieved with a 1 km horizontal resolution at nadir by the Moderate-Resolution Imaging Spectro-radiometer (MODIS) aboard the Aqua satellite (AMODIS). 1051 scenes constituted the satellite datasets for the entire period (2003–2017). Colored dissolved organic matter (CDOM) absorbance at 443 nm ($a_{CDOM}(\lambda$ =443)) was derived from spectral reflectance data using the semi-analytical algorithm of Manizza et al. (2013). $tDOC_{dat}$ concentrations were estimated by applying satellite-derived $a_{CDOM}(\lambda$=443) data to an empirical relationship between *in situ* tDOC concentration and $a_{CDOM}(\lambda$=443). This relationship ($DOC=10^{2.532}.a_{CDOM}(\lambda=443)^{0.448}$) was established using data across different seasons and areas, allowing its application to the whole AO (Matsuoka et al., 2017). The mean uncertainty of the satellite estimates of DOC concentrations was 28% (Matsuoka et al., 2017). The seasonal contribution to both *in situ* and satellite-derived tDOC data used in this study is given in Fig. 3.3.

3.2.3 Merge the *In Situ*/Satellite tDOC Data

We generated one *in situ*/satellite merged dataset for Shallow Bay, Beluga Bay and Kugmallit Bay. Between May and September (open water season), we substituted the $tDOC_{in\ situ}$ concentrations with the $tDOC_{sat}$ concentrations available. We then merged the satellite data with the $tDOC_{in\ situ}$ concentrations available between October and April to generate a merged tDOC ($tDOC_{merged}$) datasets for each outlet (step 1, Fig. 3.2). For each satellite scene, we subsampled $tDOC_{sat}$ concentrations within a 600 km^2, 306 km^2 and 441 km^2 surface area for Shallow Bay,

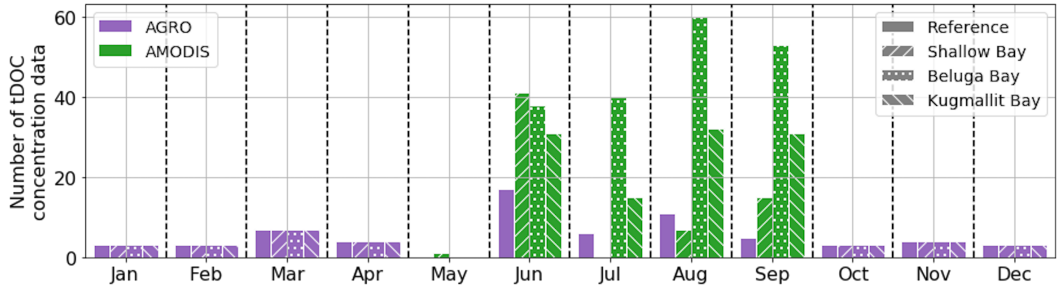

Figure 3.3: Monthly distribution of available *in situ* (AGRO) and satellite (AMODIS) tDOC concentrations over the 2003–2017 period. The solid patterns refer to the "Reference" datasets, whereas the dotted and hatched patterns refer to the "Satellite" datasets.

Beluga Bay and Kugmallit Bay, respectively (Fig. 3.1). We calculated the median of all valid pixels only when 50% had non-missing tDOC_{sat} values to limit biases due to sea ice or cloud cover. To compute the tDOC_{sat} flux, we weighted the freshwater discharge at the three delta outlets based on the channels contributions reported by Morley (2012). We estimated the percentage of the total river discharge measured at the Tsiigehtchic station that was delivered to Shallow Bay, Beluga Bay and Kugmallit Bay to 29.8%, 37.6% and 32.6%, respectively (Morley, 2012; Blackburn et al., 2015) (Fig. 3.1). To account for the water transport between the Tsiigehtchic station located 250 km upstream on the river path and the delta outlets, we applied a +1 day offset on the river discharge data. We estimated this value by multiplying the daily river discharge with the mean distance between the Tsiigehtchic station and the delta outlets (250 km), the mean width of the Mackenzie River at Tsiigehtchic (1 km) and the water level measured by the Water Survey of Canada at Tsiigehtchic station. We obtained 4 tDOC_{obs} datasets: 3 based on tDOC_{merged} data for each delta outlet (hereafter "Satellite") and 1 based on $\text{tDOC}_{in\ situ}$ data only (hereafter "Reference").

3.2.4 The LOADEST Modeling Approach

3.2.4.1 The Model Selection

We constrained the LOADEST model with time coincident observations of tDOC concentration (tDOC_{obs}) and freshwater discharge (Q) data to build up a logarithmic relationship between the tDOC load (equivalent to daily flux) and river discharge based on the following general equation (3.1):

$$\begin{aligned}\ln(L) = a_0 + a_1 \ln(Q) + a_2 \ln(Q^2) + a_3 \sin(2\pi dtime) \\ + a_4 \cos(2\pi dtime) + a_5 dtime + a_6 dtime^2,\end{aligned} \tag{3.1}$$

where L is tDOC load (kg day^{-1}), Q the river discharge ($\text{m}^3\ s^{-1}$), dtime the decimal time (YYYYMMDD) and a_n (n $\in$ [0;6]) the n regression coefficients. The multicollinearity between the explanatory variables ln Q and dtime was handled by a centering procedure as follow:

$$X_{LOADEST} = X - \overline{X} + \frac{\sum(X - \overline{X})^3}{2.\sum(X - \overline{X})^2}, \tag{3.2}$$

where X was either dtime or ln QQ. Based on the Akaike Information Criterion (AIC) (Akaike, 1974), the LOADEST approach allowed to select the best fitting model through nine different combination of the terms included in equation 3.1 (Table A.2).

We chose the model by calculating a first estimate of both ln(L) and $tDOC_{est}$ concentrations based on time coincident ArcticGRO $tDOC_{in\ situ}$ and discharge data through the automated regression model selection set in LOADEST (model 0). According to the AIC, LOADEST selected two different models as best fitting models (models 2 and 7, Table A.2). By referring to the Schwarz Posterior Probability Criterion (SPPC) also computed as an AIC comparative parameter, model 2 (equation 3.3) was identified as the most accurate:

$$\ln(L) = a_0 + a_1 \ln(Q) + a_2 \ln(Q^2). \tag{3.3}$$

Furthermore, model 2 precluded any spurious numerical trend induced by the dtime explanatory variable present in model 7. We thus assumed model 2 (Equation 3.3) as the best regression model to assess daily tDOC fluxes and concentrations entering the Mackenzie shelf.

3.2.4.2 Simulated Daily tDOC Concentration and Flux

We applied model 2 to all $tDOC_{obs}$ datasets to highlight the effect of satellite data on the tDOC flux assessment. For each $tDOC_{obs}$ datasets, we first extracted river discharge data concomitant with available $tDOC_{obs}$ data from the entire daily river discharge datasets (step 2, Fig. 3.2). In LOADEST, these data were then used to constrain model 2 to retrieve the regression coefficients (a_0, a_1 and a_2) of the model (step 3, Fig. 3.2). Finally, we ran model 2 using the regression coefficients thus obtained and forced it with the entire daily river discharge data to simulate the tDOC flux at the daily scale (step 4, Fig. 3.2). From the simulated flux, we calculated back the $tDOC_{est}$ concentrations at daily scale by dividing the daily flux by the river discharge. We thus obtained a "Reference" estimate of tDOC concentration ($tDOC_{est\_ref}$) from model 2 ran with the regression coefficients derived from the $tDOC_{in\ situ}$/Q relationship (see step 3, Fig. 3.2). Similarly, we obtained three "Satellite" estimates of tDOC concentration ($tDOC_{est\_sat}$) derived from each outlet-specific $tDOC_{merged}$/Q relationship (step 3, Fig. 3.2) for Shallow Bay, Beluga Bay and Kugmallit Bay. We give the constants obtained for each regression model in Table A.3.

3.2.5 Comparison of Simulated *Versus* Observed tDOC Concentrations

We used four comparison metrics to compare the tDOC concentrations simulated by model 2 (tDOC$_{est}$) based on the in situ data (hereafter tDOC$_{est_ref}$) and merged *in situ*/satellite data (hereafter tDOC$_{est_sat}$) with the time coincident observed (tDOC$_{obs}$) (step 5, Fig. 3.2). We calculated the correlation coefficient (r), the Nash-Sutcliffe model efficiency index (NSE), the unbiased Root Mean Square Error (URMSE), and the Median Percent Error (MPE) as follows:

$$r = \frac{\sum[(tDOC_{obs} - \overline{tDOC_{obs}}).(tDOC_{est} - \overline{tDOC_{est}})]}{\sqrt{\sum(tDOC_{obs} - \overline{tDOC_{obs}})^2 . \sum(tDOC_{est} - \overline{tDOC_{est}})^2}}, \tag{3.4}$$

$$NSE = 1 - \frac{\sum(tDOC_{obs} - tDOC_{est})^2}{\sum(tDOC_{obs} - \overline{tDOC_{obs}})^2}, \tag{3.5}$$

$$URMSE = \sqrt{\frac{\sum[(tDOC_{est} - tDOC_{obs}) - (\overline{tDOC_{est}} - \overline{tDOC_{obs}})]^2}{n}}, \tag{3.6}$$

$$MPE = Median\left(100. \left|\frac{tDOC_{est} - tDOC_{obs}}{tDOC_{obs}}\right|\right). \tag{3.7}$$

The NSE (unitless) relates the residual variance (i.e. the "noise") between the tDOC$_{est}$ and tDOC$_{obs}$ values to the variance within the tDOC$_{obs}$ values (i.e. the "information") (see Nash & Sutcliffe, 1970). A NSE value of 1 indicates that the noise is null. A NSE value near 0 means the noise is comparable to the observed variance suggesting that the simulated values are as accurate as the observed mean. A negative NSE value suggests that the mean value of observations is a better predictor than the model. The URMSE measures the size of the discrepancies between the simulated and observed values. The MPE is the median of the absolute percentage error and provides insights on the regression model accuracy.

We also calculated the relative error between the "Reference" and "Satellite" daily tDOC flux estimates as follows:

$$\delta\alpha_r = 100\frac{\sum \Phi_{Sat} - \Phi_{Ref}}{\Phi_{Ref}}, \tag{3.8}$$

where Φ_{Sat} and Φ_{Ref} are the "Satellite" and "Reference" daily tDOC flux, respectively.

3.3 Results

3.3.1 Chemodynamic Q-tDOC$_{obs}$ Relationships

The relationships between the tDOC$_{obs}$ concentrations and associated freshwater river discharge suggested the presence of two distinct clusters, which distinguished by the river discharge intensity and the source of available tDOC data (Fig. 3.4). A first cluster corresponded to the sea-ice covered season (October to April) characterized by a low river discharge and tDOC$_{in\ situ}$ concentrations only. A second cluster reflected open water (May to September) conditions with a higher river discharge and mostly tDOC$_{sat}$ concentrations. We used the Spearman correlation coefficient (r) to assess the strength of the relationships between the coincident river discharge Q and the tDOC$_{obs}$ concentrations (i.e. tDOC$_{in\ situ}$ or tDOC$_{merged}$) in the full datasets (January to December) and the same datasets but restricted to the open water season (May to September) (Table 3.1). The tDOC$_{obs}$ concentrations did not follow a Normal distribution (Shapiro test, $p < 0.05$), except for tDOC$_{in\ situ}$ during the open water season (Shapiro test, $p > 0.05$) for which a Pearson correlation coefficient was used. In all datasets, r was positive when accounting for the full ($0.48<r<0.79$) and open water ($0.39<r<0.79$) data. Compared to Q-tDOC$_{in\ situ}$ relationships, the strength of the correlation in the merged datasets varied amongst the delta outlets. The merging of satellite-derived and *in situ* tDOC concentrations increased the Q-tDOC$_{obs}$ correlation in Shallow Bay in both datasets (r=0.79) compared to Q-tDOC$_{in\ situ}$ ($0.59<r<0.68$). In Kugmallit Bay, r was similar in the full dataset (r=0.58 *versus* r=0.59) but decreased in the open water season (r=0.43 *versus* r=0.68). In Beluga Bay, r decreased in both the full (r=0.48 *versus* r=0.59) and open water (r=i0.43 *versus* r=0.68) datasets. This suggests that the strength of the Q-tDOC$_{merged}$ relationship

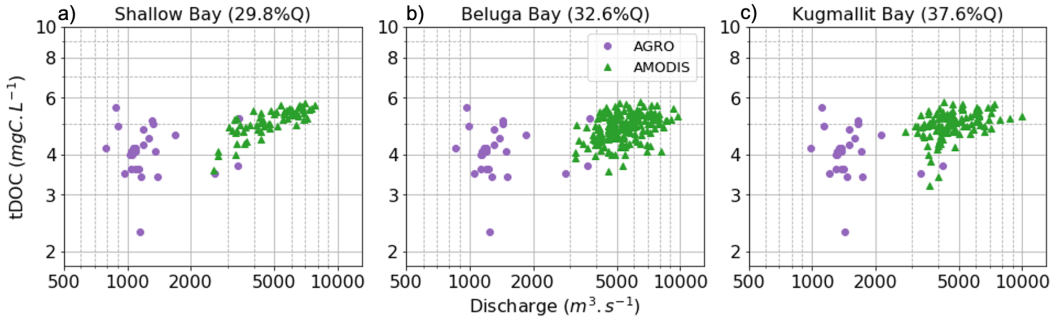

Figure 3.4: Q-tDOC relationships for the merged *in situ*-satellite datasets (tDOC$_{merged}$) on (a) Shallow Bay, (b) Beluga Bay and (c) Kugmallit Bay. Green triangles indicate the satellite tDOC concentration estimates (AMODIS). Purple dots indicate the *in situ* tDOC measurements (AGRO). Note the logarithmic scales on both axes

was sensitive to the $tDOC_{sat}$ concentration retrieved nearby each outlet of the delta, with Beluga Bay differing markedly from the other two bays.

Table 3.1: Correlation coefficients between the river discharge and the $tDOC_{in\ situ}$ ("Reference" dataset) or $tDOC_{merged}$ ("Satellite" datasets) concentrations for all data and the open water season data (May-September). Bold values indicate a Person correlation coefficient; the Spearman correlation coefficient is used otherwise (*** p-value < 0.001).

Dataset	All data	Open water data
Reference	0.59***	**0.68***
Satellite – Shallow Bay	0.79***	0.79***
Satellite – Beluga Bay	0.48***	0.39***
Satellite – Kugmallit Bay	0.58***	0.43***

3.3.2 Simulated tDOC Concentrations: Merged vs. *In Situ* Datasets

We used quantitative metrics to compare the simulated $tDOC_{est\_ref}$ and $tDOC_{est\_sat}$ concentrations with the observed $tDOC_{in\ situ}$ and $tDOC_{merged}$ concentrations, respectively (Table 3.2). The number of $tDOC_{obs}$ data increased with the inclusion of the remotely sensed $tDOC_{sat}$ estimates. In Shallow Bay, the increase reached 38% while it was 2-fold and 3-fold in Kugmallit and Beluga Bay, respectively. The data dispersion (URMSE) between $tDOC_{in\ situ}$ and $tDOC_{est\_ref}$ concentrations was 0.82 mgC L^{-1}. When using $tDOC_{est\_sat}$ estimates, URMSE decreased by 39% to 45%. The median percent error (MPE) between the $tDOC_{in\ situ}$ and the $tDOC_{est\_ref}$ concentrations was 12.7%. The MPE decreased by 2-fold (Kugmallit and Beluga bays) to 3-fold (Shallow Bay) with the $tDOC_{est\_sat}$ estimates. The correlation coefficient (r) varied little among the Reference and Satellite datasets and was relatively high (0.52–0.76), which suggested a high goodness-of-fit. With respect to the "Reference" estimates (r=0.66), r increased in Shallow Bay but decreased in Beluga Bay. The Nash-Sutcliffe model efficiency index (NSE) showed a pattern similar to that depicted by r. The NSE between the $tDOC_{in\ situ}$ and $tDOC_{est\_ref}$ concentrations was 0.44 suggesting that the regression model was a fairly good predictor of the observed concentrations. Using $tDOC_{est\_sat}$, the NSE remained positive increasing in Shallow Bay (NSE=0.58) but decreasing in Beluga Bay (NSE=0.27). Overall, $tDOC_{est\_sat}$ estimates simulated in Beluga Bay departed the most from the observed $tDOC_{merged}$ concentrations (Table 3.2). These results mirrored with the lowest Q-$tDOC_{merged}$ correlation coefficients estimated in Beluga Bay (Table 3.1).

3.3.3 Sensitivity Analysis on the Remotely-Sensed Data Subsampling

We tested the hypothesis that the predictive ability of the regression model applied to Beluga Bay was sensitive to the AMODIS data subsampling conditions. We then calculated the median of tDOC$_{sat}$ concentration estimates for each of the three new conditions: 40% of valid pixels (C40), 60% of valid pixels (C60), and a 2-fold subsampling surface area along with 50% of valid pixels (2C50). From these conditions, we simulated three new tDOC$_{est_sat}$ concentration estimates based on the three new tDOC$_{merged}$ datasets obtained according to the same method described in section 2.1.2. For each subsampling condition, we used the metrics to compare with the subsampling condition of 50% of valid pixel (C50) we previously applied (Table 3.3). Between the C50 and C60 conditions, the data quantity dropped by 45%. The correlation coefficient, the NSE and the URMSE were similar, whereas the MPE was slightly improved. Between the C50 and C40 conditions, the data quantity increased by 39% and all metrics showed limited variations. Overall, the amplitude of change of the comparison metrics between C40, C50 and C60 (Table 3.3) was much lower than between the "Reference" and "Satellite" estimates (Table 3.2 and 3.3). By contrast, a doubling of the sampled surface area (2C50, +18% of tDOC$_{sat}$ data) led to a decrease of r and the NSE compared to C40, C50, C60 and "Reference" estimate. However, no marked changes in the URMSE and MPE were observed. Increasing the number of tDOC$_{sat}$ data by widening the subsampled area decreased the strength of the correlation and increased the noise between the simulated tDOC$_{est_sat}$ and the observed tDOC$_{merged}$ concentrations. Overall, the simulated tDOC$_{est_sat}$ concentrations obtained in 2C50 departed the most from the simulated tDOC$_{est_ref}$ estimates (Table 3.2 and 3.3).

Table 3.2: Comparison metrics between the simulated tDOC$_{est_ref}$ and tDOC$_{in\ situ}$ concentrations ("Reference") and between the simulated tDOC$_{est_sat}$ and the tDOC$_{merged}$ concentrations ("Satellite").

Metrics	Reference	Satellite		
		Shallow Bay	Beluga Bay	kugmallit Bay
n	66	91	218	136
r	0.66	0.76	0.52	0.60
NSE	0.44	0.58	0.27	0.35
URMSE	0.82	0.46	0.45	0.50
MPE	12.74	4.37	5.68	6.01

n: Number of data available; r: correlation coefficient; NSE: Nash-Sutcliffe efficient index; URMSE: Unbiased Root Mean Square Error (mgC.L^{-1}); MPE: Median Percent Error

Table 3.3: Comparison metrics between the simulated $tDOC_{est\_sat}$ and the $tDOC_{merged}$ concentrations ("Satellite"). in Beluga Bay according to the C50 (50% valid pixels), C40 (40% valid pixels), C60 (60% valid pixels) and 2C50 (2-fold larger surface area + 50% valid pixels) subsampling conditions.

Metrics	C50	C40	C60	2C50
n	218	303	120	258
r	0.52	0.50	0.50	0.42
NSE	0.27	0.25	0.25	0.18
URMSE	0.45	0.47	0.47	0.45
MPE	5.68	5.83	5.01	5.66

n: Number of data available; r: correlation coefficient; NSE: Nash-Sutcliffe efficient index; URMSE: Unbiased Root Mean Square Error ($mgC.L^{-1}$); MPE: Median Percent Error

3.3.4 Annual and Seasonal Patterns of the Simulated tDOC Flux

Over 2003–2017, we simulated the yearly flux of tDOC based on the simulated $tDOC_{est\_ref}$ and the $tDOC_{est\_sat}$ concentrations obtained for the three delta outlets. We estimated the total "Satellite" flux by summing the flux simulated at each outlet. The total yearly flux was 1.47 ±0.18 (min 1.15-max 1.75) and 1.44 ±0.14 (min 1.17-max 1.66) TgC yr^{-1} for the "Reference" and "Satellite" datasets, respectively. Both flux estimates showed comparable interannual patterns. The relative error between the "Satellite" and the "Reference" estimates did not exceed 5% (Fig. 3.5). The yearly flux increased between 2004 and 2009 (1.17 to 1.66 TgC yr^{-1}) and tended to decrease between 2010 and 2017. However, the yearly flux did not show any significant interannual trend over the 15 years ($r = -0.3$, $p > 0.05$). Although we reported no substantial differences between the simulated "Reference" and "Satellite" $tDOC_{est}$ flux estimates at the annual scale, both departed at the seasonal scale (Fig. 3.6). During the seasonal peak of river discharge in May, the "Satellite" flux estimate was lower than the "Reference" flux estimate by 15% (Shallow Bay) to 20% (Beluga Bay) on average. Such a difference in the tDOC flux estimates coincides with unevenly distributed tDOC concentrations amongst the datasets in June (Fig. 3.7). By contrast, between mid-July and November the "Satellite" flux estimate was on average higher than the "Reference" flux estimate. In November, the mean difference reached 12% and 17% in Shallow Bay and Kugmallit Bay, respectively. At the interannual scale, the relative error on the total simulated tDOC flux reported at the spring river freshet exhibited a high variability (Fig. 3.8). From 2011 to 2017, the "Satellite" flux estimate was generally more than 30% lower than the "Reference" flux estimate. The highest interannual difference was reached in 2005, when the "Satellite" flux estimate was ∼60% lower than the "Reference" flux estimate.

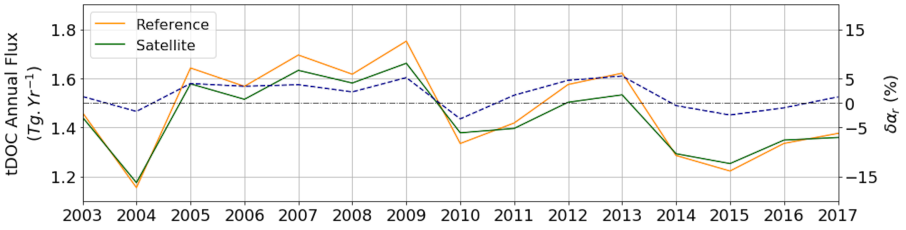

Figure 3.5: Simulated annual tDOC flux (TgC yr^{-1}) estimated from the "Reference" dataset (orange line) and the "Satellite" dataset (green line). The dashed blue line represents the error of the "Satellite" estimate relative to the "Reference" estimate ($\delta\alpha_r$, %).

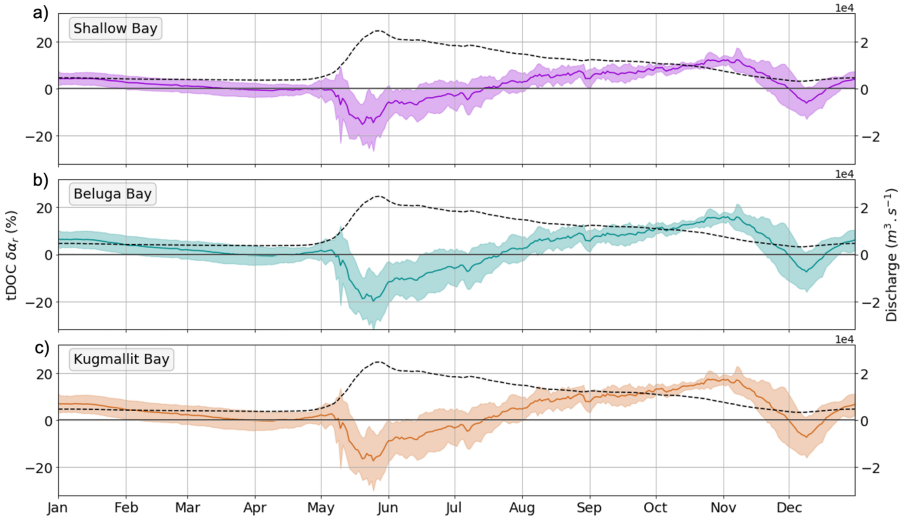

Figure 3.6: Error of the simulated daily tDOC flux estimated from the "Satellite" dataset relative to the "Reference" estimate ($\delta\alpha_r$, %) averaged over the 2003-2017 period for (a) Shallow Bay, (b) Beluga Bay and (c) Kugmallit Bay. The shaded area represents the mean $\pm$ SD. The black dashed line corresponds to the daily freshwater river discharge averaged over the 2003–2017 period.

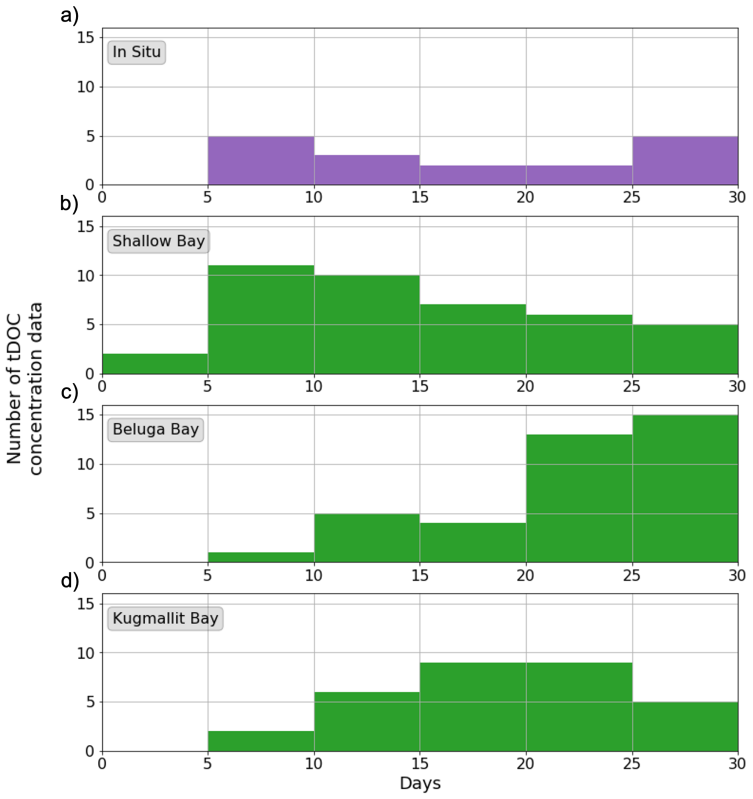

Figure 3.7: Temporal distribution in June (2003-2017) of the (a) tDOC$_{in\ situ}$ concentrations, and (b) tDOC$_{sat}$ concentrations for Shallow Bay, (c) Beluga Bay and (d) Kugmallit Bay.

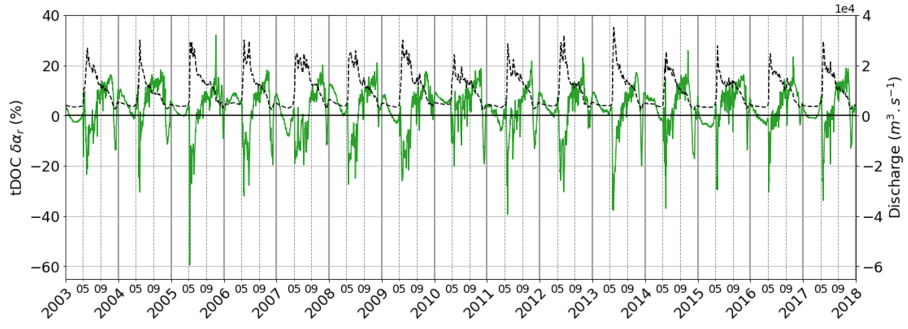

Figure 3.8: Error of the simulated daily tDOC flux estimated from the "Satellite" dataset relative to the "Reference" estimate ($\delta\alpha_r$, %) (green line) and daily freshwater river discharge (black dashed line).

3.4 Discussion

3.4.1 A Complex Land-To-Sea Interface

The presence of a chemodynamic Q-tDOC relationship, i.e. the higher the river discharge the higher the tDOC concentration, reported upstream in the Mackenzie River path is widely accepted (Raymond et al., 2007; Holmes et al., 2012; Shrestha et al., 2019). In the Peel River catchment, Shrestha et al. (2019) suggested a significant Q-tDOC correlation (r=0.52), which is in the range of the values we report in this study (0.48<r<0.79). This result suggests that the positive Q-tDOC chemodynamic relationship estimated more than 200 km upstream from the delta also applies to the fluvial-marine interface farther downstream. Our results show that the chemodynamic Q-tDOC$_{merged}$ relationship varies amongst the three delta outlets and is the weakest in Beluga Bay (r=0.48). Such a decrease in the Q-tDOC$_{merged}$ relationship for Beluga Bay suggests a less conservative behavior of the tDOC concentrations. After the spring freshet, the river water is stored in deltaic lakes and floods the vegetated floodplain (Normandin et al., 2018), which can modify its chemistry before draining to the delta channels and ultimately to the Mackenzie Shelf (Emmerton et al., 2008a). Processes like autotrophic production and leaching can enhance tDOC levels in river water over a wide range of variability (15 to 350%) as tDOC is transported through the delta (Emmerton et al., 2008a; Kipp et al., 2020). In the upper part of the delta, tDOC removal through the flocculation process (up to 45%; Kipp et al., 2020) can occur at low salinities in the more estuarine waters and can outbalance the delta enrichment effect. All these processes likely play a role in explaining the distinct Q-tDOC$_{merged}$ relationship we observe for Beluga Bay. In this part of the delta, the alluvial plain is low-lying (< 2 m) and intersected by an important network of lakes and channels. In spring, the delta is flooded with freshwater during the freshet (Mackay, 1974). In summer and fall, it is very exposed to the ocean influence and occasionally flooded when strong North-Northwestern winds trigger storm surges and marine intrusions into the delta (Mackay, 1974; Marsh & Schmidt, 1993; Manson & Solomon, 2007). Storm surges can be severe and flood the delta with saline waters over tens of kilometers inland from the coast leading to substantial changes in vegetation (Pisaric et al., 2011; Kokelj et al., 2012; Lantz et al., 2015). High surface area flooding in Beluga Bay compared to the east and west of the upper delta area (Kuenzer et al., 2015) may lead to differences in the mobilization and biogeochemistry of tDOC at the fluvial-marine transition. As satellite tDOC estimates retrieved at the fluvial-marine transition reflect the delta effect in terms of tDOC enrichment and removal, our results inform on how much

tDOC can potentially leave the delta to reach the coastal ocean.

The weaker Q-tDOC$_{merged}$ relationship reported in Beluga Bay (r=0.48), and to a lesser extent in Kugmallit Bay (r=0.58), likely explains the difference in the model performance between the three delta outlets. Overall, the use of tDOC$_{sat}$ data in the model improves the match between the simulated (tDOC$_{est_sat}$) and observed (tDOC$_{obs}$) concentrations. This is particularly true for Shallow Bay for which the Q-tDOC$_{merged}$ relationship is the strongest (r=0.79) even compared to the Q-tDOC$_{in\ situ}$ relationship (r=0.59). There is growing evidence that tDOC concentrations and quality vary in the course of the main channels of the Mackenzie Delta (Emmerton et al., 2008b; Griffin et al., 2018; Kipp et al., 2020; Schwab et al., 2020). The use of satellite tDOC retrieved in nearshore waters in the very close vicinity of the delta outlets allows for the effect of regional biogeochemical signatures to be considered in the estimated land-to-sea fluxes of tDOC. The satellite tDOC concentrations are most likely due to bio- and photo-degradation processes (Gonçalves-Araujo et al., 2015; Matsuoka et al., 2015) that occur upstream along the river path and that watersheds model are not yet able to represent (Rawlins et al., 2021). Our approach implicitly accounts for these processes without explicitly describing them as their weight on the downstream fate of tDOC is not yet well understood. Nevertheless, caution should be addressed to local non-deltaic sources of tDOC to the ocean. Offshore the delta, strong winds erode the shoreline permafrost of the Beluga Bay Islands, which may deliver extra carbon to the coastal waters (Lim et al., 2020). These inputs, however, may be limited compared to those originating from the delta (Tanski et al., 2016). Assuming a shoreline of 2077 km for our study area (Harper, 1990) and a tDOC flux of 1.37 kgC m^{-1} yr^{-1} (Bristol et al., 2021), coastal erosion would translate into a tDOC flux of $\sim$3.10–6 TgC yr^{-1} into the shelf. This flux is several order of magnitude lower than the riverine flux estimated between 1.04–1.76 TgC yr^{-1} (Macdonald et al., 1988; Dittmar & Kattner, 2003; Raymond et al., 2007; Holmes et al., 2013; Le Fouest et al., 2013).

3.4.2 The Seasonal Shift of tDOC Flux

The mean annual flux of tDOC we estimated using satellite-derived tDOC data (tDOC$_{est_sat}$= 1.44 $\pm$0.14 TgC) fits within the reported range, which was estimated from different methodologies using punctual field measurements, climatologies and/or regression model (1.04–1.76; Macdonald et al., 1988; Dittmar & Kattner, 2003; Raymond et al., 2007; Holmes et al., 2013; Le Fouest et al., 2013). The use of satellite data has no marked impact on the interannual variability but on

the seasonality of the simulated tDOC concentrations and fluxes. From May to June, when the river freshet occurs, the $tDOC_{est\_sat}$ export flux represents up to ∼40% of the total annual flux. Compared to the simulated tDOC export flux estimated from *in situ* data only, we report a decrease in the $tDOC_{est\_sat}$ flux in May at the onset of the seasonal peak of river discharge. According to the delta outlet, this decrease reaches 15% to 20%, on average, but can reach up to 60%. This decrease occurs between winter and the beginning of the open water season, when the data quantity and temporal distribution of $tDOC_{in\ situ}$ and $tDOC_{sat}$ start to differ (April-June, Fig. 3.3). In June, the $tDOC_{sat}$ data quantity is higher (31<n<41) than in the $tDOC_{in\ situ}$ dataset (n=17). While the medians of the tDOC concentration compare among the datasets ($tDOC_{in\ situ}$=5.3 $mgC.L^{-1}$, 5.0<$tDOC_{merged}$<5.4 $mgC.L^{-1}$), the amplitude of variation is lower in the $tDOC_{merged}$ dataset (4.1–5.8 $mgC.L^{-1}$) than in the $tDOC_{in\ situ}$ dataset (4.2–8.1 $mgC.L^{-1}$). The $tDOC_{in\ situ}$ data quantity is mostly evenly distributed throughout June, whereas it increases in Beluga Bay, and to a lesser extent in Kugmallit Bay, to reach a maximum at the end of June (Fig. 3.7). Such differences between the $tDOC_{in\ situ}$ and $tDOC_{sat}$ datasets likely constrain the constants obtained for each regression model (Fig. A.1), which in turn translate into different tDOC flux estimates in this period of the year when the freshet occurs (Fig. 3.6 and 3.7). Ocean color data are usually not available in May due to the presence of landfast ice in the Mackenzie Delta. Some data could be available between the landfast and pack ice but could be unreliable due to the high snow/ice albedo. New space sensors such as Sentinel-2/MSI or Landsat-8/OLI could help overcome this drawback by significantly improving the spatial resolution of imagery (∼30 m). Nevertheless, caution should be addressed to the pixel contamination due to the adjacency effect or sub-pixel-contamination, especially for landfast ice problematics. For now, uncertainties related to the lack of data during the freshet period hamper the model capacity to simulate the land-to-sea flux of tDOC in this critical period of the year.

The temporal shift in the seasonal distribution of the land-to-sea flux of tDOC induced by the use of satellite tDOC data, i.e. a decrease in May-June and an increase in July-November, may have implications on both the physical and biogeochemical settings of the coastal Beaufort Sea. In the Mackenzie Delta, tDOC has a high potential for biological degradation at the spring freshet (Gareis & Lesack, 2020; Behnke et al., 2021). A decrease of the riverine flux in May-June would imply that a lesser fraction of bioavailable tDOC would be delivered and potentially processed by heterotrophic bacteria within the marine ecosystem (Colatriano et al., 2018; Vaqué et al., 2019). In turn, as most of the tDOC is colored (∼94% Matsuoka et al., 2017) and then absorbs light,

phytoplankton might leverage more favorable light conditions in this period because less tDOC would be delivered by the Mackenzie Delta to the coastal waters. Whether such a decrease of the tDOC flux at the spring freshet will have a substantial impact on the heterotrophic-autotrophic balance remains to be determined. In contrast, tDOC is rather refractory in summer, because the biological removal is enhanced and the enrichment limited along the river path (Holmes et al., 2008). A steady increase of the tDOC flux between July and November as we report in our study could then translate into a greater proportion of tDOC that escapes remineralization and accumulates in the oceanic waters. Because the interannual variability of this seasonal shift is high, such biogeochemical responses might be exacerbated in the future. This is particularly true in a context of Arctic warming, which is expected to alter both the river discharge seasonality and the quality of the tDOC exported (see Behnke et al., 2021).

3.4.3 Future Developments

Using satellite tDOC data, we increased the size of the dataset available during the ice-free period by more than 39%, which is comparable to the study of Griffin et al. (2018) focused on inland waters within the Mackenzie River. The chemodynamic relationships and metrics we estimated for Beluga Bay suggest that the median of the satellite-derived tDOC concentration was sensitive to the subsampling procedure of the remote sensing scenes. The sensitivity analysis suggests that the model is not highly sensitive to the number of valid pixels in satellite scenes but rather to the size of the subsampled surface area. As a larger subsampled area may reflect more contrasted environmental conditions, it may alter the value of the tDOC concentration median. Compared to the other two delta outlets, the differences between the simulated and observed tDOC concentrations reported for Beluga Bay could then indicate a different tDOC dynamics within the land-to-sea interface. For all bays, the robustness of the model to the number of data within a subsampled area allows for some flexibility in the methodology, because it may offset potential issues related to cloud and/or sea ice cover. In addition, we will leverage newer space sensors such as Sentinel-2/MSI or Landsat-8/OLI to improve the spatial and temporal resolution (i.e. high-resolution ocean color data are available every 3–5 days when all available sensors are used) of radiometric records in nearshore Arctic environments. If the pixel contamination due to sea ice could be overcome, such remotely sensed data would provide tDOC concentrations estimates at the immediate vicinity of the streams' mouth, hence limiting the effect of tDOC degradation/enrichment occurring upstream on the delta estimate. With respect to river discharge, we used daily time-series measured $\sim$100 km upstream the delta to constrain the regression model within the upper part of

the delta at the land-ocean transition. The forthcoming Surface Water and Ocean Topography (SWOT) space mission that aims to measure river water surface elevation, top width, and free-surface slope might allow periodic estimation of freshwater discharge for Arctic rivers wider than 50 m (Biancamaria et al., 2016; Durand et al., 2016). As tDOC concentrations are also related to the watershed slope (Connolly et al., 2020), these new promising data combined with satellite tDOC retrievals in nearshore waters might help refine the land-to-sea flux of tDOC in the upper Mackenzie Delta.

Since the past 17 years, the ArcticGRO/PARTNERS program led to a large and very highly valuable dataset of water quality for the Mackenzie River. The sampling frequency is on a monthly basis spanning from January to December with a mean sampling frequency of about 4 days each year. In the Arctic, the retrieval of tDOC from space is limited to the open water season (mostly from June to September). *In situ* measurements of freshwater discharge and tDOC concentrations at the sea ice break-up and spring freshet are hence essential to constrain a regression model as we used in our study and to generate a realistic seasonal cycle of tDOC concentration and flux. In a context of Arctic warming, it is important to maintain and eventually extend such a water quality monitoring to gain robustness in model predictions. Besides, new datasets such as for the Mackenzie river temperature (Tokuda et al., 2019) could further be used to improve the regression models and then to better predict the seasonal to interannual tDOC dynamics (see Shrestha et al., 2019) in response to climate change.

3.5 Conclusion

This study investigated the value of merging riverine *in situ* tDOC concentrations with satellite ocean-color estimates retrieved at the three main outlets of the second largest Arctic Delta to assess the seasonal to interannual flux of tDOC to the coastal AO. By using satellite observations, we show that we can substantially increase the quantity of data available during the open water season to constrain predictive regression models. We also identified a spatial variability in the tDOC concentrations and flux amongst the three main delta outlets likely reflecting distinct biogeochemical patterns within the land-to-sea interface. The robustness of the approach suggests it could be applied to other Arctic deltas/estuaries to assess the pan-Arctic flux of tDOC if reliable remotely sensed tDOC data are available in such complex land-to-sea interfaces (see Juhls et al., 2020)). However, our results also highlight that such predictive models would require more

in situ and satellite-derived tDOC data especially in fall-winter and at the sea ice breakup to improve their ability to resolve the strong seasonal variability that prevails in such critical and remote environments. There is evidence now that the Arctic permafrost thaw alters both quantitatively and qualitatively the coastal waters biogeochemistry. It then motivates the need to quantify the land-to-sea fluxes of terrestrial organic matter at high spatial and temporal resolution to further investigate the coastal ecosystem response at the synoptic and seasonal time scales at which operates the physical-biogeochemical coupling in the ocean. In addition, the fraction of terrestrial organic matter outgassed into CO_2 through marine physicochemical and microbial processes remains very uncertain although it might unbalance the delicate air-sea gas exchanges. Assessing in a robust way the terrestrial fluxes of organic matter to the coastal ocean is thus paramount to better understand and predict how changes in the land-sea linkages might alter the coastal carbon budget and air-sea CO_2 fluxes at regional scale in the AO.

CHAPTER

4

BIOGEOCHEMICAL RIVER RUNOFF DRIVES INTENSE COASTAL ARCTIC OCEAN CO_2 OUTGASSING

Abstract

Arctic warming alters land-to-sea fluxes of nutrients and organic matter, which impact air-sea carbon exchange. Here we use an ocean-biogeochemical model of the southeastern Beaufort Sea (SBS) to investigate the role of Mackenzie River biogeochemical discharge in modulating air-sea CO_2 fluxes during 2000–2019. The contribution of 6 biogeochemical discharge constituents leads to a net CO_2 outgassing of 0.13 TgC yr^{-1}, with a decrease in the coastal SBS carbon sink of 0.23 TgC yr^{-1} and 0.4 TgC yr^{-1} due to riverine dissolved organic and inorganic carbon, respectively. Years with high (low) discharge promote more CO_2 outgassing (uptake) from the river plume. These results demonstrate that the Mackenzie River modulates the capacity of the SBS to act as a sink or source of atmospheric CO_2. Our work suggests that accurate model representation of land-to-sea biogeochemical coupling can be critical for assessing present-day Arctic coastal ocean response to the rapidly changing environment.

Plain Language Summary

We modeled the discharge of freshwater and 6 biogeochemical constituents from the Mackenzie River into the southeastern Beaufort Sea (SBS) to study their impact on ocean-atmosphere carbon dioxide (CO_2) fluxes during 2000–2019. We find that biogeochemical constituents from river runoff promote CO_2 outgassing to the atmosphere in the river plume region. Dissolved inorganic carbon is the main contributor to this phenomenon, with river discharge events driving pulses of intense CO_2 outgassing during ice-free periods. Our results show that the capacity of the SBS to act as an atmospheric CO_2 sink or source is strongly related to interannual variability in biogeochemical river discharge. Our results highlight the increased coupling of Arctic land-ocean biogeochemical systems under rapid environmental changes.

4.1 Introduction

The Arctic Ocean (AO) is estimated to be a carbon sink of roughly 118 to 180 TgC yr^{-1} (Arrigo et al., 2010; Yasunaka et al., 2018; Manizza et al., 2019). Its net contribution to global CO_2 uptake is massive relative to its surface area (Bates & Mathis, 2009). However, whether the coastal periphery, which occupies approximately 50% of the AO (e.g., Carmack et al., 2006), acts

as a net atmospheric CO_2 source or sink, remains poorly understood (Forest et al., 2014; Roobaert et al., 2019). For example, warming-induced changes in land-to-sea fluxes of freshwater associated with biogeochemical variables (Tank et al., 2012, 2016; Mann et al., 2022) can drive CO_2 outgassing rather than CO_2 uptake (Roobaert et al., 2019; Lacroix et al., 2021). An improved understanding of the effect of freshwater-biogeochemical discharge from Arctic rivers is therefore critical for accurately estimating AO air-sea CO_2 exchange.

Arctic rivers transport 11% of global freshwater to the world's ocean (McClelland et al., 2012) and contribute half of the net freshwater input to the AO (Brown et al., 2020). Additionally, these rivers transport significant amounts of inorganic nutrients and organic matter into the coastal zone (Dittmar & Kattner, 2003; Holmes et al., 2012; Le Fouest et al., 2013; Juhls et al., 2020; Rawlins et al., 2021), with part of the organic matter signal originating from thawing of northern permafrost and peatlands (Hugelius et al., 2014; Schuur et al., 2015). While riverine inorganic nutrients promote phytoplankton growth and enhance nearshore CO_2 uptake, fluxes of terrestrial organic matter and in particular dissolved organic carbon (tDOC), support favorable conditions for CO_2 production (Kirchman et al., 2009). Once in coastal waters, tDOC is reprocessed by mechanisms such as flocculation (Kipp et al., 2020), photodegradation (Belanger et al., 2006; Aarnos et al., 2018), or bacterial degradation (Ortega-Retuerta et al., 2012; Colatriano et al., 2018; Bruhn et al., 2021). The latter two mechanisms produce dissolved inorganic carbon (DIC) that increases the partial pressure of CO_2 (pCO_2), which in turn can promote CO_2 outgassing if seawater pCO_2 exceeds atmospheric pCO_2.

Since the 1970s, the Arctic has warmed three time faster than anywhere else on Earth (AMAP, 2021), inducing large changes in its hydrological cycle (Box et al., 2019; Brown et al., 2020; Saito et al., 2021). This warming has dramatically altered Arctic watersheds and rivers, which play an important role in shaping the physical and biogeochemical setting of the coastal AO. Along with a 0.22% yr^{-1} intensification of river discharge since 1984 (Feng et al., 2021), accelerated permafrost thaw (Slater & Lawrence, 2013; McGuire et al., 2016; Chadburn et al., 2017; Langer et al., 2022) 1) changes the quantity and the quality (i.e., sources, compositions, and bioavailability) of tDOC exported to the AO (Mann et al., 2022; Matsuoka et al., 2022) and 2) increases connectivity between watersheds and marine ecosystems. Recent work shows that permafrost-driven carbon in the Mackenzie River mouth was observed even in early spring/summer, typically when only modern (i.e., young) organic matter has been observed (Schwab et al., 2020), highlighting the ongoing,

rapid Arctic warming. In addition to tDOC, pan-Arctic rivers also act as large conveyor belts of terrestrial dissolved inorganic carbon (tDIC) to the ocean (Tank et al., 2012). While DIC upwelled from depth is known to trigger outgassing in coastal regions (Mol et al., 2018), quantification of tDIC release and associated CO_2 outgassing driven by Arctic river plumes has received far less attention and remains highly uncertain.

The sparse observational record in Arctic coastal waters has led to large uncertainty estimates of coastal CO_2 flux (Yasunaka et al., 2018; Landschützer et al., 2020). Although the impact of riverine input to the Arctic Ocean has already been considered in a few modeling studies (Manizza et al., 2019; Terhaar et al., 2019, 2021b; Mathis et al., 2022), these previous studies either lack nearshore data constraints or do not include realistic representation of dissolved carbon river runoff. Additionally, the strong differences between individual Arctic river systems (Brown et al., 2020) motivates the need to investigate regional land-to-sea coupling in order to infer its effects at the AO scale. In the context of rapid watershed modification, it is also timely to gain understanding on the ecosystem response to seasonal-to-interannual variability in riverine discharge (Brown et al., 2020; Gelfan et al., 2017).

Here we use a regional ocean-ice-biogeochemistry model (ECCO-Darwin) to understand how freshwater and matter transported by Arctic rivers modulate air-sea CO_2 fluxes in the coastal AO. We focus on the southeastern Beaufort Sea (SBS), where outflow from the Mackenzie River makes this region, with the Siberian shelf (McClelland et al., 2012), one of the most riverine-influenced of all pan-Arctic shelves with respect to its size and river runoff (Macdonald et al., 1989; Carmack et al., 2004). The remainder of the paper is organized as follows. First, we describe the regional model set-up and simulation of the SBS carbon cycle. Second, we quantify the contribution of Mackenzie constituents to coastal air-sea CO_2 flux. Third, we characterize intense outgassing events that develop under specific discharge conditions and quantify the interannual variability in coastal air-sea CO_2 fluxes driven by land-to-sea export. Finally, we conclude by highlighting the critical processes that drive AO land-to-sea coupling of carbon and make recommendations for future modeling efforts.

4.2 Methods

The SBS model is a regional set-up adapted from the global-ocean ECCO-Darwin biogeochemistry state estimate described in Carroll et al. (2020, 2022). ECCO-Darwin assimilates both physical (Wunsch et al., 2009) and biogeochemical (Menemenlis, Fukumori, & Lee, 2005) observations and is used for generating initial, open, and surface boundary conditions. The general set-up of the regional model (hereafter referred to as ED-SBS) is detailed in Text A1. In the following section, we provide the specific details required for the regional Arctic set-up.

The biogeochemical component of the model explicitly simulates cycling of carbon, nitrogen, phosphorus, silica, iron, and oxygen as they transition between inorganic, living, and dead organic pools; the model also simulates the carbonate cycle. In addition, the ED-SBS has four key plankton functional types (PFTs) characteristic of the western AO: diatoms, large eukaryotes, and small and large zooplankton. To represent the observed phytoplankton biomass that is maintained under sea ice in winter, no mortality or grazing occur when phytoplankton biomass is below 0.05 mmolC m^{-3} (Randelhoff et al., 2020; Hoppe, 2022).

ED-SBS also includes terrestrial inputs from the Mackenzie River. We prescribed daily freshwater discharge, river temperature, and six biogeochemical components (Table A.4 and Text A2) at the three major outlets of the Mackenzie Delta: Shallow Bay, Beluga Bay, and Kugmallit Bay (Fig. A.2). Freshwater and biogeochemical river fluxes were distributed over a group of grid cells located within Shallow Bay (29.8%), Beluga Bay (37.6%), and Kugmallit Bay (32.6%) (Bertin et al., 2022). Freshwater discharge and river temperature were forced by daily gauge measurements of the Water Survey of Canada (WSC) from the Arctic Great River Observatory (Fig. A.3; Shiklomanov et al., 2021) and by the Tokuda et al. (2019) dataset, respectively. Riverine biogeochemical components include tDOC, terrestrial dissolved organic nitrogen (tDON), phosphorus (tDOP), tDIC, alkalinity (tAlk), and inorganic silica (tDSi). tDIC and tDOC were computed based on chemodynamic relationships between discharge and concentration (Tank et al., 2012; Bertin et al., 2022) using a nonlinear load estimation method (Text A2). tAlk was computed using a Alk:DIC ratio of 0.93 (Tank et al., 2012) and tDOC was split into to semi-labile (DOC_{sl}) and semi-refractory (DOC_{sr}) pools. DOC_{sl} and DOC_{sr} were implicitly remineralized into DIC at rates of 1 month and 10 years (Manizza et al., 2009, 2011), respectively. tDON, tDOP, and tDSi concentrations were computed using the GlobalNEWS2 annual climatology (Mayorga et al., 2010).

A suite of 8 simulations were integrated and analyzed for the 2000–2019 period (Table A.5). The run "Q+Temp" included only freshwater discharge (Q) and river temperature and served as a reference run. The runs "All Interannual" and "All Climatology" included all riverine physical and biogeochemical inputs calculated, respectively, with interannual and climatological forcing; climatologies were estimated by averaging daily time series. The effect of each group of riverine biogeochemical components was analyzed by removing one by one the associated inputs: run "No tDOC" included all but tDOC, run "No tDIC" included all but tDIC and tAlk, and run "No Nutrients" included all but tDON, tDOP, and tDSi. Finally, two runs were designed to assess model sensitivity to zero biogeochemical input; The "No river" run did not included any riverine inputs from the Mackenzie River and the "Q" run included only the freshwater discharge with river temperature set to the sea-surface temperature (SST) value of the wet grid cell. A plume region delimited by Mulligan and Perrie (2019) observations at isohaline S=27 was computed to evaluate the contribution of the Mackenzie plume to CO_2 fluxes and net primary production (NPP) in the SBS. The plume region was coherent with the Mackenzie inner-shelf sub-region determined by a neural network (not shown), which combined 17 years of satellite data acquired by the Aqua-MODIS sensor (Hilborn & Devred, 2022).

Table 4.1: Net air-sea CO_2 fluxes and net primary production (NPP) during 2000–2019 calculated in the river plume area (S<27)

Model Run	Net CO_2 flux (TgC yr^{-1})	NPP (TgC yr^{-1})
No river	-0.20±0.06 (-51%)[a]	0.51±0.08 (-12%)[a]
Q	-0.42 ± 0.05 (1%)[a]	0.57 ± 0.06 (-1%)[a]
Q+Temp	-0.41 ± 0.06	0.58 ± 0.07
All Interannual	0.13 ± 0.10 (-132%)[a]	0.70 ± 0.06 (+21%)[a]
No Nutrients	0.21 ± 0.10	0.58 ± 0.07
No tDOC	-0.10 ± 0.06	0.70 ± 0.06
No tDIC-tAlk	-0.27 ± 0.06	0.70 ± 0.06
All Climatology	0.13 ± 0.08	0.70 ± 0.06

[a]values in brackets indicates difference with "Q+Temp" simulation

4.3 Contribution of River Components to Mackenzie Plume Air-sea CO_2 Flux

For the 2000–2019 period, using all river inputs in the ED-SBS model ("All Interannual") results in an annual-mean CO_2 outgassing of 0.13±0.10 TgC yr^{-1} within the plume region (Table 4.1 and Fig. 4.1). This estimate falls outside the range reported in previous studies (-0.9±0.5 to -4.3±2.5 TgC yr^{-1}; Manizza et al., 2013; Evans et al., 2015; Manizza et al., 2019; Ouyang et al., 2021) that categorize the SBS as a weak-to-moderate CO_2 sink (see also Roobaert et al., 2019; Dai et al., 2022). However, the lack of nearshore data (which do not cover a large part of the river plume) or lack of terrestrial inputs (missing tDIC-tAlk input or poorly-resolved tDOC remineralization), can explain this discrepancy. With no riverine biogeochemistry in the river plume ("Q+Temp" run), the plume region transitions to a CO_2 sink (-0.41 TgC yr^{-1}, Table 4.1), highlighting the key role of the Mackenzie river in modulating air-sea CO_2 flux. We estimate that the biogeochemical plume ventilates 0.54±0.16 TgC yr^{-1} to the atmosphere, which corresponds to about 7% of the annual-mean riverine input of both tDIC and tDOC (Table A.4).

Including riverine nutrients (tDON, tDOP, and tDSi) increases NPP by 21%, resulting in an uptake of 0.08 TgC yr^{-1} by the coastal AO ("All Interannual" run and "No Nutrients" run, Table 4.1). The riverine nutrient contribution to NPP is comparable to previously reported values in the region (≥9.8%; Terhaar et al., 2021b) and also in Arctic (Lena River, 34%; Lacroix et al., 2020) and non-Arctic (Amazon River, 21%; Louchard et al., 2021) river systems. However, as a caveat the riverine tDON and tDOP used in ED-SBS may be overestimated relative to other observations (Table A.4). In the absence of riverine nutrients ("No Nutrients" run), the coastal Beaufort Sea's net CO_2 flux to the atmosphere is strengthened due to weaker biological uptake. In ED-SBS, riverine tDIC drives an outgassing of 0.40 TgC yr^{-1} in the coastal AO, which is ∼2 times higher than the tDOC contribution (0.23 TgC yr^{-1}). This results from higher tDIC supply in the Mackenzie River compared to tDOC (Table A.4), demonstrating that tDIC plays a crucial role in carbon cycling on the Mackenzie Shelf.

In Arctic river waters, tDOC originating from permafrost thaw can exhibit fast remineralization rates (7 days; Spencer et al., 2015), depending on the season and soil characteristics in various watersheds (Bruhn et al., 2021). Additionally, tDOC lability varies significantly according to the soil type, to which marine microbes respond differently (Bruhn et al., 2021; Drake et al., 2018).

tDOC is thus a complex pool of molecules characterized by a large spectrum of lifetimes (Dittmar et al., 2021) that makes it challenging to represent in biogeochemical models. In this study, we represent tDOC based on our best knowledge of the Mackenzie River system by separating it into fast-reacting (50%) and slow-reacting (50%) pools. According to this parameterization, the model was able to correctly reproduce the DOC concentrations retrieved by satellite (Fig. A.5, r = 0.65; Matsuoka et al., 2017, 2022). In our simulations, tDIC plays a greater role than tDOC in the air-sea CO_2 balance in the Beaufort Sea (see Tank et al., 2012; Mol et al., 2018). This contrasts with results from Terhaar et al. (2019) that assumed the immediate remineralization of all tDOC into DIC and predicted a greater effect of tDOC compared to tDIC on air-sea CO_2 flux. Our results emphasize the critical role of tDOC remineralization in ocean-atmosphere carbon exchange, highlighting the importance of accurately representing the fate of riverine carbon in models.

Turning off all Mackenzie River inputs ("No river") results in a 51% weaker net CO_2 sink, along with a 12% decrease in NPP (Table 4.1). This response results from 1) higher CO_2 solubility in less-saline waters and 2) enhanced DIC uptake by phytoplankton blooms promoted by increased upper-ocean stratification (Carmack & Macdonald, 2002; Ardyna & Arrigo, 2020) in the "Q+Temp" run. In contrast, the effect of river temperature on air-sea CO_2 exchange is negligible. We find that ED-SBS underestimates observed SST (OSTIA; Good et al., 2020), especially in the coastal zone influenced by the Mackenzie River plume (Fig. A.6; Nguyen et al., 2021). This mismatch can be explained by two primary reasons. First, the uppermost vertical layer in ED-SBS is 10-m thick, which does not fully resolve the fine-scale vertical stratification driven by the river plume, which has been observed to be roughly 2–3m deep (Mulligan & Perrie, 2019). Second, ED-SBS does not include thermal effects from the colored and optically-active tDOC fraction (Hill, 2008; Matsuoka et al., 2017; Soppa et al., 2019; Pefanis et al., 2020) which likely influenced SST in this region.

4.4 Biogeochemically-induced Outgassing Events in the SBS

"All Interannual" and "All Climatology" simulate a general sink of carbon in the SBS (blue colors, Fig. 4.1a), balanced by short lived intense outgassing as a result of riverine input (red colors, Fig. 4.1a). In this study, an outgassing event is defined as a net CO_2 flux to the atmosphere exceeding 2 GgC d^{-1} within the river plume region. While both runs exhibit similar net CO_2

fluxes (Table 4.1), specifically in terms of the number of outgassing events (191–192) and net carbon ventilated (787–815 GgC), disparities occur at seasonal and interannual timescales (Fig. 4.1b). In July, after the peak of discharge, the "All Interannual" run increases CO_2 outgassed by discrete events by 31%. From year to year, the number of events and carbon outgassed also strongly differs between the two runs (Fig. A.7). This highlights the influence of riverine interannual variability in modulating the frequency and intensity of plume-driven CO_2 outgassing in the SBS.

We find that the absence of tDIC and tAlk input ("No tDIC-tAlk" run), and tDOC ("No tDOC" run) to a lesser extent, strongly limits CO_2 outgassing events, (Fig. 4.1c and 4.2a). Coastal waters deprived of these inputs become a net CO_2 sink over the two decades, with the number of outgassing events decreasing from 192 ("All Interannual") to 26 in "No tDOC" and to only 1 event in "No tDIC-tAlk" (Fig. 4.2a). Therefore, including tDIC, tAlk and tDOC forcing is necessary for accurately simulating seasonal carbon dynamics in the SBS between July to October (Table A.6). We find that outgassing events start in mid-July, which coincides with the decline in near-shore sea-ice (Fig. 4.2; Carmack et al., 2004) that confines the river plume and dampens the intensity of outgassing hotspots. 85% of the outgassing events occur in August and September, when phytoplankton decline (Fig. 4.2b) and tDIC/tDOC inputs are maintained by high discharge rates (Fig. A.3), promoting air-sea CO_2 exchange in ice-free waters with low productivity. Finally, outgassing declines in October, following seasonal decline in river's carbon supply.

We find that ED-SBS exhibits broad-scale consistency in both time and space with the ob-

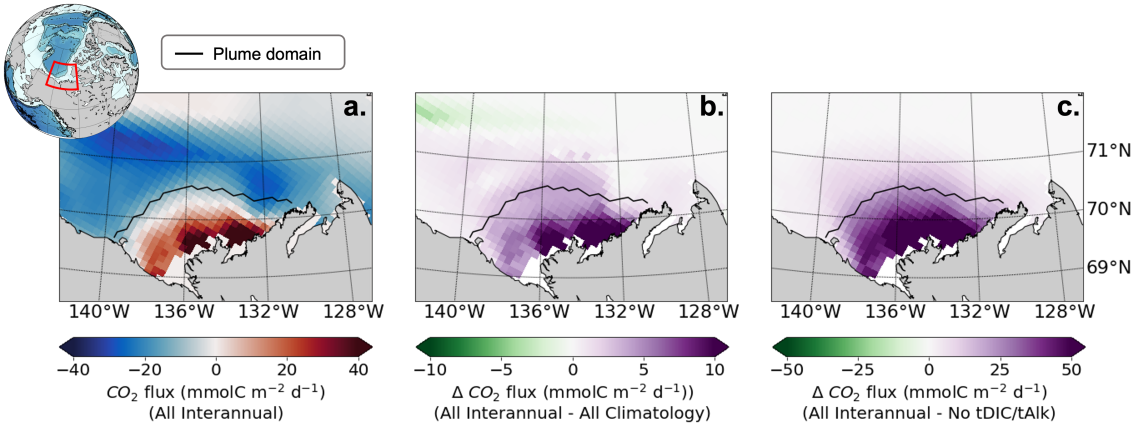

Figure 4.1: (a) Net air-sea CO_2 flux simulated by the "All Interannual" run during the 08/23/2007 outgassing event and difference with (b) "All Climatology" and (c) "No tDOC" runs. Positive (negative) values indicate CO_2 outgassing (ingassing). Top left inset shows the ED-SBS model region in a global context. Black solid lines indicate the plume region (S<27).

served circulation patterns (Fig. A.4, Lin et al., 2020) and NPP and net CO_2 flux products. Over the 2000–2017 period, the "All Interannual" run is able to accurately simulate both seasonal and interannual variability within the range of mean product amplitude and bloom phenology (Fig. 4.2a and 4.3a, Bélanger et al., 2013; Lewis et al., 2020). In terms of net CO_2 flux, ED-SBS simulates higher CO_2 uptake compared to Yasunaka et al. (2018) and Landschützer et al. (2020) (Fig. 4.2c). We note that these interpolated-based products lack nearshore observations which prevents a more robust comparison along the coastal periphery and does not indicate a model discrepancy. On interannual timescales, ED-SBS net CO_2 flux falls within the Yasunaka et al. (2018) error bounds (Fig. 4.3b).

We observe a positive linear relationship (r = 0.91) between interannual variability in Mackenzie River discharge and net annual CO_2 flux ("All Interannual" - "All Climatology" values). This

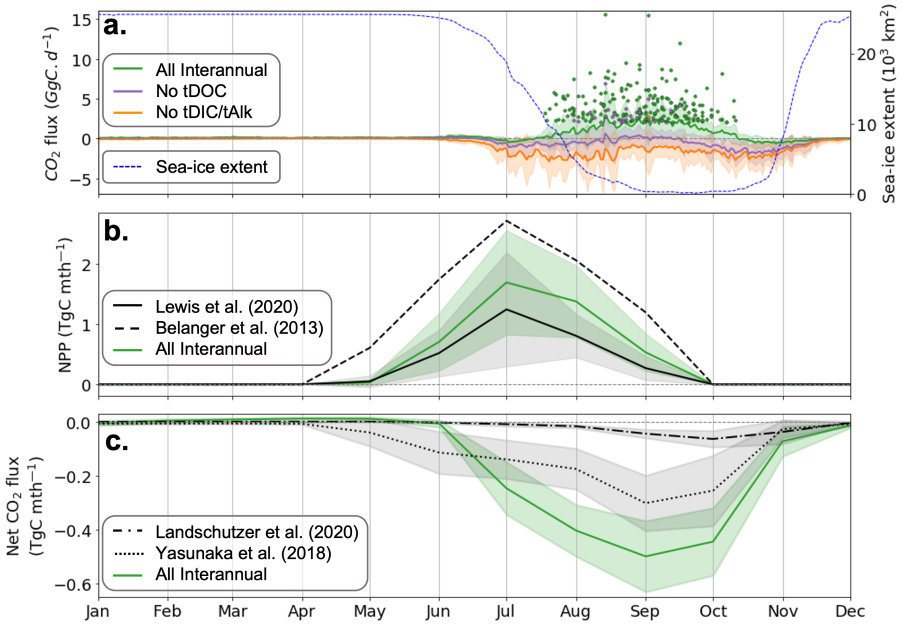

Figure 4.2: (a) 2000–2019 daily net CO_2 flux (TgC d^{-1}) simulated by the "All Interannual" run (green solid line), "No tDOC" run (purple solid line) and "No tDIC/tAlk" run (orange solid line) in the plume domain (see Fig. A.2). Green, purple and orange dots show the net CO_2 flux driven by individual outgassing events simulated in "All Interannual", "No tDOC" and "No tDIC/tAlk" runs, respectively. Positive (negative) values indicate CO_2 outgassing (ingassing). The simulated sea ice extent (10^3 km^2) is overlaid (blue dashed line). 2000–2017 seasonal (b) NPP and (c) net CO_2 flux (TgC mth^{-1}) from "All Interannual" run (green solid line) and observed by satellite (solid black line, Lewis et al. (2020); dashed black line, Bélanger et al. (2013); dash-dotted black line, Landschützer et al. (2020), and dotted black line, Yasunaka et al. (2018)) over the full model domain (see Fig. A.2). For all panels, the shaded envelop indicates the standard deviation computed for every seasonal cycles.

result suggests that low discharge promotes CO_2 uptake and high discharge drives CO_2 outgassing (Fig.4.3c). Interannual variability in river discharge is thus an important driver of the capacity of the coastal AO to capture or release CO_2 to the atmosphere. In a recent study, Ouyang et al. (2021) simulated interannual variability in CO_2 uptake across the western Arctic using a data-driven box model, but without including Mackenzie River discharge. Ouyang et al. (2021) obtained a better fit between their model and the observations in the Canada Basin and Chukchi Sea compared to Beaufort Shelf that is highly influenced by the Mackenzie River. Our results suggest that excluding the effect of the pan-Arctic river systems and their biogeochemical constituents in an ocean biogeochemistry model might hamper complete assessment of coastal air-sea CO_2 fluxes on interannual timescales.

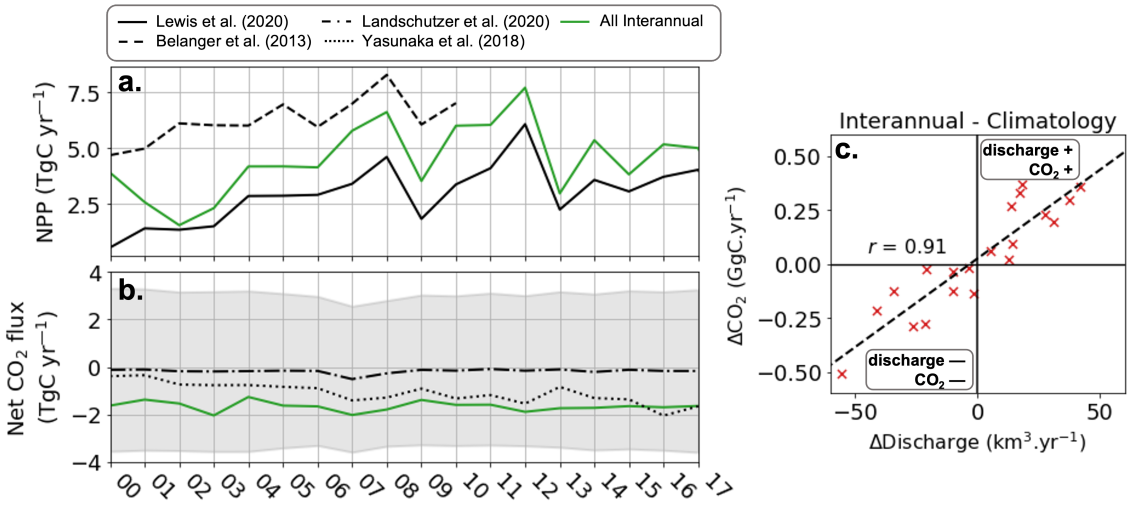

Figure 4.3: Interannual (a) NPP and (b) net CO_2 flux (TgC yr^{-1}) in the "All Interannual" run (green solid line) and observed by satellite (solid black line, Lewis et al. (2020); dashed black line, Bélanger et al. (2013); dash-dotted black line, (Landschützer et al., 2020) and dotted black line, Yasunaka et al. (2018)) over the full model domain (see Fig. A.2). Positive (negative) values indicate CO_2 outgassing (ingassing). The shaded envelop indicates the net CO_2 flux error associated to Yasunaka et al. (2018) data. (c) Relationship between net annual CO_2 flux vs. annual Mackenzie discharge interannual variability.

4.5 Conclusion and Future Directions

We investigated how the Mackenzie River plume modulates the capacity of the SBS to act as a sink or source of CO_2 to the atmosphere. ED-SBS compares well to both time-coincident satellite and observation products and provides key mechanistic insight on the contribution of riverine freshwater and biogeochemistry to air-sea CO_2 fluxes in this rapidly-changing region. We have

several critical results:

1. During the 2000–2019 period, the Mackenzie River plume drives net CO_2 outgassing (0.13 ± 0.10 TgC yr^{-1}), resulting from tDIC and tDOC inputs that ventilate 0.40 and 0.23 TgC yr^{-1} to the atmosphere, respectively.

2. tDIC riverine discharge contributes twice as much as tDOC in driving outgassing conditions; we identified 192 discrete CO_2 outgassing events, which mainly occur during ice-free periods.

3. Interannual variability of the Mackenzie River discharge strongly modulates air-sea CO_2 flux, with more outgassing occurring when discharge is high and more uptake when discharge is low.

Despite the tiny scale of the plume outgassing relative to the entire Arctic shelf (Dai et al., 2022), this study improves the mechanistic understanding of the processes controlling the seasonal air-sea CO_2 fluxes in the Mackenzie shelf and provides a set of new software tools that can help refine the pan-Arctic coastal carbon budget. We suggest that tDIC can be a key driver of ocean outgassing, which might be relevant to other tDIC-dominated river systems (Li et al., 2017). As suggested by recent observational-based coastal air-sea CO_2 flux estimates (Roobaert et al., 2019; Landschützer et al., 2020), we also demonstrate that large spatial heterogeneity exists near river mouths, such as the Mackenzie Delta (Fig. 4.1), which indicates that localized outgassing along the Arctic coastal periphery may result in a weaker AO CO_2 sink than previously expected (Dai et al., 2022). These results also stress the importance of including all river freshwater and biogeochemical discharge constituents in AO numerical ocean simulations and highlight that previous studies which do not include these processes may overestimate the AO CO_2 sink (Manizza et al., 2019; Ouyang et al., 2021). Pan-Arctic rivers are important contributors to the budget of freshwater (Serreze et al., 2006) and inorganic and organic matter in the coastal AO (Holmes et al., 2012; Tank et al., 2012). Fluxes from these large river system are projected to increase in the future with the intensification of the Arctic hydrologic cycle (Brown et al., 2020; Saito et al., 2021), river discharge (Ahmed et al., 2020; Feng et al., 2021), and permafrost thaw (Schuur et al., 2015; McGuire et al., 2016). As suggested by our study, representing the large interannual variability in riverine export of tDIC and tDOC to the coastal AO is critical for predicting how these changes may alter future carbon cycling on Arctic shelves. This requires quantifying the quantity, type, and lability of riverine nutrients, as well as the timing with which they are delivered to coastal waters.

Measurements of nutrient distributions are needed as close as possible to the mouths of large deltas and estuaries, which could prevent biases due to removal/addition processes taking place upstream in watersheds (Emmerton et al., 2008a; Schwab et al., 2020). This is particularly true for tDOC originating from thawing permafrost, which has a much older ^{14}C age and is more labile than tDOC from contemporary sources. Furthermore, we report significant outgassing in late summer, which is coincident with maximum seasonal depth of the permafrost active layer (Schuur et al., 2015; Lacroix et al., 2022). Future soil warming (Slater & Lawrence, 2013) could promote the release of permafrost-derived tDOC in coastal waters (Matsuoka et al., 2022), potentially increasing river-driven outgassing. However, the actual amount of permafrost tDOC exported into the ocean still remains highly uncertain (Schwab et al., 2020). Recent autonomous systems (Juhls et al., 2020) and methods which merge *in-situ* and remotely-sensed data (Bertin et al., 2022) provide a new AO monitoring frameworks, but they are still unable to track seasonal-to-interannual changes in tDOC lability in response to rapid changes in permafrost conditions. We stress that knowledge of the riverine tDOC signal and how it will change in time and space is pivotal, as this determines remineralization pathways and key timescales within the carbon cycle. Concerning tDIC, concentrations are indirectly estimated from ions present in river water (Tank et al., 2012), whose monitoring primarily relies on the ArcticGRO pan-Arctic program (Holmes et al., 2012). Such a database and continuity in monitoring programs are essential for tracking seasonal-to-interannual variations of tDIC alongside those of tDOC. This is important as the riverine tDIC:tDOC ratio exhibits large variations at the pan-Arctic scale (Fig. A.5).

In the Eurasian AO, the tDIC:tDOC ratio falls between 1.0–1.5, while it is as high as 4.5 on the North American side (Holmes et al., 2012; Tank et al., 2012). There is far more tDOC delivered by large rivers in the Eurasian shelf seas, so outgassing events might not be driven by the processes we have identified in the SBS. With ongoing Arctic warming, an improved understanding of seasonal-to-interannual variability in tDOC concentrations and fluxes are thus required to improve the ability of AO simulations to quantify the relative contribution of tDOC and tDIC to air-sea CO_2 fluxes in these productive shelf regions.

We find that the CO_2 outgassing signal is sensitive to the choice of vertical model resolution. Additional experiments (not shown) demonstrate that with finer vertical resolution in the upper layer, CO_2 fluxes are increased and tend to promote more outgassing. Therefore, we recommend that future models use coastal observations to optimize their land-to-sea boundary conditions. This

is also critical for the implementation of riverine fluxes of particulate matter, which are subject to vertical sedimentation. The Mackenzie shelf receives as much terrestrial particulate organic carbon (tPOC) as tDOC (1.6 TgC yr^{-1}; Bertin et al., 2022) from both the river (0.7 TgC yr^{-1}; McClelland et al., 2016) and coastal erosion (0.9 TgC yr^{-1}; Nielsen et al., 2022). Once in shallow waters, tPOC is resuspended from bottom sediments to the water column (Jong et al., 2020) and transported farther offshore (Forest et al., 2014). Resuspension cycles constantly bring tPOC back to surface waters where it can be oxidized (Massicotte et al., 2021; Galeron et al., 2018) and degraded by bacteria to be ultimately outgassed as CO_2 (Jong et al., 2020). However, representing tPOC in regional models is not trivial as it requires coupling with bottom sediments and fine grid resolution in order to resolve the physical (i.e. tides, waves) and biogeochemical processes that drive tPOC dynamics.

Both tPOC and tDOC also produce a browning of shelf waters, with potential consequences for near-surface light penetration. Therefore, future models will need to include this process as it will impact the delicate balance between CO_2 uptake through NPP and regeneration through bacterial respiration. Finally, we suggest that future efforts focus more on the role of tPOC in driving air-sea CO_2 flux. Since the 2000s, coastal erosion has reached high rates (up to -1.8m yr^{-1} along the US Beaufort Sea coast; Irrgang et al., 2022) expected to rise in the future (more than -3m yr^{-1}; Nielsen et al., 2022) in the North American Arctic. An explicit representation of terrestrial POC may be required to produce a more holistic view on how land-to-sea connectivity would drive carbon flows in an Arctic "green belt", which is already facing rapid and drastic environmental changes. Furthermore, Arctic deltas are projected to become less ice-dominated and more exposed to wave erosion in the future (Overeem et al., 2022; Odériz et al., 2022), bringing more uncertainty to the projected AO carbon cycle.

CHAPTER

5

PAVING THE WAY TO AN IMPROVED REPRESENTATION OF tDOC AND PHYSICAL PLUME: A SENSITIVITY ANALYSIS

Abstract

Processes affecting riverine dissolved organic carbon (DOC) removal across the land-to-ocean aquatic continuum (LOAC) are still poorly constrained in Arctic models, leading to large uncertainties in simulated air-sea CO_2 fluxes within Arctic river plumes. We use an ocean-sea ice-biogeochemichal model of the Southeastern Beaufort Sea (SBS) to analyze the sensitivity of the simulated physics and biogeochemistry to different parameterizations of the Mackenzie River inputs and vertical grid of the model. We show that tDOC quality and lifetime largely modulate the SBS capacity to act as a source (-0.29 TgC yr^{-1}) or sink (0.1 TgC yr^{-1}) of CO_2. Adding tDOC flocculation turns ED-SBS as a weak sink (-0.04 TgC yr^{-1}) close to equilibrium, hence preventing the outgassing of 0.14 TgC yr^{-1} in the scenario with a rapid tDOC turnover (0.1 TgC yr^{-1}). In terms of physics, increasing the vertical stratification of the riverine plume triggers the highest CO_2 outgassing, which is 3.5 times more important (0.45 TgC yr^{-1}) than in the scenario with a rapid tDOC turnover (0.10 TgC yr^{-1}). However, though simulated SST better match observations, the increased stratification of the plume also results in unrealistic simulated DOC concentrations pointing out issues on ED-SBS capacity to properly represent key processes of the land-to-sea interface. Tackling the way Arctic models consider this interface is required to simulate realistic fields both physical and biogeochemical prior to move towards very high resolution Arctic models.

5.1 Introduction

A tenth of the global freshwater volume (Opsahl et al., 1999) flows towards the Arctic Ocean (AO) that represents only $\sim$1% of the global oceanic volume. Half of this freshwater takes its origin from Pan-Arctic rivers (Brown et al., 2020) that discharge 5,169 km^3 yr^{-1} of freshwater into the AO (Feng et al., 2021). The dynamics of Arctic shelves that account for 50% of the basin area (Carmack et al., 2006) is then strongly constrained by the riverine forcing. Fresh and warm plumes spread into the AO driving strong stratification (Brown et al., 2020; Lenn et al., 2022) and variability in near-shore sea-ice phenology (Nghiem et al., 2014; Park et al., 2020). Rivers also drain vast watershed (Vörösmarty et al., 2000) and mobilize huge amounts of biogeochemical constituents (Dittmar & Kattner, 2003; Le Fouest et al., 2013) across very different landscapes. Riverine inorganic nutrients exported into the AO support growth of marine phytoplankton that could contribute to a sink of atmospheric carbon estimated to 118 to 180 TgC yr^{-1} at the basin scale (Arrigo et al., 2010; Yasunaka et al., 2018; Manizza et al., 2019). In contrast, the substantial

amount of riverine dissolved carbon in the organic (tDOC; 17–26 TgC yr^{-1}; Le Fouest et al., 2013) and inorganic (tDIC; 57 TgC yr^{-1}; Tank et al., 2012) form promote CO_2 outgassing from the AO (Terhaar et al., 2019; Bertin et al., 2023). While tDIC directly contributes to outgassing, tDOC must first be degraded into the DIC form through processes that remain challenging to include in biogeochemical models.

In the global ocean, DOC is continuously exported from continents, biologically produced, and degraded. As a result of this cycling, DOC exhibits a wide range of composition classified into five compartments according to their turnover rates τ (intrinsic recalcitrance concept; Lønborg et al., 2020; Dittmar et al., 2021): labile (τ=hours to days), semi-labile (τ=weeks to months), semi-refractory (τ=decades), refractory (τ=thousand years) and ultra-refractory (τ=ten thousand years). In the AO, DOC has very different sources (Bauer & Bianchi, 2011; Schuur et al., 2015; Kaiser et al., 2017) and is mostly semi-labile and semi-refractory. tDOC mainly originates from vascular plant (Bianchi, 2011; Amon et al., 2012) and exhibits modern forms of carbon with monthly turnover rates (Holmes et al., 2008). In contrast, permafrost thaw releases more ancient forms of tDOC characterized by faster turnover rates ($\sim$2weeks; Spencer et al., 2015). The ratio between modern and ancient tDOC that fuels the semi-labile pool is very uncertain as it can differ across the seasons and years (Schwab et al., 2020; Matsuoka et al., 2022). Other DOC forms in coastal waters mainly come from autochtonous and allochtonous dead organic matter already reprocessed and enter within the semi-refractory category (τ=7 to 10 years; Hansell et al., 2004; Manizza et al., 2009). The tDOC contribution to the semi-labile and semi-refractory pools in plume waters is still poorly known. Wickland et al. (2012) estimate the fraction of semi-labile tDOC in Arctic rivers between 10 to 45% based on the DIN:DOC ratio. However, the percentage of semi-labile tDOC biologically available is strongly season-dependent and varies between the river systems (Wickland et al., 2012). Furthermore, recent experiment reported that the fraction of biologically available tDOC changes as it mixes in the river plume (Matsubara et al., 2022).

Additionally, the quick response of the AO to climate change complexifies the understanding of such intricate processes (Lønborg et al., 2020; Schwab et al., 2020). The increase of river discharge (Ahmed et al., 2020; Feng et al., 2021) associated with the accelerated permafrost thaw rich of 1,400-1,600 Gt of frozen organic carbon (Tarnocai et al., 2009) might trigger significant and irreversible changes in the biogeochemistry of coastal waters exposed to sea-ice melt (Saito et al., 2021; Schuur et al., 2015, 2022). This is particularly true for tDOC removal processes that

depend on temperature, salinity and light. Microbial activity considered as a major pathway in the remineralization of DOC into DIC (Holmes et al., 2008) is highly constrained by temperature (Ortega-Retuerta et al., 2012). DOC photodegradation is also a prominent process, accounting for 5 to 38% of DIC production in coastal Arctic waters (Belanger et al., 2006; Aarnos et al., 2018). At the land to sea interface, the mixing of riverine freshwater with saline waters promotes flocculation effects (Sholkovitz, 1976). This process is thought to be responsible for a DOC loss as high as 45% in very close vicinity of the Mackenzie Delta (Kipp et al., 2020).

Given the complexity of DOC degradation in Arctic coastal waters and the regional disparities of bioavailable tDOC (Wickland et al., 2012), it is very timely to gain a better understanding on the tDOC mechanistic processes driving the carbon biogeochemistry and resulting air-sea CO_2 fluxes. Recent modeling efforts have been done this way (Manizza et al., 2019; Terhaar et al., 2019; Lacroix et al., 2020; Mathis et al., 2022; Gibson et al., 2022), even if tDOC related processes are often very simplified. In these models, tDOC inputs are calculated from climatologies extracted from the C:P ratio in organic matter (Lacroix et al., 2020; Mathis et al., 2022) or annual budget data (Global NEWS; Terhaar et al., 2019; Manizza et al., 2019). The degradation rate of DOC is either set as very long (1 to 10 years Manizza et al., 2019; Mathis et al., 2022) or instantaneous (DOC directly converted into DIC; Terhaar et al., 2019). Additionally, riverine fluxes are simulated within top surface layers deeper than 10 m depth, which is not representative of the plume thickness generally measured in large arctic rivers (2 to 5 m for the Lena and Mackenzie River; Guieu et al., 1996; Macdonald & Yu, 2006). To that respect, such a diversity in the river plumes parameterization likely has important implications for the simulated biogeochemistry, which is thus very timely to consider.

In this study, we analyze the sensitivity of the Southeastern Beaufort Sea (SBS) physics and biogeochemistry to a range of physical and biogeochemical parameterizations of the Mackenzie River inputs and vertical grid in ED-SBS. We aim to quantify the range of simulated response in terms of ocean and sea-ice properties and carbon biogeochemistry, as well as to provide insights on present-day limitations. The paper is organized as follows: we first describe the main characteristics of the regional ocean-sea ice-biogeochemical set up for the SBS. Second, we analyze how different model parameterizations alter the simulated physics and biogeochemistry. Finally, we discuss pathways to models improvement and provide guidance for a better estimation of carbon fluxes in river-influenced Arctic seas.

5.2 Methods

We used the ECCO-Darwin Southeastern Beaufort Sea model (ED-SBS; see Bertin et al., 2023), a regional configuration of the global-ocean ECCO-Darwin biogeochemistry state estimate described in Carroll et al. (2020, 2022). The physical model is based on the ECCOv4 (LLC270) global ocean and sea-ice configuration (H. Zhang et al., 2018) and coupled online with the Darwin ocean ecology and carbon chemistry models (Dutkiewicz et al., 2013; Follows et al., 2007). The model has an average 12 km horizontal spacing distributed on a curvilinear grid. The vertical grid has 44 unevenly spaced levels, ranging from 10 m thick near the surface to 307 meters near the ocean bottom. The biogeochemical component of the model explicitly simulates cycling of carbon, nitrogen, phosphorus, silica, iron, and oxygen as they transition between inorganic, living, and dead organic pools; the model also simulates the carbonate cycle (Follows et al., 2006). ED-SBS simulates four plankton functional types (PFTs) characteristic of the AO communities present in the SBS: diatoms, large eukaryotes, and small and large zooplankton. ED-SBS was forced by the initial and boundary conditions extracted from Carroll et al. (2020) simulations, except for oceanic DOC extracted from Bertin et al. (2023). The model and the land-to-sea forcing are fully detailed in Bertin et al. (2023).

The ED-SBS configuration was designed to enhance the ECCO-Darwin ability to represent processes associated with the land-to-sea continuum of the AO. The main improvements, applied to the Mackenzie River runoff and to the oceanic DOC degradation scheme, are summarized below and fully detailed in Bertin et al. (2023). The oceanic DOC is represented by 2 different explicit state variables: DOC_{sl} and DOC_{sr} that simulate the dynamics of semi-labile and semi-refractory DOC pools, respectively. The degradation of DOC was implicitly simulated using a constant rate (λ in s^{-1}) such as $\lambda=1/\tau$, with τ=10 years (Manizza et al., 2009) and τ=1 month, respectively (Bertin et al., 2023). Daily riverine inputs of freshwater and six biogeochemical tracers were distributed over the three main Mackenzie Delta outlets according to (see Morley, 2012; Bertin et al., 2022): Shallow Bay (29.8%), Beluga Bay (37.6%), and Kugmallit Bay (32.6%). Freshwater discharge was forced by daily gauge measurements from the Arctic Great River Observatory (AGRO; Shiklomanov et al., 2021) and was associated with daily river temperature extracted from the Tokuda et al. (2019) dataset. Daily riverine forcings of terrestrial dissolved organic nitrogen

(tDON), phosphorus (tDOP) and inorganic silica (tDSi) were calculated from the GlobalNEWS2 annual climatology (Mayorga et al., 2010). Daily riverine forcings of tDOC and tDIC were calculated from interannual time series based on AGRO and Tank et al. (2012) data, respectively Bertin et al. (2023). We calculated the riverine alkalinity (tAlk) flux using an tAlk:tDIC ratio of 0.93 characteristic of the Mackenzie River(Tank et al., 2012).

A suite of 5 simulations were integrated and analyzed for 2009. In the baseline simulation (hereby referred as Run$_{base}$), tDOC is equally distributed among the semi-labile (50%) and semi-refractory (50%) oceanic tracers, and the degradation rate of semi-labile tDOC (τ_{DOC_l}) is set to 1 month Bertin et al. (2023). In Run$_{remin}$, tDOC semi-labile fraction is smaller (20%) and is recycled at a slower rate (τ_{DOC_l}= 3 months) (Holmes et al., 2008; Wickland et al., 2012) than in Run$_{base}$. Run$_{floc}$ is same as Run$_{base}$, except that we implicitly include the tDOC flocculation loss process (45%;Kipp et al. (2020)). In Run$_{floc}$, ED-SBS is thus constrained by only 55% of the total tDOC load. Run$_{strat}$ is same as Run$_{base}$, except that we refined the thickness of the top sea surface grid cell (10 m in Run$_{base}$) to 3 m in accordance with the thickness measured in the Mackenzie River plume ((2-4 m; Macdonald & Yu, 2006; Mulligan & Perrie, 2019)). In this run, the original 10 m thick grid cell was discretized into three layers of 3 m, 3 m and 4 m from the top to the bottom. Finally, Run$_{strat+floc}$ is a combination of both Run$_{strat}$ and Run$_{floc}$. The characteristics of all simulations are summarized in Table 5.1.

The simulated data (X$_{mod}$) were compared with time and space coincident observations (X$_{obs}$). Observations were from the summer 2009 Malina cruise (30 July to 25 August,Fig 5.2a; Massicotte et al., 2021; Forest et al., 2014), derived from satellite-*in situ* merged datasets (Good et al., 2020) and derived from satellite sensors (Matsuoka et al., 2017). Observations are at the surface and include mixed layer depth (MLD; Massicotte et al., 2021), *in situ* DIC and DOC concentra-

Table 5.1: ED-SBS sensitivity simulations tested and their characteristics

Simulation	tDOC distribution (DOC$_{sl}$:DOC$_{sr}$)	DOC$_{sl}$ turnover rate	Flocculation	Surface layer thickness
Run$_{base}$	50:50	1 month	No	10 m
Run$_{remin}$	20:80	3 months	No	10 m
Run$_{floc}$	50:50	1 month	Yes	10 m
Run$_{strat}$	50:50	1 month	No	3 m
Run$_{strat+floc}$	50:50	1 month	Yes	3 m

tions (Massicotte et al., 2021), remotely sensed DOC (Matsuoka et al., 2017), *in situ* air-sea CO_2 fluxes (Forest et al., 2014), sea surface temperature (SST; Good et al., 2020) and sea-ice extent estimates (Good et al., 2020). The observed and simulated day of retreat (DOR) of sea-ice, which correspond to the first Julian day when sea-ice cover falls below 15 %, was calculated according to Steele et al. (2019). The model-observations comparisons were evaluated according to the following metrics:

$$r = \frac{\sum[(X_{obs} - \overline{X_{obs}}).(X_{mod} - \overline{X_{mod}})]}{\sqrt{\sum(X_{obs} - \overline{X_{obs}})^2 . \sum(X_{mod} - \overline{X_{mod}})^2}}, \tag{5.1}$$

$$MPE = Median\left(100. \left|\frac{X_{mod} - X_{obs}}{X_{obs}}\right|\right), \tag{5.2}$$

$$NSE = 1 - \frac{\sum(X_{obs} - X_{mod})^2}{\sum(X_{obs} - \overline{X_{obs}})^2}, \tag{5.3}$$

$$URMSE = \sqrt{\frac{\sum[(X_{mod} - X_{obs}) - (\overline{X_{mod}} - \overline{X_{obs}})]^2}{n}}, \tag{5.4}$$

where n is the number of data. r is the correlation coefficient and measures the strength of the model-data relationship. The median of the absolute percentage error (MPE) measures the accuracy the regression between the model and the observations. The Nash-Sutcliffe model efficiency index (NSE) is an indicator of the predictive skill of the model (see Nash & Sutcliffe, 1970). The model is a good descriptor the observations when the residual variance (i.e. the "noise") is close to 0, resulting in a NSE value of 1. If the noise is comparable to the observational variance, the NSE value is near 0 suggesting that simulated values are as accurate as the observed mean. A negative NSE value suggests that the observational mean is a better predictor than the model. The Unbiased Root Mean Square Error (URMSE) measures the size of the discrepancies between the simulated and observed values.

5.3 Results

5.3.1 Sensitivity to tDOC parameterization

Here we compare the response of ED-SBS to three different parameterization of tDOC and assess the model capacity to match the observations (Table 5.2). Figure 5.1 shows the spatial distribution of surface DOC concentrations simulated in Run_{base} and retrieved from space during the

summer Malina cruise. With respect to both DOC and DIC concentrations, Run$_{base}$ gives a reasonable description of the observations (Table 5.2). Correlation coefficients r range between 0.61 (DIC) and 0.78 (DOC) suggesting the model captures between 37 and 61 % of the observational variance. The model-data regression has a middle-range accuracy for DOC (47.7<MPE<56.5) and a good accuracy for DIC (MPE$\sim$5.1). The data dispersion for DOC is high compared to the averages but comparable for both observational datasets (URMSE 68 mmolC m^{-3}). For DIC, dispersion is similar (URMSE=73.2 mmolC m^{-3}) but low relative to the averages. NSE is an indicator of which, between the model and the observations, best describes the system. For DOC, both NSE are negative but NSE is higher with satellite data (-0.17) suggesting ED-SBS is close to be as accurate as the observations (NSE=0). The higher number of data used for the model-satellite comparison (n=12,393) likely explains this result. For DIC, ED-SBS is a better descriptor (NSE=-0.64) than DOC (NSE=-1.94) from the Malina dataset. Compared to DIC and DOC, the metrics calculated for the air-sea CO_2 fluxes overall suggest larger discrepancies with the measurements.

In Run$_{remin}$, the fraction of semi-labile DOC is lower and remineralized at a slower rate than in Run$_{base}$. It translates into a mean DOC concentration 18 to 25 % higher in Run$_{remin}$ (Table 5.2). The difference is much lower for DIC (-0.09 %). For DOC, all comparison metrics, except r, suggest a lower predictive ability of ED-SBS compared to Run$_{base}$. This is not the case for DIC, for which MPE (-12 %) and NSE (-58 %) are improved. With respect to air-sea CO_2 fluxes, the

Table 5.2: Model-observations comparisons for surface DOC and DIC concentrations (mmolC m^{-3}) and net air-sea CO_2 fluxes (TgC yr^{-1}) with Run$_{base}$, Run$_{remin}$, and Run$_{floc}$. n is the number of data, r the correlation coefficient, MPE the median of the absolute percentage error, NSE the Nash-Sutcliffe model efficiency index, and URMSE the Unbiased Root Mean Square Error (mmolC m^{-3} or TgC yr^{-1}). DOC$_{sat}$ are remotely sensed data while DOC are Malina measurements.

Variable	Run	n	r	MPE	NSE	URMSE	average$_{obs}$ $\pm$ std	average$_{mod}$ $\pm$ std
	Run$_{base}$		0.67	47.7	-0.17	68.1		161 $\pm$ 88
[a]DOC$_{sat}$	Run$_{remin}$	12,393	0.66	76.9	-1.07	75.6	116 $\pm$ 75	193 $\pm$ 100
	Run$_{floc}$		0.65	32.9	0.42	56.8		122 $\pm$ 50
	Run$_{base}$		0.78	56.5	-1.94	68.4		166 $\pm$ 103
DOC	Run$_{remin}$	56	0.77	87.2	-4.08	80.7	98 $\pm$ 56	196 $\pm$ 117
	Run$_{floc}$		0.78	31.7	0.28	37.7		127 $\pm$ 57
	Run$_{base}$		0.61	5.08	-0.64	73.2		1930 $\pm$ 65
DIC	Run$_{remin}$	56	0.61	4.43	-0.37	73.9	1838 $\pm$ 92	1916 $\pm$ 68
	Run$_{floc}$		0.61	4.73	-0.55	73.6		1926 $\pm$ 67
	Run$_{base}$		0.14	115.6	-1.99	6.43		-1.21 $\pm$ 5.78
CO_2 flux	Run$_{remin}$	56	0.33	91.0	-1.30	5.09	-1.85 $\pm$ 3.73	-4.31 $\pm$ 4.93
	Run$_{floc}$		0.23	99.7	-1.20	5.52		-2.33 $\pm$ 5.02

[a]From June to September

comparison metrics remain poor but suggest an improvement in the model capacity to describe the observations.

In Run$_{floc}$, the tDOC load in ED-SBS is reduced by 45 % that translates into 26 to 35 % less DOC at the sea surface (Table 5.2). The simulated DOC concentrations are closer to observations than in Run$_{base}$. MPE is reduced by 31 to 44 %, NSE values turn positive suggesting ED-SBS becomes a good predictor of the observations, and data show 16 to 45 % less dispersion. Simulated DIC concentrations show a better agreement with observations in terms of NSE and MPE than in Run$_{base}$, but to a lesser extent compared to Run$_{remin}$. As for DIC, the metrics suggest a slight improvement in the model predictive ability in terms of air-sea CO_2 fluxes, but to a lesser extent compared to Run$_{remin}$.

Overall, Run$_{base}$ and Run$_{floc}$ best compare with the observed DOC concentrations (Table 5.2). In contrast, Run$_{remin}$ shows a better but still limited capacity to describe air-sea CO_2 fluxes and, to a lesser extent DIC concentrations. Run$_{base}$ and Run$_{floc}$ show the closest match with the mean air-sea CO_2 flux estimated from the Malina cruise data (-1.85 $\pm$ 3.73 mmolC m^{-2} d^{-1}) with simulated means of -1.21 $\pm$ 5.78 mmolC m^{-2} d^{-1} and -2.33 $\pm$ 5.02 mmolC m^{-2} d^{-1}, respectively. Run$_{remin}$ departs the most from the mean air-sea CO_2 flux estimated from the Malina cruise data with a simulated mean of -4.31 $\pm$ 4.93 mmolC m^{2} d^{-1}).

Simulated air-sea CO_2 fluxes were integrated yearly and over the domain shown in Figure 5.3a. In Run$_{base}$, ED-SBS simulates a net ocean outgassing of 0.1 TgC yr^{-1}. With tDOC floccu-

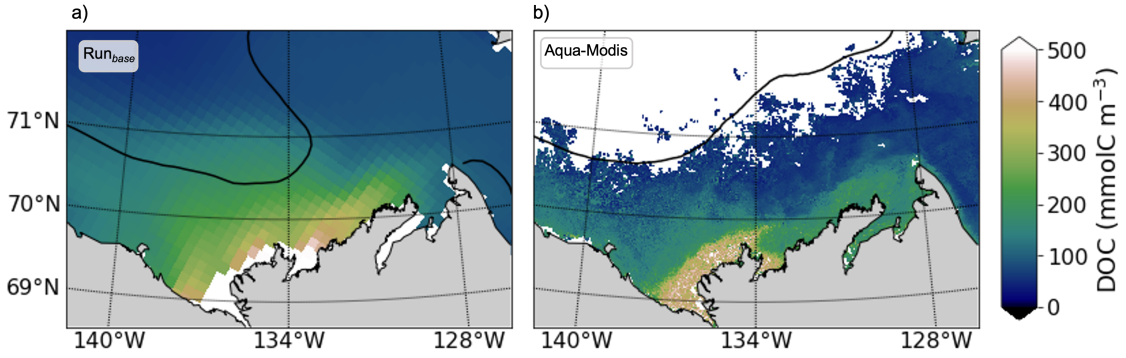

Figure 5.1: Sea surface DOC concentration (mmolC m^{-3}) and 15% sea-ice cover front (black solid line) simulated in Run$_{base}$ (a) and derived from space remote sensing (b) during the summer 2009 Malina cruise.

lation, ED-SBS turns as a weak CO_2 sink (-0.04 TgC yr^{-1}) close to equilibrium (Run$_{floc}$). The ocean pumping is highly promoted (-0.29 TgC yr^{-1}) by a weaker DOC remineralization and no flocculation (Run$_{remin}$).

5.3.2 Sensitivity to the river plume stratification: physics

In Run$_{base}$, the top surface layer of ED-SBS is 10 m thick, which is ∼3-fold higher than the observed Mackenzie plume thickness (2-4 m; Macdonald & Yu, 2006; Mulligan & Perrie, 2019). In Run$_{strat}$, we discretized the thickness of the surface top grid cell into three layers of 3 m, 3 m and 4 m from the top to the bottom.

In the delta vicinity and offshore waters, ED-SBS overestimates the observed MLD in Run$_{base}$, whereas a better fit is obtained with Run$_{strat}$ (Fig. 5.2, top panels). In Run$_{strat}$, all metrics are improved, except for correlation (Table 5.3). ED-SBS gets much closer to be as accurate as the observations (NSE=-0.65), with a 66 % and 31 % lower MPE and URMSE, respectively. A lower r and a still negative NSE can result from MLD values simulated offshore (>71°N) never exceeding ∼6 m (Fig. 5.2 c). As a response to the increased stratification, Run$_{strat}$ promotes a wider spreading of the river plume. The 25.0 isohaline chosen as an indicator of the plume boundary (Macdonald & Yu, 2006) shows that the plume spreads farther West along with an improvement

Table 5.3: Model-observations comparisons for sea surface temperature (SST, °C), DOC (mmolC m^{-3}), mixed layer depth (MLD), and salinity (SSS). SST$_{sat}$ and DOC$_{sat}$ are remotely sensed data while MLD, SSS, SST and DOC are Malina measurements.

Variable	Run	n	r	MPE	NSE	URMSE	average$_{obs}$ ± std	average$_{mod}$ ± std
[a]SST$_{sat}$	Run$_{base}$	157,964	0.77	45.7	0.55	1.55	0.54 ± 2.42	0.09 ± 1.89
	Run$_{strat}$		0.88	31.6	0.76	1.19		0.49 ± 2.52
[b]DOC$_{sat}$	Run$_{base}$	12,393	0.67	47.7	-0.17	68.1	116 ± 75	161 ± 88
	Run$_{strat}$		0.61	199	-26.7	287		388 ± 327
MLD	Run$_{base}$	56	0.53	87.2	-7.49	3.77	7.8 ± 2.7	14.7 ± 5.6
	Run$_{strat}$		0.27	29.3	-0.65	2.59		4.4 ± 0.7
SSS	Run$_{base}$	55	0.62	6.00	0.25	3.59	24.6 ± 4.4	26.0 ± 3.8
	Run$_{strat}$		0.66	6.72	0.13	3.94		23.4 ± 5.2
SST	Run$_{base}$	55	0.68	88.8	-0.14	2.00	2.81 ± 2.70	0.75 ± 2.13
	Run$_{strat}$		0.78	58.1	0.47	1.93		2.42 ± 3.00
DIC	Run$_{base}$	56	0.61	5.08	-0.64	73.2	1838 ± 92	1930 ± 65
	Run$_{strat}$		0.49	4.07	0.15	84.0		1830 ± 92
DOC	Run$_{base}$	56	0.78	56.51	1.94	68.4	98 ± 56	166 ± 103
	Run$_{strat}$		0.72	285	-71.7	350		428 ± 390

[a]From August to October
[b]From June to September

of the simulated MLD (Fig. 5.2, ac). At the stations located within the plume in Run$_{strat}$ plume but outside the plume in Run$_{base}$ (Figure5.2 bc), MLD simulated in Run$_{strat}$ are 4-7 m and so very consistent with observations.

The comparison metrics do not suggest any marked improvement in the ED-SBS ability to simulate SSS in Run$_{strat}$. In contrast, the simulated increase in stratification translates into higher simulated SST means (0.49 $\pm$ 2.52 °C and 0.54 $\pm$ 2.42 °C matching the remotely sensed and Malina grid points, respectively; Table 5.3) that better match with the observational means (0.54 $\pm$ 2.42 °C and 2.81 $\pm$ 2.70 °C for the remotely sensed and Malina data, respectively). Overall, the metrics suggest ED-SBS improves its ability to simulate SST (Table 5.3). This is particularly true in regard to the accuracy of the linear regression model between simulated and observed data (MPE) and to the ED-SBS predictive skill (NSE), which are particularly higher in Run$_{strat}$. With respect to remotely sensed data, simulated SST increases earlier in the season to reach a better match with observations during the open water period (August-October) (Figure5.2d). Nevertheless, Run$_{base}$ and Run$_{strat}$ both fail to simulate the early season warming (June to July) of the top surface layer. Run$_{strat}$ still underestimates SST (Fig. 5.4a), which is consistent with an overestimation of the simulated sea-ice cover (up to 40 %, Fig. 5.4b) and DOR (up to 1 month, Fig. 5.4c). Nevertheless, the increase of SST in the top surface layer associated with the larger extent

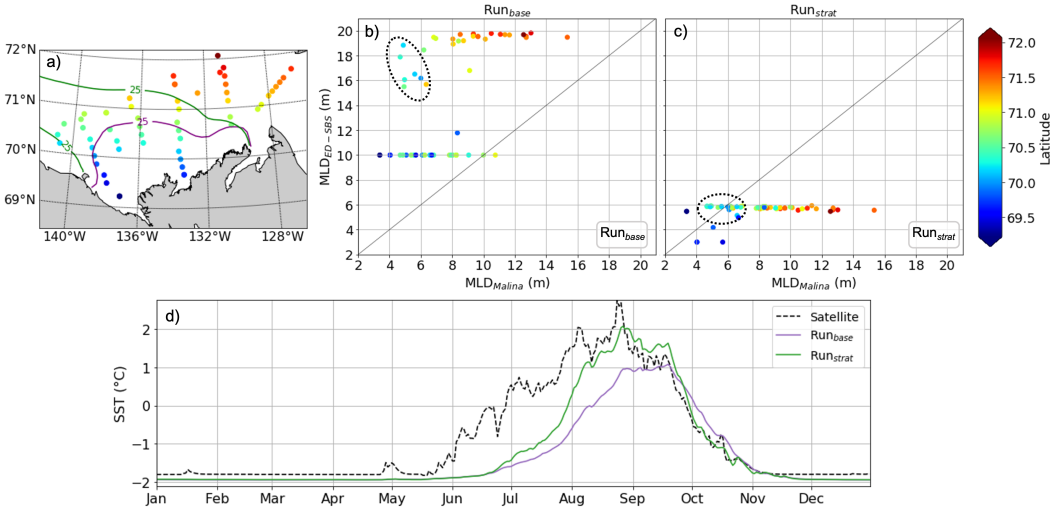

Figure 5.2: a) Location of the Malina cruise sampling stations with the 25 isohaline overlaid for Run$_{base}$ (solid purple line) and Run$_{strat}$ (solid green line). MLD model-observations comparison for (b) Run$_{base}$ (c) and Run$_{strat}$. The color scale represents the latitude of the matching points. d) Seasonal evolution of the satellite-derived and simulated daily SST on ED-SBS domain. On panels a) and b), the black circular shape indicates the stations situated within the plume in Run$_{strat}$ but outside the plume in Run$_{base}$.

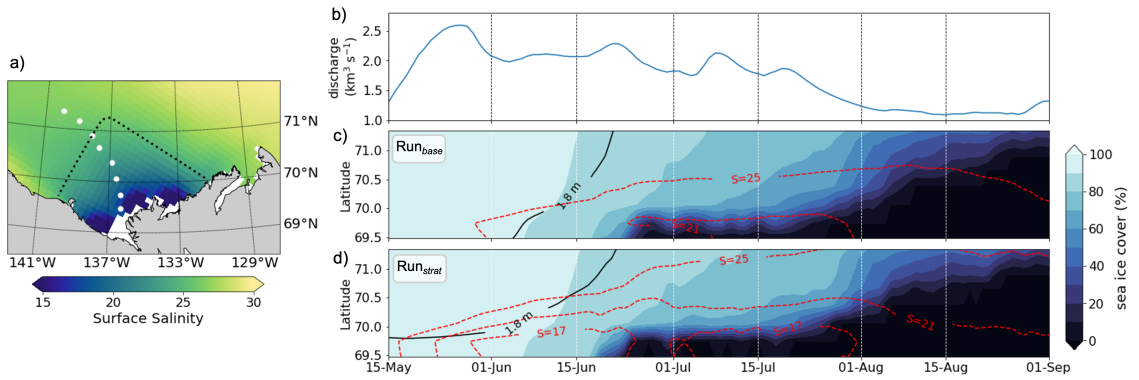

Figure 5.3: (a) Mean SSS simulated between June to September in Run$_{strat}$, (b) Mackenzie River discharge (km^3 s^{-1}), and Hovmöller plots showing the percentage of sea-ice cover in (c) Run$_{base}$ and (d) Run$_{strat}$ along the transect shown in panel a (white dots). On panels c) and d), the black and red lines indicate the simulated sea-ice thickness and sea surface isohalines, respectively.

of the simulated river plume simulated in Run$_{strat}$ dampens the DOR overestimation by about a week (Fig. 5.4ce). During the river freshet period, sea-ice cover is 100 % all over the river plume area in both Run$_{base}$ and Run$_{strat}$ (Fig. 5.3cd). However, in Run$_{strat}$, the warmer river freshwater spreads more under the ice (Fig. 5.3d). As a consequence, sea-ice thickness decreases (Fig. 5.3d) indicating enhanced bottom sea-ice melt triggered by the warmer river waters. During the second peak of river discharge between mid-June and early July, sea-ice cover shrinks at higher rates in Run$_{strat}$.

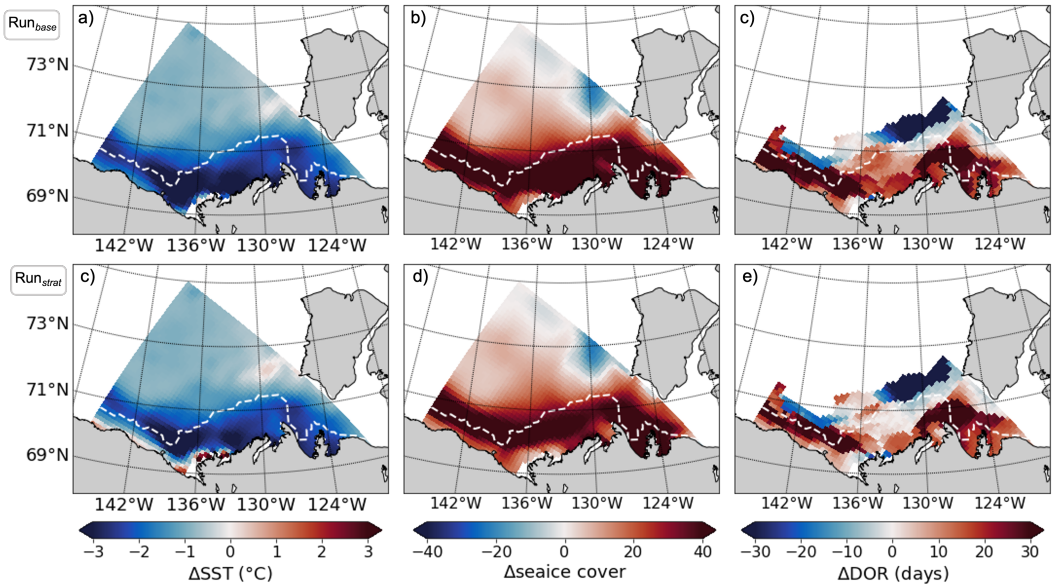

Figure 5.4: model-observations difference for (a) mean SST (June to July), (b) mean sea-ice cover (June to July) and (c) DOR with Run$_{base}$ (upper panels) and Run$_{strat}$ (lower panels). A model underestimation (overestimation) is represented in blue (red) shades.

5.3.3 Sensitivity to the river plume stratification: biogeochemistry

As a consequence of a stronger vertical stratification induced by a thinner top surface layer, all riverine nutrients in Run$_{strat}$ dilute within a smaller cell volume, which in turn increases their concentrations (Fig. 5.6ab). With more nutrients at the sea surface, ED-SBS simulates a 10% increase of PP in the river plume area (Domain in Fig. 5.3a) compared to Run$_{strat}$. However, simulated surface DOC concentrations and net air-sea CO_2 fluxes are the most impacted by the changes induced in the simulated physics (Table 5.3 and Fig. 5.5).

In Run$_{strat}$, the simulated means of surface DOC concentration more than double compared to Run$_{base}$ (Table 5.3). They depart even more from the observational mean by a factor 3 to 4. The correlation gets weaker, the accuracy of the linear regression model decreases by a factor up to 5, and the data dispersion reaches unrealistic values (287-350 mmolC m^{-3}). ED-SBS becomes a very poor predictor (NSE$\ll$0) of surface DOC concentrations. With respect to DIC, the comparison metrics show contrasted results on ED-SBS capacity to describe the observations (Table 5.3). In Run$_{strat}$, ED-SBS gains in accuracy (NSE=0.15) and simulates mean conditions (1830 $\pm$ 92 mmolC m^{-3}) in better accordance with the observations (1838 $\pm$ 92 mmolC m^{-3}). However, the correlation gets weaker and the dispersion slightly higher.

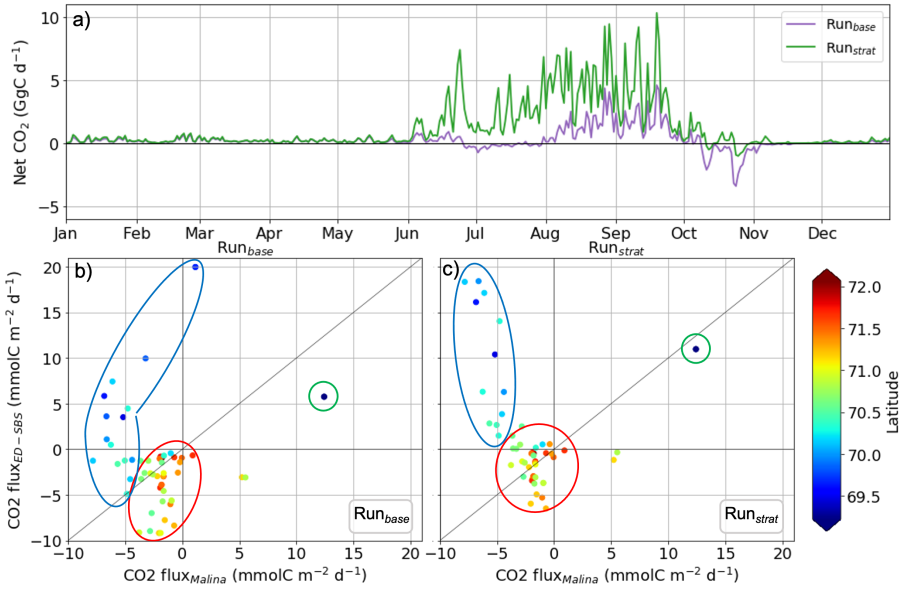

Figure 5.5: a) Simulated net daily air-sea CO_2 fluxes (GgC d^{-1}) spatially-integrated over the domain delimited by black dotted lines shown in Fig. 5.3. Model-observations comparison for (b) Run$_{base}$ and (c) Run$_{strat}$ (mmolC m^{-2} d^{-1}). The color scale represents the latitude of the model-observations matching points. The red and blue circular shapes show the matching points located north and south of 70.5°N, respectively. The green circular shape indicates the Shallow Bay station (<69.5°N).

Similarly, simulated air-sea CO_2 fluxes that depend on surface DOC and DIC concentrations are less consistent with *in situ* estimates in the river-influenced domain south of 70.5°N (Fig. 5.5bc), except an estuarine station near Shallow Bay (<69.5°N). The model-observations consistency is however improved above 70.5°N in waters less impacted by the river plume and where the simulated CO_2 outgassing weakens. Such a contrasted spatial pattern suggests that a DIC source might be underestimated in the model, such as shelf break upwellings. On a yearly basis, it results that Run$_{strat}$ simulates the highest CO_2 outgassing, which is 3.5-times more (0.45 TgC yr^{-1}) than in Run$_{base}$ (0.10 TgC yr^{-1}). In addition, this simulated outgassing occurs in June (Fig. 5.5), so 2 months earlier than in Run$_{base}$ (0.10 TgC yr^{-1}).

In ED-SBS, the riverine forcing is limited to the top surface layer and only on a few grid cells to get a realistic spatial distribution of the riverine inputs. However, figure 5.6c shows that this parameterization leads to unrealistic surface DOC concentrations with simulated values reaching up to 5,000 mmolC m^{-3}. In a last run (Run$_{strat+floc}$), we assess the effect of tDOC flocculation on the reported discrepancies between the simulated and remotly-sensed DOC concentrations. It results that adding tDOC flocculation in Run$_{strat}$ increases the NSE from -26.7 to -5.87 and decreased the URMSE from 287 to 147 mmolC m^3. Based on these two metrics, Run$_{strat+floc}$ is

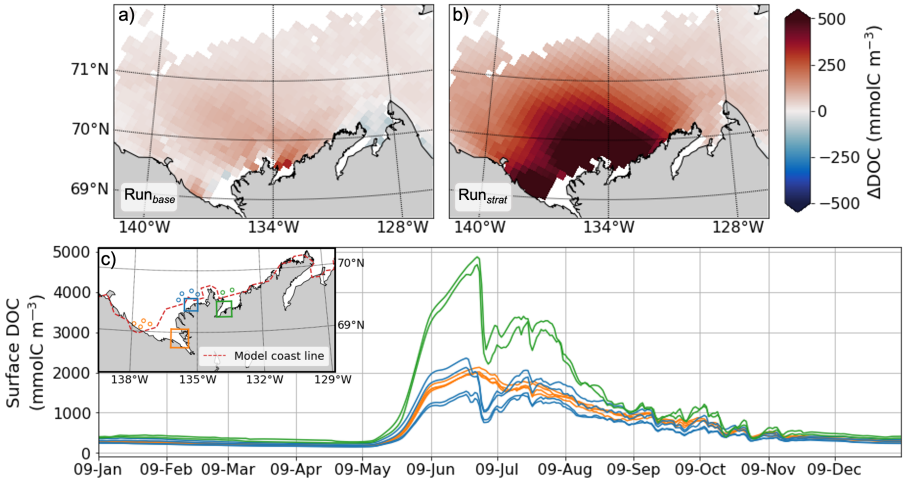

Figure 5.6: Mean difference between remotely-sensed and simulated surface DOC concentrations (mmol C m^{-3}) with (a) Run$_{base}$ and (b) Run$_{strat}$; a model underestimation (overestimation) is represented in blue (red) shades. (c) Surface DOC concentration (mmolC m^{-3}) simulated in Run$_{base}$ within grid cells receiving the riverine tDOC forcing; the grid cell location is indicated on the inset overlaid and colors represent the three major Mackenzie River outlets used to constrain the river forcing: Shallow Bay (orange), Beluga Bay (blue) and Kugmallit Bay (green).

improved with respect to Run$_{strat}$ but ED-SBS is still a poor predictor (NSE<0) with simulated DOC concentrations showing an high dispersion with regard to observations.

5.4 Discussion and conclusion

In this study, we quantify the sensitivity of ED-SBS to different parameterizations of the Mackenzie River and vertical grid resolution. Our results show that the model simulates very contrasting responses that reflect large uncertainties on predictions. In arctic watersheds, carbon fluxes are deeply altered by the unprecedented changes that the Arctic is undergoing (Schuur et al., 2015, 2022; Schwab et al., 2020; Saito et al., 2021). This translate into a wide range of reported tDOC quality, especially in terms of bioavailability once in nearshore and coastal waters (Kaiser et al., 2017; Mann et al., 2022). In this study, we have tested a high (Run$_{base}$) and low (Run$_{remin}$) tDOC remineralization scenario, both realistically constrained based on observations reported over the past 20 years (F. Joux, unpublished data from Nunataryuk Campaign, Holmes et al., 2008; Wickland et al., 2012; Shen et al., 2012). Unsurprisingly, tDOC recycling strongly modulates the ingassing or outgassing capacity of the ocean. However, we are not yet in the capacity to assess the most plausible trend as we are still very limited by the scarcity of carbon chemistry data in nearshore and coastal arctic waters. Most datasets exclude river-influenced waters (Yasunaka et al., 2018) or face a critical lack in data (Landschützer et al., 2020; Ouyang et al., 2021) making regional model studies rely on sporadic but still highly valuable synoptic field surveys (Forest et al., 2014).

In addition to tDOC quality, ED-SBS is also very responsive to chemical processes occurring at the freshwater-marine transition. Flocculation is reported as an important removal processes of tDOC in the Mackenzie and Lena deltas (Gonçalves-Araujo et al., 2015; Kipp et al., 2020), while it is not apparent in other Arctic estuaries (Amon & Meon, 2004; Clark et al., 2022). Flocculation of organic carbon is very complex to represent in models as it depends on numerous interacting processes involving water temperature, suspended solid concentration, and bacteria (Droppo et al., 1998; Lasareva et al., 2019). Flocculation in the delta may also alter the quantity of tDOP truly reaching coastal marine waters, whose remineralization into dissolved inorganic phosphorus can promote phytoplankton growth and then CO_2 uptake. Such biogeochemical processes require attention in predictive models as they may play an important role in the oceanic

CO_2 ingassing/outgassing balance as well as in the availability of organic matter farther on shelf. Beyond the freshwater-marine transition, tDOC is remineralized into DIC an important driver of the air-sea CO_2 fluxes. In ED-SBS, tDOC is degraded into DIC through a temperature-dependent function that implicitly represents the action of bacterioplankton. Representing tDOC remineralization in Arctic models is however not trivial and is receiving a growing attention. tDOC is a complex mixture that encompasses a wide range of molecular compounds degraded across a wide range of time scales (Lønborg et al., 2020; Dittmar et al., 2021). Recent studies, investigated the DOC removal across the land-ocean aquatic continuum (LOAC) with emphasis on photodegradation processes (Anderson et al., 2019; Clark et al., 2022). A new type of model based on the emergent recalcitrance concept (Dittmar et al., 2021) emerges with a more ecosystem representation of the microbial degradation (microbe-network model; Mentges et al., 2019, 2020; Zakem et al., 2021). Initially designed to simulate refractory DOC pool (degradation over decades), the microbe-network models could improve the simulation of DOC microbial degradation across the LOAC.

The response of the coastal ocean to riverine biogeochemical fluxes is also highly constrained by the physical settings of the regional model. We show that the simulated physics and biogeochemistry is very sensitive to the thickness of the plume. In Run$_{strat}$, riverine biogeochemical tracers enter the model within the 3 m top grid cell only, which is a realistic scheme with regard to observations (Macdonald & Yu, 2006; Mulligan & Perrie, 2019). The simulated physics is improved, but simulated tDOC concentrations are largely beyond the reported background. A solution could be to spread the freshwater discharge and riverine concentrations across several deeper grid cell to prevent any overshooting of concentration. However, it could imply nutrients to cycled in a different way than those entering only at the surface as not evenly exposed to same light and mixing conditions. Inorganic nutrients would be made unavailable for phytoplankton as delivered within the aphotic zone. Similarly, tDOC might not undergo photodegradation and get more easily mixed up in depth. Future ways to overcome such an issue might imply for instance to extend farther the lateral distribution of the riverine tracers according our knowledge of the main and minor delta mouths. The lateral surface diffusivity could also be increased to promote more lateral transport of the riverine tracers near their entry point in the model. This issue related to the riverine plume representation in arctic models is also highly related to the lateral resolution of model grid.

ED-SBS has a ∼10 km lateral resolution, which is nearly twice the estimated radius of baroclinic deformation estimated for the Canadian Archipelago and Beaufort Sea shelf (∼6 km; Nurser & Bacon, 2014). This means that the model does not reach yet the horizontal scale at which rotation effects become as important as buoyancy effects. This is important as it can alter the lateral transport of the riverine tracers off the coastline, but also the transport of the simulated sea-ice. As shown in this study, the timing of sea-ice opening/melting, freshwater discharge and air-sea CO_2 fluxes are highly related. With a finer lateral resolution below the estimated 6 km Rossby radius of deformation (Nurser & Bacon, 2014), we might expect from ED-SBS very different simulated oceanic and sea-ice conditions, especially in spring when sea-ice melts and the freshwater discharge reaches a seasonal maximum (Macdonald & Yu, 2006; Nghiem et al., 2014). In addition, a more detailed resolution of the coastline could facilitate a better representation of the terrestrial inputs of freshwater and nutrients in the model, alongside an improved representation of the ocean physics.

To conclude, we show that ED-SBS forced with tDOC fluxes and remineralization rates based on the observational range simulates the coastal SBS either as a source or a sink of CO_2, which departs from the most recent estimates (Terhaar et al., 2019; Lacroix et al., 2020). We also suggest that a refinement of the vertical grid improves the simulated SST of the riverine plume but also leads to spurious concentrations of the simulated biogeochemical tracers. This highlights that assessing the contribution of riverine biogeochemical tracers to the carbon cycle is very challenging in the Arctic, maybe more than elsewhere on the globe. First, the LOAC is a complex mosaic of landscape and soils that quickly respond to the rising air temperatures. Second, Arctic rivers flows in shelves whose dynamics is highly constrained by sea-ice imposing to models to reproduce complex plume-ice interactions in the appropriate way. Third, the remoteness of both the Arctic LOAC and shelf seas strongly impedes their monitoring and then robust model-observation comparisons at the land-to-sea interface.

In regard to these limitations, we believe that such an assessment of the rivers' contribution to the Arctic carbon cycle relies first on our capacity to generate consistent interannual time series of key biogeochemical tracers as the interannual signature of river plumes on air-sea CO_2 fluxes can be very high (Bertin et al., 2022, 2023). This can be achieved by merging *in situ* and remote sensing data (Bertin et al., 2022) and by taking advantage of recent advances made by watersheds models (e.g. ORCHIDEE model; Bowring et al., 2019, 2020) in simulating varying

semi-labile:semi-refractory tDOC ratios. Increasing the vertical and horizontal resolution in regional models is also a requisite to link the terrestrial inputs to the models' grids in a realistic physical and biogeochemical way, but also to predict their fate in the simulated elemental cycles. Regional approaches with an improved representation of deltas and estuaries can pave the way to future upscaling at the pan-Arctic scale for a better prediction of the rapidly changing Arctic carbon cycle.

CHAPTER

6 CONCLUSIONS

An ocean-sea ice-biogeochemical model (ED-SBS) was adapted to the SBS to investigate the effects of the Mackenzie River plume on the interannual (2000-2019) variability of air-sea CO_2 fluxes. Interannual land-to-sea fluxes of tDOC and tDIC/tAlk conveyed by the Mackenzie River were for the first time implemented in such a regional modeling framework. ED-SBS simulated NPP and net CO_2 fluxes consistent with available observations from the seasonal to interannual scale. Considering two qualitatively different tDOC pools (semi-labile and semi-refractory) improved our ability to simulate in coastal waters DOC concentrations close to both *in situ* measurements and remotely-sensed estimates. To that respect, ED-SBS provides new and robust insights on the contribution of tDOC to air-sea CO_2 fluxes in close vicinity of the land-to-sea interface :

- Merging riverine *in situ* tDOC concentrations with remotely-sensed estimates retrieved in the outermost vicinity of the Mackenzie Delta substantially increases the quantity of data during the open water season to compute land-to-sea fluxes of tDOC. The resulting interannual tDOC fluxes estimated at three major delta outlets reveal a shift in the seasonal distribution of the fluxes when compared to flux estimates based only on *in situ* data collected several hundred kilometers upstream in the river path. The spatial variability in the tDOC concentrations and flux amongst the three main delta outlets likely reflect distinct biogeochemical patterns affecting the quality and quantity of tDOC within the land-to-sea interface. Robust terrestrial tDOC fluxes to the coastal ocean are thus paramount to better understand and predict how changes in the land-sea linkages might alter the coastal carbon budget and air-sea CO_2 fluxes at the regional scale in the AO.

- Net air-sea CO_2 fluxes simulated in the Mackenzie River plume in 2000–2019 reveal CO_2 outgassing driven by the land-to-sea flux of carbon. The contribution of both riverine tDIC and tDOC to CO_2 outgassing (0.63 TgC yr^{-1}) is 8 times higher than phytoplankton contribution to CO_2 uptake (0.08 TgC yr^{-1}; Fig. 6.1). tDIC is estimated to contribute twice as much as tDOC to CO_2 outgassing, emphasizing all the importance of monitoring riverine tDIC in large Arctic rivers. The interannual variability of the Mackenzie River discharge strongly modulates the delicate air-sea CO_2 balance, which strengthens the need for implementing interannual runoff forcings in models and thus pursuing/reinforcing the monitoring of the land-to-sea interface.

- In addition to the river forcing, ED-SBS is also sensitive to the way the riverine biogeochemical tracers are transported and transformed once in the coastal ocean. Different ED-SBS parameterizations of tDOC lability and lifetime based on observations make the simulated

ocean either release (0.10 TgC yr^{-1}) or absorb CO_2 (-0.29 TgC yr^{-1}) (Δ = -0.39 TgC yr^{-1}; Fig. 6.1). tDOC flocculation could retain up to 0.14 TgC yr^{-1} within the ocean. In terms of physics, an improved representation of plume-driven stratification in ED-SBS translates into more CO_2 outgassing (0.35 TgC yr^{-1}) but very unrealistic surface DOC concentrations. These sensitivity analyses show how much the ocean capacity to act as a source or sink of CO_2 is still very uncertain in Arctic models. The representation of key mechanistic processes remains challenging and needs to be carefully considered in models to improve air-sea CO_2 flux estimates in the under-sampled coastal AO.

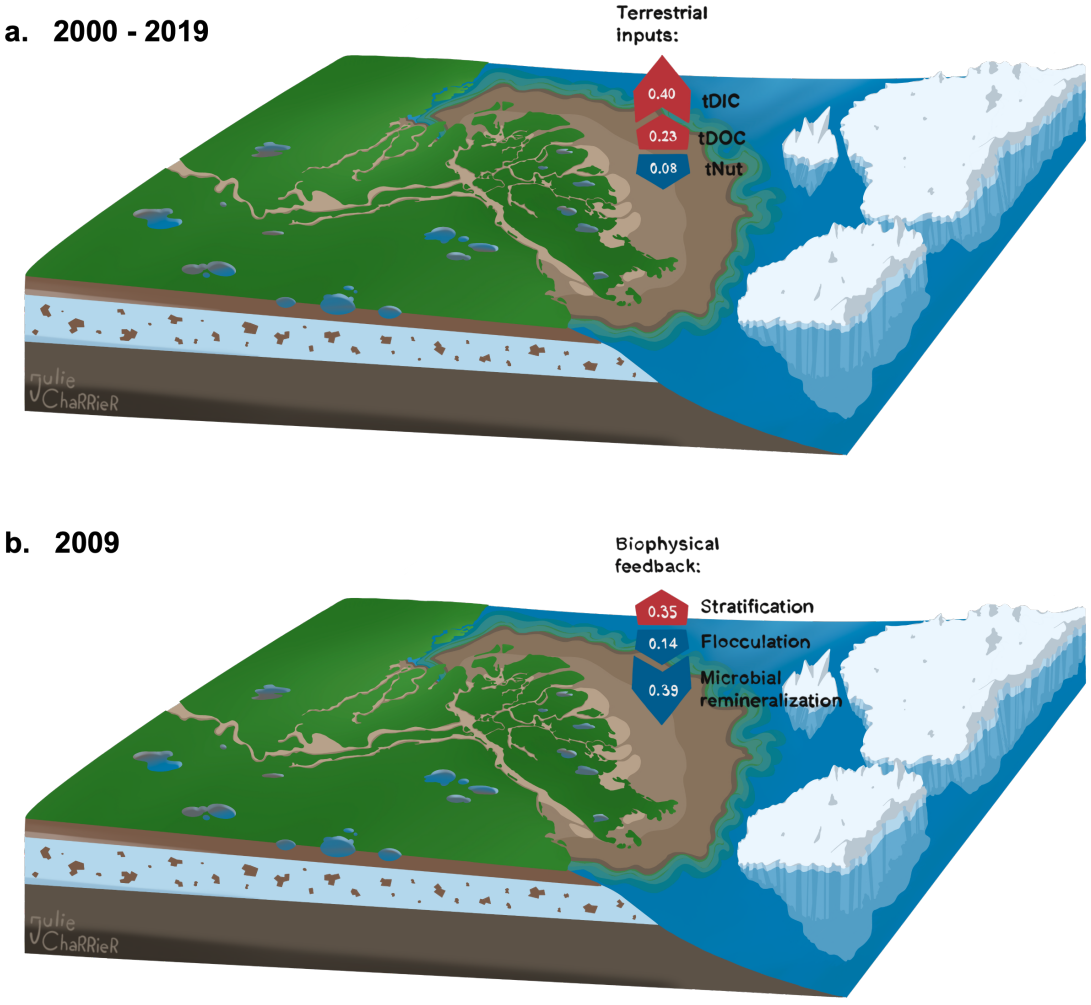

Figure 6.1: Schematic representation of the Mackenzie Delta and coastal waters highlighting the key results of the PhD thesis. Simulated CO_2 fluxes (TgC yr^{-1}) are shown and represented by arrows. Values are differences between runs with and without targeted biogeochemical tracers (upper panel) or biophysical processes (lower panel). Panels (a) and (b) represent simulated conditions for the 2000-2019 and 2009 periods, respectively. (Designed by Julie Charrier).

CHAPTER

7 PERSPECTIVES

The work undertaken during this PhD sheds light on the large range of variability of simulated CO_2 fluxes within a coastal Arctic sea under the strong influence of riverine waters. It also underlines the many challenges that remain to be tackled to gain more confidence on the mass fluxes of carbon between land, ocean and atmosphere in the Arctic. In this section, I introduce several future research pathways that could contribute to improve our ability to assess the land-to-sea flux of carbon and to predict their impact on the carbon cycle.

7.1 Towards a wider consideration of parameters driving the land-to-sea flux of carbon

In pan-Arctic rivers, chemodynamic relationships capture between 31 and 79 % (Griffin et al., 2018; Shrestha et al., 2019; Bertin et al., 2022) of DOC concentration variability meaning that other parameters could be considered to get more accurate land-to-sea flux of tDOC. Shrestha et al. (2019) propose to supplement non-linear fitting models with air temperature measurements as an indicator of seasonality. Additional parameters susceptible to depict the quantitative and qualitative dynamics of DOC could also be considered. Because of light absorbance (a_{CDOM}), the colored fraction of dissolved organic matter (CDOM) can explain 88 to 94 % of DOC variability at pan-Arctic scale (Matsuoka et al., 2017; Griffin et al., 2018), but also has a potential to provide extra information on tDOC photodegradation (Grunert et al., 2018). Besides, watersheds characteristics such as topography, vegetation or lakes abundance inform on tDOC origin and its potential to be degraded by microbes (Kaiser et al., 2017). Pooled together, this information might improve time series of land-to-sea flux of tDOC, but our lack of knowledge on the relationships linking all these variables together is the key limitation. To meet this purpose, artificial intelligence (AI) can help combine relevant and explanatory variables as already done for the open ocean (Roshan & DeVries, 2017). The fact that it requires large dataset still represents a major drawback in Arctic regions. However, collaborative open access platform such ©DataStream that host all data available in Canadian regions pave the way to bridge this gap. The availability of satellite data in such remote regions is also a prerequisite. Spectroradiometers onboard Aqua and LANDSAT satellites contribute to retrieve a_{CDOM} (Matsuoka et al., 2017; Griffin et al., 2018) and other landscape characteristics such as land temperature, vegetation (Nill et al., 2019) or flood duration on floodplains (Normandin et al., 2018). Recently, the SWOT mission launched high performance altimeters that would be able to provide large amounts of freshwater discharge data directly in river outlets (Biancamaria et al., 2016; Durand et al., 2016). The NASA's Plankton,

Aerosol, Cloud, ocean Ecosystem (PACE) mission planed to be launched in 2024 will send into orbit new advanced instruments also to support the need of large Earth observation dataset. Efforts as the Arctic-COLORS (Coastal Land Ocean Interactions in the Arctic) program will certainly contribute to merge all these dataset and better understand the fate of terrigenous carbon in remote Arctic coastal waters.

7.2 Explicit representation of the microbial degradation of organic matter

ED-SBS was developed based on a multi-compartment and implicit model of organic matter degradation (Multi-G model) in agreement with our best knowledge on DOC microbial degradation in the AO (Holmes et al., 2008; Wickland et al., 2012; Shen et al., 2012). Whilst providing a first order representation of the microbial degradation activity , the Multi-G model excludes any mass transfer related to the stock of heterotrophic bacteria. Explicit models of heterotrophic bacteria are available including a wide range of complexity in their ability to represent mechanistic processes at stake in the cycling and respiration of organic matter (Eichinger et al., 2011). For instance, Monod models with heterotrophic bacteria as a state variable allow microbial respiration to be simulated through a bacterial growth efficiency (BGE; Monod, 1942; Anderson & Williams, 1999; Eichinger et al., 2006). This kind of model was already successfully implemented in the global ECCO-Darwin configuration with the addition of a simplified nutrients co-limitation (constant rate) and temperature modulation (Zakem et al., 2018). Next generation of ED-SBS is already under development to simulate bacteria based on Zakem et al. (2018) Monod model along with Arctic-adapted PFTs. However, this type of model poorly describes the molecular diversity of the DOC pool, the different time scales associated to those pools, and their recycling into both DIC but also into more recalcitrant DOC. A new generation of models based on the emergent recalcitrance concept (Wagner et al., 2020; Dittmar et al., 2021) attempt to address this issue by simulating the recalcitrant DOC pool (degradation rates longer than decades), which is still largely unresolved by classic models (Mentges et al., 2019, 2020; Zakem et al., 2021). In such models, heterotrophic bacteria are represented as an ecosystem composed several types of bacteria with their own properties able to degrade several types of DOC compounds. Using this approach in ED-SBS would allow to consider finer temporal scales of tDOC degradation and then to simulate recalcitrant DOC in biogeochemical models as ECCO-Darwin.

7.3 The biophysical feedback of Colored Dissolved Organic Matter (CDOM)

ED-SBS sensitivity experiments conducted in this PhD thesis showed that the physics of the plume largely impacts the biogeochemistry and hence air-sea CO_2 fluxes estimates. However, how biogeochemistry could alter the simulated physics was not investigated. Optical properties of autochtonous CDOM were reported to substantially attenuate light and to increase SST in the AO through radiative heating of the ocean surface (Hill, 2008; Pefanis et al., 2020). In the AO, the radiative heating induced by autochtonous CDOM was shown to promote sea ice melt (Pefanis et al., 2020). Considering the large amount of CDOM exported by rivers towards Arctic shelves (Stedmon et al., 2011; Matsuoka et al., 2017), this effect is expected to be even greater at the coast (Gnanadesikan et al., 2019; Soppa et al., 2019). The interaction between CDOM and the light spectrum decreases exponentially from near UV to visible light (300 to $\sim$650 nm). However, the only few models explicitly simulating a CDOM state variable (then expressed in mass) are focused solely on the photosynthetically active Radiation (PAR) (Gnanadesikan et al., 2019; Pefanis et al., 2020; Neumann et al., 2021). However, data from the ANR Malina project (2008-2012) suggest that 40 % of the total light spectrum is absorbed by CDOM in the near-UV. Accounting for the full sepctrum of shortwave radiation (near-UV to infrared) is thus required to assess any possible optical feedback of terrestrial CDOM on the ocean physics and thus biogeochemistry. A next generation of ED-SBS is under development (not presented in the thesis since more exploratory) to include an explicit CDOM state variable constrained by riverine tDOC from the Mackenzie and interacting with the full integrated light spectrum. Coupled to the recent developments of version 5 of ECCO-Dawin model, which includes a radiative transfer model (Dutkiewicz et al., 2015), it might further contribute to improve ED-SBS ability to predict the ocean state estimate of the SBS.

References

Aarnos, H., Gélinas, Y., Kasurinen, V., Gu, Y., Puupponen, V.-M., & Vähätalo, A. V. (2018). Photochemical mineralization of terrigenous DOC to dissolved inorganic carbon in ocean. *Global Biogeochemical Cycles*, *32*(2), 250–266. doi: https://doi.org/10.1002/2017GB005698

Adcroft, A., & Campin, J.-M. (2004). Rescaled height coordinates for accurate representation of free-surface flows in ocean circulation models. *Ocean Modelling*, *7*(3-4), 269–284. doi: https://doi.org/10.1016/j.ocemod.2003.09.003

Ahmed, R., Prowse, T., Dibike, Y., Bonsal, B., & O'Neil, H. (2020). Recent trends in freshwater influx to the Arctic Ocean from four major Arctic-draining rivers. *Water*, *12*(4). doi: https://doi.org/10.3390/w12041189

Akaike, H. (1974). A new look at the statistical model identification. *IEEE transactions on automatic control*, *19*(6), 716–723. doi: https://doi.org/10.1109/TAC.1974.1100705

Åkerman, H. J., & Johansson, M. (2008). Thawing permafrost and thicker active layers in sub-arctic Sweden. *Permafrost and periglacial processes*, *19*(3), 279–292. doi: https://doi.org/10.1002/ppp.626

AMAP. (2021). Arctic Climate Change Update 2021: Key Trends and Impacts. *Summary for Policy-makers. Arctic Monitoring and Assessment Programme (AMAP)*.

Amon, R. M., & Meon, B. (2004). The biogeochemistry of dissolved organic matter and nutrients in two large Arctic estuaries and potential implications for our understanding of the Arctic Ocean system. *Marine Chemistry*, *92*(1-4), 311–330. doi: https://doi.org/10.1016/j.marchem.2004.06.034

Amon, R. M., Rinehart, A., Duan, S., Louchouarn, P., Prokushkin, A., Guggenberger, G., ... Zhulidov, A. (2012). Dissolved organic matter sources in large Arctic rivers. *Geochimica et Cosmochimica Acta*, *94*, 217–237. doi: https://doi.org/10.1016/j.gca.2012.07.015

Anderson, T. R., Rowe, E., Polimene, L., Tipping, E., Evans, C., Barry, C., ... Waska, H. (2019). Unified concepts for understanding and modelling turnover of dissolved organic matter from freshwaters to the ocean: the uniDOM model. *Biogeochemistry*, *146*(2), 105–123. doi: https://doi.org/10.1007/s10533-019-00621-1

Anderson, T. R., & Williams, P. J. l. B. (1999). A one-dimensional model of dissolved organic carbon cycling in the water column incorporating combined biological-photochemical decomposition. *Global Biogeochemical Cycles*, *13*(2), 337–349. doi: https://doi.org/10.1029/1999GB900013

Ardyna, M., & Arrigo, K. R. (2020). Phytoplankton dynamics in a changing Arctic Ocean. *Nature Climate Change*, *10*(10), 892–903. doi: https://doi.org/10.1038/s41558-020-0905-y

Arrigo, K. R., Pabi, S., van Dijken, G. L., & Maslowski, W. (2010). Air–sea flux of CO_2 in the Arctic Ocean, 1998–2003. *Journal of Geophysical Research: Biogeosciences*, *115*. doi: https://doi.org/10.1029/2009JG001224

Arrigo, K. R., & van Dijken, G. L. (2015). Continued increases in Arctic Ocean primary production. *Progress in Oceanography*, *136*, 60–70. doi: https://doi.org/10.1016/j.pocean.2015.05.002

Arzhanov, M., Eliseev, A., & Mokhov, I. (2013). Impact of climate changes over the extratropical land on permafrost dynamics under RCP scenarios in the 21st century as simulated by the IAP RAS climate model. *Russian meteorology and hydrology*, *38*(7), 456–464. doi: https://doi.org/10.3103/S1068373913070030

Bartsch, A., Höfler, A., Kroisleitner, C., & Trofaier, A. M. (2016). Land cover mapping in northern high latitude permafrost regions with satellite data: Achievements and remaining challenges. *Remote Sensing*, *8*(12), 979. doi: https://doi.org/10.3390/rs8120979

Bates, N., & Mathis, J. (2009). The Arctic Ocean marine carbon cycle: evaluation of air–sea CO_2 exchanges, ocean acidification impacts and potential feedbacks. *Biogeosciences*, *6*(11), 2433–2459. doi: https://doi.org/10.5194/bg-6-2433-2009

Bauer, J., & Bianchi, T. (2011). Dissolved Organic Carbon Cycling and Transformation. *Treatise on estuarine and coastal science*, *5*, 7–67. doi: https://doi.org/10.1016/B978-0-12-374711-2.00502-7

Behnke, M. I., McClelland, J. W., Tank, S. E., Kellerman, A. M., Holmes, R. M., Haghipour, N., ... Spencer, R. G. M. (2021). Pan-Arctic riverine dissolved organic matter: Synchronous molecular stability, shifting sources and subsidies. *Global Biogeochemical Cycles*, *35*(4). doi: https://doi.org/10.1029/2020GB006871

Bélanger, S., Babin, M., & Tremblay, J.-É. (2013). Increasing cloudiness in Arctic damps the increase in phytoplankton primary production due to sea ice receding. *Biogeosciences*, *10*(6), 4087–4101. doi: https://doi.org/10.5194/bg-10-4087-2013

Belanger, S., Xie, H., Krotkov, N., Larouche, P., Vincent, W. F., & Babin, M. (2006). Photomineralization of terrigenous dissolved organic matter in Arctic coastal waters from 1979 to 2003: Interannual variability and implications of climate change. *Global Biogeochemical Cycles*, *20*(4). doi: https://doi.org/10.1029/2006GB002708

Bertin, C., Carroll, D., Menemenlis, D., Dutkiewicz, S., Zang, H., Matsuoka, A., ... Le Fouest, V. (2023). Biogeochemical river runoff drives intense coastal Arctic Ocean CO_2 outgassing. *Geophysical Research Letters*, *50*. doi: https://doi.org/10.1029/2022GL102377

Bertin, C., Matsuoka, A., Mangin, A., Babin, M., & Le Fouest, V. (2022). Merging Satellite and *in situ* Data to Assess the Flux of Terrestrial Dissolved Organic Carbon From the Mackenzie River to the Coastal Beaufort Sea. *Frontiers in Earth Science*, *10*. doi: https://doi.org/10.3389/feart.2022.694062

Biancamaria, S., Lettenmaier, D. P., & Pavelsky, T. M. (2016). The SWOT mission and its capabilities for land hydrology. In *Remote sensing and water resources* (pp. 117–147). Springer. doi: https://doi.org/10.1007/s10712-015-9346-y

Bianchi, T. S. (2011). The role of terrestrially derived organic carbon in the coastal ocean: A changing paradigm and the priming effect. *Proceedings of the National Academy of Sciences*, *108*(49), 19473–19481. doi: https://doi.org/10.1073/pnas.1017982108

Blackburn, J., She, Y., Hicks, F., & Nafziger, J. (2015). Ice effects on flow distributions in the Mackenzie Delta. In *Proceedings of 18th workshop on the hydraulics of ice covered rivers, quebec city, quebec* (pp. 18–20).

Bowring, S. P., Lauerwald, R., Guenet, B., Zhu, D., Guimberteau, M., Regnier, P., ... Ciais, P. (2020). ORCHIDEE MICT-LEAK (r5459), a global model for the production, transport, and transformation of dissolved organic carbon from Arctic permafrost regions–Part 2: Model evaluation over the Lena River basin. *Geoscientific Model Development*, *13*(2), 507–520. doi: https://doi.org/10.5194/gmd-13-507-2020

Bowring, S. P., Lauerwald, R., Guenet, B., Zhu, D., Guimberteau, M., Tootchi, A., ... Ciais, P. (2019). ORCHIDEE MICT-LEAK (r5459), a global model for the production, transport, and transformation of dissolved organic carbon from Arctic permafrost regions–Part 1: Rationale, model description, and simulation protocol. *Geoscientific Model Development*, *12*(8), 3503–3521. doi: https://doi.org/10.5194/gmd-12-3503-2019

Box, J. E., Colgan, W. T., Christensen, T. R., Schmidt, N. M., Lund, M., Parmentier, F.-J. W., ... Olsen, M. S. (2019). Key indicators of Arctic climate change: 1971–2017. *Environmental Research Letters*, *14*(4). doi: https://doi.org/10.1088/1748-9326/aafc1b

Bristol, E. M., Connolly, C. T., Lorenson, T. D., Richmond, B. M., Ilgen, A. G., Choens, R. C., ... McClelland, J. W. (2021). Geochemistry of coastal permafrost and erosion-driven organic matter fluxes to the Beaufort Sea near Drew Point, Alaska. *Frontiers in Earth Science*, *8*.

doi: https://doi.org/10.3389/feart.2020.598933

Brix, H., Menemenlis, D., Hill, C., Dutkiewicz, S., Jahn, O., Wang, D., ... Zhang, H. (2015). Using Green's Functions to initialize and adjust a global, eddying ocean biogeochemistry general circulation model. *Ocean Modelling*, *95*, 1–14.

Brown, K. A., Holding, J. M., & Carmack, E. C. (2020). Understanding regional and seasonal variability is key to gaining a Pan-Arctic perspective on Arctic Ocean freshening. *Frontiers in Marine Science*, *7*. doi: https://doi.org/10.3389/fmars.2020.00606

Bruhn, A. D., Stedmon, C. A., Comte, J., Matsuoka, A., Speetjens, N. J., Tanski, G., ... Sjöstedt, J. (2021). Terrestrial dissolved organic matter mobilized from eroding permafrost controls microbial community composition and growth in Arctic coastal zones. *Frontiers in Earth Science*, *9*. doi: https://doi.org/10.3389/feart.2021.640580

Burn, C. R., & Kokelj, S. V. (2009). The environment and permafrost of the Mackenzie Delta area. *Permafrost and periglacial processes*, *20*(2), 83–105. doi: https://doi.org/10.1002/ppp.655

Carmack, E. C., Barber, D., Christensen, J., Macdonald, R., Rudels, B., & Sakshaug, E. (2006). Climate variability and physical forcing of the food webs and the carbon budget on panarctic shelves. *Progress in Oceanography*, *71*(2-4), 145–181. doi: https://doi.org/10.1016/j.pocean.2006.10.005

Carmack, E. C., & Macdonald, R. W. (2002). Oceanography of the Canadian Shelf of the Beaufort Sea: a setting for marine life. *Arctic*, 29–45. doi: https://www.jstor.org/stable/40512418

Carmack, E. C., Macdonald, R. W., & Jasper, S. (2004). Phytoplankton productivity on the Canadian Shelf of the Beaufort Sea. *Marine Ecology Progress Series*, *277*, 37–50. doi: https://doi.org/10.3354/meps277037

Carroll, D., Menemenlis, D., Adkins, J., Bowman, K., Brix, H., Dutkiewicz, S., ... Zhang, H. (2020). The ECCO-Darwin data-assimilative global ocean biogeochemistry model: Estimates of seasonal to multidecadal surface ocean pCO_2 and air–sea CO_2 flux. *Journal of Advances in Modeling Earth Systems*, *12*(10). doi: https://doi.org/10.1029/2019MS001888

Carroll, D., Menemenlis, D., Dutkiewicz, S., Lauderdale, J. M., Adkins, J. F., Bowman, K. W., ... Zhang, H. (2022). Attribution of Space-Time Variability in Global-Ocean Dissolved Inorganic Carbon. *Global Biogeochemical Cycles*, *36*(3). doi: https://doi.org/10.1029/2021GB007162

Chadburn, S., Burke, E., Cox, P., Friedlingstein, P., Hugelius, G., & Westermann, S. (2017). An observation-based constraint on permafrost loss as a function of global warming. *Nature Climate Change*, *7*(5), 340–344. doi: https://doi.org/10.1038/nclimate3262

Charette, M. A., Kipp, L. E., Jensen, L. T., Dabrowski, J. S., Whitmore, L. M., Fitzsimmons, J. N., ... Zhang, R. (2020). The Transpolar Drift as a source of riverine and shelf-derived trace elements to the central Arctic Ocean. *Journal of Geophysical Research: Oceans*, *125*(5), e2019JC015920. doi: https://doi.org/10.1029/2019JC015920

Clark, J. B., Mannino, A., Tzortziou, M., Spencer, R. G., & Hernes, P. (2022). The Transformation and Export of Organic Carbon Across an Arctic River-Delta-Ocean Continuum. *Journal of Geophysical Research: Biogeosciences*, *127*(12), e2022JG007139. doi: https://doi.org/10.1029/2022JG007139

Colatriano, D., Tran, P. Q., Guéguen, C., Williams, W. J., Lovejoy, C., & Walsh, D. A. (2018). Genomic evidence for the degradation of terrestrial organic matter by pelagic Arctic Ocean Chloroflexi bacteria. *Communications biology*, *1*(1). doi: https://doi.org/10.1038/s42003-018-0086-7

Connolly, C. T., Cardenas, M. B., Burkart, G. A., Spencer, R. G., & McClelland, J. W. (2020). Groundwater as a major source of dissolved organic matter to Arctic coastal waters. *Nature communications*, *11*(1), 1–8. doi: https://doi.org/10.1038/s41467-020-15250-8

Coupel, P., Matsuoka, A., Ruiz-Pino, D., Gosselin, M., Marie, D., Tremblay, J.-É., & Babin, M.

(2015). Pigment signatures of phytoplankton communities in the Beaufort Sea. *Biogeosciences*, *12*(4), 991–1006. doi: https://doi.org/10.5194/bg-12-991-2015

Dai, M., Su, J., Zhao, Y., Hofmann, E. E., Cao, Z., Cai, W.-J., ... Wang, Z. (2022). Carbon fluxes in the Coastal Ocean: Synthesis, boundary processes, and future trends. *Annual Review of Earth and Planetary Sciences*, *50*, 593–626. doi: https://doi.org/10.1146/annurev-earth-032320-090746

Dittmar, T., & Kattner, G. (2003). The biogeochemistry of the river and shelf ecosystem of the Arctic Ocean: a review. *Marine chemistry*, *83*, 103–120. doi: https://doi.org/10.1016/S0304-4203(03)00105-1

Dittmar, T., Lennartz, S. T., Buck-Wiese, H., Hansell, D. A., Santinelli, C., Vanni, C., ... Hehemann, J.-H. (2021). Enigmatic persistence of dissolved organic matter in the ocean. *Nature Reviews Earth & Environment*, *2*(8), 570–583. doi: https://doi.org/10.1038/s43017-021-00183-7

Dobinski, W. (2011). Permafrost. *Earth-Science Reviews*, *108*(3-4), 158–169. doi: https://doi.org/10.1016/j.earscirev.2011.06.007

Doxaran, D., Devred, E., & Babin, M. (2015). A 50% increase in the mass of terrestrial particles delivered by the Mackenzie River into the Beaufort Sea (Canadian Arctic Ocean) over the last 10 years. *Biogeosciences*, *12*(11), 3551–3565. doi: https://doi.org/10.5194/bg-12-3551-2015

Drake, T. W., Guillemette, F., Hemingway, J. D., Chanton, J. P., Podgorski, D. C., Zimov, N. S., & Spencer, R. G. (2018). The ephemeral signature of permafrost carbon in an Arctic fluvial network. *Journal of Geophysical Research: Biogeosciences*, *123*(5), 1475–1485. doi: https://doi.org/10.1029/2017JG004311

Droppo, I., Jeffries, D., Jaskot, C., & Backus, S. (1998). The prevalence of freshwater flocculation in cold regions: a case study from the Mackenzie River Delta, Northwest Territories, Canada. *Arctic*, 155–164. doi: https://doi.org/10.14430/arctic1056

Durand, M., Gleason, C., Garambois, P.-A., Bjerklie, D., Smith, L., Roux, H., ... Vilmin, L. (2016). An intercomparison of remote sensing river discharge estimation algorithms from measurements of river height, width, and slope. *Water Resources Research*, *52*(6), 4527–4549. doi: https://doi.org/10.1002/2015WR018434

Dutkiewicz, S., Follows, M. J., & Bragg, J. G. (2009). Modeling the coupling of ocean ecology and biogeochemistry. *Global Biogeochemical Cycles*, *23*(4). doi: https://doi.org/10.1029/2008GB003405

Dutkiewicz, S., Hickman, A., Jahn, O., Gregg, W., Mouw, C., & Follows, M. (2015). Capturing optically important constituents and properties in a marine biogeochemical and ecosystem model. *Biogeosciences*, *12*(14), 4447–4481. doi: https://doi.org/10.5194/bg-12-4447-2015

Dutkiewicz, S., Scott, J. R., & Follows, M. (2013). Winners and losers: Ecological and biogeochemical changes in a warming ocean. *Global Biogeochemical Cycles*, *27*(2), 463–477. doi: https://doi.org/10.1002/gbc.20042

Eichinger, M., Poggiale, J.-C., & Sempéré, R. (2011). Toward a mechanistic approach to modeling bacterial DOC pathways: a review. *Science*, 66–68. doi: https://doi.org/10.1126/science.opms.sb0001

Eichinger, M., Poggiale, J.-C., Van Wambeke, F., Lefèvre, D., & Sempéré, R. (2006). Modelling DOC assimilation and bacterial growth efficiency in biodegradation experiments: a case study in the Northeast Atlantic Ocean. *Aquatic microbial ecology*, *43*(2), 139–151. doi: https://doi.org/10.3354/ame043139

Else, B., Papakyriakou, T., Galley, R., Mucci, A., Gosselin, M., Miller, L., ... Thomas, H. (2012). Annual cycles of pCO_{2sw} in the southeastern Beaufort Sea: New understandings of air–sea CO_2 exchange in arctic polynya regions. *Journal of Geophysical Research: Oceans*,

117(C9).

Emmerton, C. A., Lesack, L. F., & Vincent, W. F. (2008b). Nutrient and organic matter patterns across the Mackenzie River, estuary and shelf during the seasonal recession of sea-ice. *Journal of Marine Systems*, *74*(3-4), 741–755. doi: https://doi.org/10.1016/j.jmarsys.2007.10.001

Emmerton, C. A., Lesack, L. F. W., & Vincent, W. F. (2008a). Mackenzie River nutrient delivery to the Arctic Ocean and effects of the Mackenzie Delta during open water conditions. *Global Biogeochemical Cycles*, *22*(1). doi: https://doi.org/10.1029/2006GB002856

Evans, W., Mathis, J. T., Cross, J. N., Bates, N. R., Frey, K. E., Else, B. G., ... Takahashi, T. (2015). Sea-air CO_2 exchange in the western Arctic coastal ocean. *Global Biogeochemical Cycles*, *29*(8), 1190–1209. doi: https://doi.org/10.1002/2015GB005153

Fekete, B. M., Vörösmarty, C. J., & Grabs, W. (2002). High-resolution fields of global runoff combining observed river discharge and simulated water balances. *Global Biogeochemical Cycles*, *16*(3), 15–1. doi: https://doi.org/10.1029/1999GB001254

Feng, D., Gleason, C. J., Lin, P., Yang, X., Pan, M., & Ishitsuka, Y. (2021). Recent changes to Arctic river discharge. *Nature communications*, *12*(1). doi: https://doi.org/10.1038/s41467-021-27228-1

Follows, M. J., & Dutkiewicz, S. (2011). Modeling diverse communities of marine microbes. *Annual review of marine science*, *3*(1), 427–451. doi: https://doi.org/10.1146/annurev-marine-120709-142848

Follows, M. J., Dutkiewicz, S., Grant, S., & Chisholm, S. W. (2007). Emergent biogeography of microbial communities in a model ocean. *science*, *315*(5820), 1843–1846. doi: https://doi.org/10.1126/science.1138544

Follows, M. J., Ito, T., & Dutkiewicz, S. (2006). On the solution of the carbonate chemistry system in ocean biogeochemistry models. *Ocean Modelling*, *12*(3–4), 290–301. doi: https://doi.org/10.1016/j.ocemod.2005.05.004

Forest, A., Coupel, P., Else, B., Nahavandian, S., Lansard, B., Raimbault, P., ... Babin, M. (2014). Synoptic evaluation of carbon cycling in the Beaufort Sea during summer: contrasting river inputs, ecosystem metabolism and air–sea CO_2 fluxes. *Biogeosciences*, *11*(10), 2827–2856. doi: https://doi.org/10.5194/bg-11-2827-2014

Fritz, M., Vonk, J. E., & Lantuit, H. (2017). Collapsing arctic coastlines. *Nature Climate Change*, *7*(1), 6–7. doi: https://doi.org/10.1038/nclimate3188

Fukumori, I. (2002). A partitioned kalman filter and smoother. *Monthly Weather Review*, *130*(5), 1370–1383. doi: https://doi.org/10.1175/1520-0493(2002)130<1370:APKFAS>2.0.CO;2

Galeron, M.-A., Radakovitch, O., Charrière, B., Vaultier, F., Volkman, J. K., Bianchi, T. S., ... Rontania, J.-F. (2018). Lipoxygenase-induced autoxidative degradation of terrestrial particulate organic matter in estuaries: A widespread process enhanced at high and low latitude. *Organic Geochemistry*, *115*, 78–92. doi: https://doi.org/10.1016/j.orggeochem.2017.10.013

Gareis, J. A., & Lesack, L. F. (2020). Ice-out and freshet fluxes of CO_2 and CH_4 across the air–water interface of the channel network of a great Arctic delta, the Mackenzie. *Polar Research*. doi: https://doi.org/10.33265/polar.v39.3528

Gelfan, A., Gustafsson, D., Motovilov, Y., Arheimer, B., Kalugin, A., Krylenko, I., & Lavrenov, A. (2017). Climate change impact on the water regime of two great Arctic rivers: modeling and uncertainty issues. *Climatic change*, *141*(3), 499–515. doi: https://doi.org/10.1007/s10584-016-1710-5

Gent, P. R., & Mcwilliams, J. C. (1990). Isopycnal mixing in ocean circulation models. *Journal of Physical Oceanography*, *20*(1), 150–155. doi: https://doi.org/10.1175/1520-0485(1990)020<0150:IMIOCM>2.0.CO;2

Gibson, G. A., Elliott, S. M., Piliouras, A., Kinney, J. L., & Jeffery, N. (2022). Assessing the potential impact of river chemistry on Arctic coastal production. *Frontiers in Marine Science*, 675.

Gnanadesikan, A., Kim, G. E., & Pradal, M.-A. S. (2019). Impact of colored dissolved materials on the annual cycle of sea surface temperature: Potential implications for extreme ocean temperatures. *Geophysical Research Letters*, *46*(2), 861–869. doi: https://doi.org/10.1029/2018GL080695

Gonçalves-Araujo, R., Stedmon, C. A., Heim, B., Dubinenkov, I., Kraberg, A., Moiseev, D., & Bracher, A. (2015). From fresh to marine waters: Characterization and fate of dissolved organic matter in the Lena River Delta Region, Siberia. *Frontiers in Marine Science*, *2*, 108. doi: https://doi.org/10.3389/fmars.2015.00108

Good, S., Fiedler, E., Mao, C., Martin, M. J., Maycock, A., Reid, R., ... Worsfold, M. (2020). The current configuration of the OSTIA system for operational production of foundation sea surface temperature and ice concentration analyses. *Remote Sensing*, *12*(4). doi: https://doi.org/10.3390/rs12040720

Griffin, C., McClelland, J., Frey, K., Fiske, G., & Holmes, R. (2018). Quantifying CDOM and DOC in major Arctic rivers during ice-free conditions using Landsat TM and ETM+ data. *Remote Sensing of Environment*, *209*, 395–409. doi: https://doi.org/10.1016/j.rse.2018.02.060

Grunert, B. K., Mouw, C. B., & Ciochetto, A. B. (2018). Characterizing CDOM spectral variability across diverse regions and spectral ranges. *Global Biogeochemical Cycles*, *32*(1), 57–77. doi: https://doi.org/10.1002/2017GB005756

Guieu, C., Huang, W. W., Martin, J.-M., & Yong, Y. Y. (1996). Outflow of trace metals into the Laptev Sea by the Lena River. *Marine Chemistry*, *53*(3-4), 255–267. doi: https://doi.org/10.1016/0304-4203(95)00093-3

Hansell, D. A., Kadko, D., & Bates, N. R. (2004). Degradation of terrigenous dissolved organic carbon in the western Arctic Ocean. *Science*, *304*(5672), 858–861. doi: https://doi.org/10.1126/science.1096175

Harper, J. R. (1990). Morphology of the Canadian Beaufort Sea coast. *Marine Geology*, *91*(1-2), 75–91. doi: https://doi.org/10.1016/0025-3227(90)90134-6

Herlemann, D. P., Manecki, M., Meeske, C., Pollehne, F., Labrenz, M., Schulz-Bull, D., ... Jürgens, K. (2014). Uncoupling of bacterial and terrigenous dissolved organic matter dynamics in decomposition experiments. *PloS one*, *9*(4). doi: https://doi.org/10.1371/journal.pone.0093945

Hilborn, A., & Devred, E. (2022). Delineation of Eastern Beaufort Sea sub-regions using self-organizing maps applied to 17 years of MODIS-Aqua data. *Frontiers in Marine Science*, 1061. doi: https://doi.org/10.3389/fmars.2022.912865

Hill, V. J. (2008). Impacts of chromophoric dissolved organic material on surface ocean heating in the Chukchi Sea. *Journal of Geophysical Research: Oceans*, *113*(C7). doi: https://doi.org/10.1029/2007JC004119

Holmes, R. M., Coe, M. T., Fiske, G. J., Gurtovaya, T., McClelland, J. W., Shiklomanov, A. I., ... Zhulidov, A. V. (2013). Climatic change and global warming of inland waters. *In Climate change impacts on the hydrology and biogeochemistry of Arctic rivers*, 1–26.

Holmes, R. M., McClelland, J. W., Peterson, B. J., Tank, S. E., Bulygina, E., Eglinton, T. I., ... Zimov, S. A. (2012). Seasonal and annual fluxes of nutrients and organic matter from large rivers to the Arctic Ocean and surrounding seas. *Estuaries and Coasts*, *35*(2), 369–382. doi: https://doi.org/10.1007/s12237-011-9386-6

Holmes, R. M., McClelland, J. W., Raymond, P. A., Frazer, B. B., Peterson, B. J., & Stieglitz, M. (2008). Lability of DOC transported by Alaskan rivers to the Arctic Ocean. *Geophysical*

Research Letters, *35*(3). doi: https://doi.org/10.1029/2007GL032837

Holmes, R. M., McClelland, J. W., Tank, S. E., Spencer, R. G., & Shiklomanov, A. I. (2021). *ArcticGRO Water Quality Dataset* (Tech. Rep.). Version 2021-05-27, available at: https://arcticgreatrivers.org/data/.

Hoppe, C. J. (2022). Always ready? Primary production of Arctic phytoplankton at the end of the polar night. *Limnology and Oceanography Letters*, *7*(2), 167–174. doi: https://doi.org/10.1002/lol2.10222

Hugelius, G., Strauss, J., Zubrzycki, S., Harden, J. W., Schuur, E., Ping, C.-L., ... Kuhry, P. (2014). Estimated stocks of circumpolar permafrost carbon with quantified uncertainty ranges and identified data gaps. *Biogeosciences*, *11*(23), 6573–6593. doi: https://doi.org/10.5194/bg-11-6573-2014

Irrgang, A. M., Bendixen, M., Farquharson, L. M., Baranskaya, A. V., Erikson, L. H., Gibbs, A. E., ... Jones, B. M. (2022). Drivers, dynamics and impacts of changing Arctic coasts. *Nature Reviews Earth & Environment*, *3*(1), 39–54. doi: https://doi.org/10.1038/s43017-021-00232-1

Jong, D., Bröder, L., Tanski, G., Fritz, M., Lantuit, H., Tesi, T., ... Vonk, J. E. (2020). Nearshore zone dynamics determine pathway of organic carbon from eroding permafrost coasts. *Geophysical research letters*, *47*(15). doi: https://doi.org/10.1029/2020GL088561

Juhls, B., Stedmon, C. A., Morgenstern, A., Meyer, H., Hölemann, J., Heim, B., ... Overduin, P. P. (2020). Identifying drivers of seasonality in Lena River biogeochemistry and dissolved organic matter fluxes. *Frontiers in Environmental Science*, *8*. doi: https://doi.org/10.3389/fenvs.2020.00053

Juranek, L. W. (2022). Changing biogeochemistry of the Arctic Ocean: Surface nutrient and CO_2 cycling in a warming, melting north. *Oceanography*, *35*(2), 1–12. doi: https://doi.org/10.5670/oceanog.2022.120

Kaiser, K., Canedo-Oropeza, M., McMahon, R., & Amon, R. M. (2017). Origins and transformations of dissolved organic matter in large Arctic rivers. *Scientific reports*, *7*(1), 1–11. doi: https://doi.org/10.1038/s41598-017-12729-1

Kicklighter, D. W., Hayes, D. J., McClelland, J. W., Peterson, B. J., McGuire, A. D., & Melillo, J. M. (2013). Insights and issues with simulating terrestrial DOC loading of Arctic river networks. *Ecological Applications*, *23*(8), 1817–1836. doi: https://doi.org/10.1890/11-1050.1

Kipp, L. E., Henderson, P. B., Wang, Z. A., & Charette, M. A. (2020). Deltaic and estuarine controls on Mackenzie River solute fluxes to the Arctic Ocean. *Estuaries and coasts*, *43*(8), 1992–2014. doi: https://doi.org/10.1007/s12237-020-00739-8

Kirchman, D. L., Morán, X. A. G., & Ducklow, H. (2009). Microbial growth in the polar oceans—role of temperature and potential impact of climate change. *Nature Reviews Microbiology*, *7*(6), 451–459. doi: https://doi.org/10.1038/nrmicro2115

Kokelj, S. V., Lantz, T. C., Solomon, S., Pisaric, M. F., Keith, D., Morse, P., ... Esagok, D. (2012). Using multiple sources of knowledge to investigate northern environmental change: regional ecological impacts of a storm surge in the outer Mackenzie Delta, NWT. *Arctic*, 257–272. doi: https://doi.org/10.14430/arctic4214

Kuenzer, C., Klein, I., Ullmann, T., Foufoula Georgiou, E., Baumhauer, R., & Dech, S. (2015). Remote sensing of river delta inundation: Exploiting the potential of coarse spatial resolution, temporally-dense MODIS time series. *Remote Sensing*, *7*(7), 8516–8542. doi: https://doi.org/10.3390/rs70708516

Lacroix, F., Ilyina, T., & Hartmann, J. (2020). Oceanic CO_2 outgassing and biological production hotspots induced by pre-industrial river loads of nutrients and carbon in a global modeling approach. *Biogeosciences*, *17*(1), 55–88. doi: https://doi.org/10.5194/bg-2019-152

Lacroix, F., Ilyina, T., Laruelle, G. G., & Regnier, P. (2021). Reconstructing the preindustrial coastal carbon cycle through a global ocean circulation model: was the global continental shelf already both autotrophic and a CO_2 sink? *Global Biogeochemical Cycles*, *35*(2). doi: https://doi.org/10.1029/2020GB006603

Lacroix, F., Zaehle, S., Caldararu, S., Schaller, J., Stimmler, P., Holl, D., ... Göckede, M. (2022). Mismatch of N release from the permafrost and vegetative uptake opens pathways of increasing nitrous oxide emissions in the high Arctic. *Global Change Biology*, *28*(20), 5973–5990. doi: https://doi.org/10.1111/gcb.16345

Lammers, R. B., Shiklomanov, A. I., Vörösmarty, C. J., Fekete, B. M., & Peterson, B. J. (2001). Assessment of contemporary Arctic river runoff based on observational discharge records. *Journal of Geophysical Research: Atmospheres*, *106*(D4), 3321–3334. doi: https://doi.org/10.1007/978-3-030-50930-9_7

Landschützer, P., Gruber, N., & Bakker, D. C. (2016). Decadal variations and trends of the global ocean carbon sink. *Global Biogeochemical Cycles*, *30*(10), 1396–1417. doi: https://doi.org/10.1002/2015GB005359

Landschützer, P., Laruelle, G. G., Roobaert, A., & Regnier, P. (2020). A uniform pCO_2 climatology combining open and coastal oceans. *Earth System Science Data*, *12*, 2537–2553.

Langer, M., Nitzbon, J., Groenke, B., Assmann, L.-M., Schneider von Deimling, T., Stuenzi, S. M., & Westermann, S. (2022). The evolution of Arctic permafrost over the last three centuries. *EGUsphere*. doi: https://doi.org/10.5194/egusphere-2022-473

Lantz, T. C., Kokelj, S. V., & Fraser, R. H. (2015). Ecological recovery in an Arctic delta following widespread saline incursion. *Ecological Applications*, *25*(1), 172–185. doi: https://doi.org/10.1890/14-0239.1

Lasareva, E. V., Parfenova, A. M., Romankevich, E. A., Lobus, N. V., & Drozdova, A. N. (2019). Organic matter and mineral interactions modulate flocculation across Arctic river mixing zones. *Journal of Geophysical Research: Biogeosciences*, *124*(6), 1651–1664. doi: https://doi.org/10.1029/2019JG005026

Le Fouest, V., Babin, M., & Tremblay, J.-É. (2013). The fate of riverine nutrients on Arctic shelves. *Biogeosciences*, *10*(6), 3661–3677. doi: https://doi.org/10.5194/bg-10-3661-2013

Lenn, Y.-D., Fer, I., Timmermans, M.-L., & MacKinnon, J. A. (2022). Mixing in the Arctic Ocean. In *Ocean mixing* (pp. 275–299). Elsevier. doi: https://doi.org/10.1016/B978-0-12-821512-8.00018-9

Lewis, K., Van Dijken, G., & Arrigo, K. R. (2020). Changes in phytoplankton concentration now drive increased Arctic Ocean primary production. *Science*, *369*(6500), 198–202. doi: https://doi.org/10.1126/science.aay8380

Li, M., Peng, C., Wang, M., Xue, W., Zhang, K., Wang, K., ... Zhu, Q. (2017). The carbon flux of global rivers: A re-evaluation of amount and spatial patterns. *Ecological Indicators*, *80*, 40–51. doi: https://doi.org/10.1016/j.ecolind.2017.04.049

Liao, C., Zhuang, Q., Leung, L. R., & Guo, L. (2019). Quantifying Dissolved Organic Carbon Dynamics Using a Three-Dimensional Terrestrial Ecosystem Model at High Spatial-Temporal Resolutions. *Journal of Advances in Modeling Earth Systems*, *11*(12), 4489–4512. doi: https://doi.org/10.1029/2019MS001792

Lim, M., Whalen, D., J. Mann, P., Fraser, P., Berry, H. B., Irish, C., ... Woodward, J. (2020). Effective monitoring of permafrost coast erosion: Wide-scale storm impacts on outer islands in the Mackenzie Delta area. *Frontiers in Earth Science*, *8*. doi: https://doi.org/10.3389/feart.2020.561322

Lin, P., Pickart, R. S., Fissel, D., Ross, E., Kasper, J., Bahr, F., ... Wiese, F. K. (2020). Circulation in the vicinity of Mackenzie Canyon from a year-long mooring array. *Progress in Oceanography*, *187*, 102396. doi: https://doi.org/10.1016/j.pocean.2020.102396

Lin, P., Pickart, R. S., Fissel, D. B., Borg, K., Melling, H., & Wiese, F. K. (2021). On the nature of wind-forced upwelling and downwelling in Mackenzie Canyon, Beaufort Sea. *Progress in Oceanography*, *198*, 102674. doi: https://doi.org/10.1016/j.pocean.2021.102674

Lizotte, M., Juhls, B., Matsuoka, A., Massicotte, P., Mével, G., Anikina, D. O. J., ... Babin, M. (2022). Nunataryuk field campaigns: Understanding the origin and fate of terrestrial organic matter in the coastal waters of the Mackenzie Delta region. *Earth System Science Data Discussions*, 1–46. doi: https://doi.org/10.5194/essd-2022-163

Lønborg, C., & Álvarez-Salgado, X. A. (2012). Recycling versus export of bioavailable dissolved organic matter in the coastal ocean and efficiency of the continental shelf pump. *Global biogeochemical cycles*, *26*(3). doi: https://doi.org/10.1029/2012GB004353

Lønborg, C., Carreira, C., Jickells, T., & Álvarez-Salgado, X. A. (2020). Impacts of global change on ocean dissolved organic carbon (DOC) cycling. *Frontiers in Marine Science*, *7*. doi: https://doi.org/10.3389/fmars.2020.00466

Losch, M., Menemenlis, D., Campin, J.-M., Heimbach, P., & Hill, C. (2010). On the formulation of sea-ice models. Part 1: Effects of different solver implementations and parameterizations. *Ocean Modelling*, *33*(1-2), 129–144. doi: https://doi.org/10.1016/j.ocemod.2009.12.008

Louchard, D., Gruber, N., & Münnich, M. (2021). The impact of the Amazon on the biological pump and the air–sea CO_2 balance of the Western Tropical Atlantic. *Global Biogeochemical Cycles*, *35*(6). doi: https://doi.org/10.1029/2020GB006818

Macdonald, R. W., Carmack, E. C., McLaughlin, F., Iseki, K., Macdonald, D., & O'brien, M. (1989). Composition and modification of water masses in the Mackenzie Shelf Estuary. *Journal of Geophysical Research: Oceans*, *94*(C12), 18057–18070. doi: https://doi.org/10.1029/JC094iC12p18057

Macdonald, R. W., Iseki, K., O'Brien, M. C., McLaughlin, F A, M., D, M., ... Miskulin, G. (1988). NOGAP B-6. *Volume 5, Chemical data collected in the Beaufort Sea and Mackenzie River Delta, March-July 1987.*

Macdonald, R. W., Wong, C., & Erickson, P. E. (1987). The distribution of nutrients in the southeastern Beaufort Sea: Implications for water circulation and primary production. *Journal of Geophysical Research: Oceans*, *92*(C3), 2939–2952. doi: https://doi.org/10.1029/JC092iC03p02939

Macdonald, R. W., & Yu, Y. (2006). The Mackenzie Estuary of the Arctic Ocean. *Estuaries*, 91–120. doi: https://doi.org/10.1007/698_5_027

MacGilchrist, G., Garabato, A. N., Tsubouchi, T., Bacon, S., Torres-Valdés, S., & Azetsu-Scott, K. (2014). The Arctic Ocean carbon sink. *Deep Sea Research Part I: Oceanographic Research Papers*, *86*, 39–55. doi: https://doi.org/10.1016/j.dsr.2014.01.002

Mackay, J. R. (1974). *The Mackenzie Delta area, N.W.T* (M. Geological Survey of Canada Dept. of Energy & Resources, Eds.).

Manizza, M., Follows, M., Dutkiewicz, S., McClelland, J., Menemenlis, D., Hill, C., ... Peterson, B. (2009). Modeling transport and fate of riverine dissolved organic carbon in the Arctic Ocean. *Global Biogeochemical Cycles*, *23*(4). doi: https://doi.org/10.1029/2008GB003396

Manizza, M., Follows, M., Dutkiewicz, S., Menemenlis, D., Hill, C., & Key, R. (2013). Changes in the Arctic Ocean CO_2 sink (1996–2007): A regional model analysis. *Global Biogeochemical Cycles*, *27*(4), 1108–1118. doi: https://doi.org/10.1002/2012GB004491

Manizza, M., Follows, M. J., Dutkiewicz, S., Menemenlis, D., McClelland, J. W., Hill, C., ... Key, R. M. (2011). A model of the Arctic Ocean carbon cycle. *Journal of Geophysical Research: Oceans*, *116*. doi: https://doi.org/10.1029/2011JC006998

Manizza, M., Menemenlis, D., Zhang, H., & Miller, C. E. (2019). Modeling the recent changes in the Arctic Ocean CO_2 sink (2006–2013). *Global Biogeochemical Cycles*, *33*(3), 420–438. doi: https://doi.org/10.1029/2018GB006070

Mann, P. J., Davydova, A., Zimov, N., Spencer, R., Davydov, S., Bulygina, E., ... Holmes, R. (2012). Controls on the composition and lability of dissolved organic matter in Siberia's Kolyma River basin. *Journal of Geophysical Research: Biogeosciences*, *117*. doi: https://doi.org/10.1029/2011JG001798

Mann, P. J., Eglinton, T. I., McIntyre, C. P., Zimov, N., Davydova, A., Vonk, J. E., ... Spencer, R. G. (2015). Utilization of ancient permafrost carbon in headwaters of Arctic fluvial networks. *Nature Communications*, *6*(1). doi: https://doi.org/10.1038/ncomms8856

Mann, P. J., Strauss, J., Palmtag, J., Dowdy, K., Ogneva, O., Fuchs, M., ... Juhls, B. (2022). Degrading permafrost river catchments and their impact on Arctic Ocean nearshore processes. *Ambio*, *51*(2), 439–455. doi: https://doi.org/10.1007/s13280-021-01666-z

Manson, G. K., & Solomon, S. M. (2007). Past and future forcing of beaufort sea coastal change. *Atmosphere-Ocean*, *45*(2), 107–122. doi: https://doi.org/10.3137/ao.450204

Marsh, P., & Schmidt, T. (1993). Influence of a Beaufort Sea storm surge on channel levels in the Mackenzie Delta. *Arctic*, 35–41. doi: https://doi.org/10.14430/arctic1319

Marshall, J., Adcroft, A., Hill, C., Perelman, L., & Heisey, C. (1997). A finite-volume, incompressible Navier Stokes model for studies of the ocean on parallel computers. *Journal of Geophysical Research: Oceans*, *102*, 5753–5766. doi: https://doi.org/10.1029/96JC02775

Martens, J., Wild, B., Semiletov, I., Dudarev, O. V., & Gustafsson, Ö. (2022). Circum-Arctic release of terrestrial carbon varies between regions and sources. *Nature communications*, *13*(1), 1–10. doi: https://doi.org/10.1038/s41467-022-33541-0

Massicotte, P., Amon, R. M., Antoine, D., Archambault, P., Balzano, S., Bélanger, S., ... Babin, M. (2021). The MALINA oceanographic expedition: how do changes in ice cover, permafrost and UV radiation impact biodiversity and biogeochemical fluxes in the Arctic Ocean? *Earth System Science Data*, *13*(4), 1561–1592. doi: https://doi.org/10.5194/essd-2020-252

Mathis, M., Logemann, K., Maerz, J., Lacroix, F., Hagemann, S., Chegini, F., ... Schrum, C. (2022). Seamless integration of the coastal ocean in global marine carbon cycle modeling. *Journal of Advances in Modeling Earth Systems*, *14*(8). doi: https://doi.org/10.1029/2021MS002789

Matsubara, F., Wild, B., Martens, J., Andersson, A., Wennström, R., Bröder, L., ... Gustafsson, Ö. (2022). Molecular-Multiproxy Assessment of Land-Derived Organic Matter Degradation over Extensive Scales of the East Siberian Arctic Shelf Seas. *Global Biogeochemical Cycles*, *36*. doi: https://doi.org/10.1029/2022GB007428

Matsuoka, A., Babin, M., & Devred, E. C. (2016). A new algorithm for discriminating water sources from space: A case study for the southern Beaufort Sea using MODIs ocean color and SMOS salinity data. *Remote Sensing of Environment*, *184*, 124–138. doi: https://doi.org/10.1016/j.rse.2016.05.006

Matsuoka, A., Babin, M., & Vonk, J. E. (2022). Decadal trends in the release of terrigenous organic carbon to the Mackenzie Delta (Canadian Arctic) using satellite ocean color data (1998–2019). *Remote Sensing of Environment*, *283*, 113322. doi: https://doi.org/10.1016/j.rse.2022.113322

Matsuoka, A., Boss, E., Babin, M., Karp-Boss, L., Hafez, M., Chekalyuk, A., ... Bricaud, A. (2017). Pan-Arctic optical characteristics of colored dissolved organic matter: Tracing dissolved organic carbon in changing Arctic waters using satellite ocean color data. *Remote sensing of Environment*, *200*, 89–101. doi: https://doi.org/10.1016/j.rse.2017.08.009

Matsuoka, A., Ortega-Retuerta, E., Bricaud, A., Arrigo, K. R., & Babin, M. (2015). Characteristics of colored dissolved organic matter (CDOM) in the Western Arctic Ocean: Relationships with microbial activities. *Deep Sea Research Part II: Topical Studies in Oceanography*, *118*, 44–52. doi: https://doi.org/10.1016/j.dsr2.2015.02.012

Mayorga, E., Seitzinger, S. P., Harrison, J. A., Dumont, E., Beusen, A. H., Bouwman, A., ... Van Drecht, G. (2010). Global nutrient export from WaterSheds 2 (NEWS 2): model development and implementation. *Environmental Modelling & Software*, *25*(3), 837–853. doi: https://doi.org/10.1029/2018GB006070

McClelland, J., Holmes, R., Dunton, K., & Macdonald, R. (2012). The arctic ocean estuary. *Estuaries and Coasts*, *35*(2), 353–368. doi: https://doi.org/10.1007/s12237-010-9357-3

McClelland, J., Holmes, R., Peterson, B., Raymond, P., Striegl, R., Zhulidov, A., ... Griffin, C. (2016). Particulate organic carbon and nitrogen export from major Arctic rivers. *Global biogeochemical cycles*, *30*(5), 629–643. doi: https://doi.org/10.1002/2015GB005351

McGuire, A. D., Anderson, L. G., Christensen, T. R., Dallimore, S., Guo, L., Hayes, D. J., ... Roulet, N. (2009). Sensitivity of the carbon cycle in the Arctic to climate change. *Ecological Monographs*, *79*(4), 523–555. doi: https://doi.org/10.1890/08-2025.1

McGuire, A. D., Koven, C., Lawrence, D. M., Clein, J. S., Xia, J., Beer, C., ... Zhuang, Q. (2016). Variability in the sensitivity among model simulations of permafrost and carbon dynamics in the permafrost region between 1960 and 2009. *Global Biogeochemical Cycles*, *30*(7), 1015–1037. doi: https://doi.org/10.1002/2016GB005405

Menemenlis, D., Fukumori, I., & Lee, T. (2005). Using Green's functions to calibrate an ocean general circulation model. *Monthly weather review*, *133*(5), 1224–1240. doi: https://doi.org/10.1175/MWR2912.1

Menemenlis, D., Hill, C., Adcrocft, A., Campin, J.-M., Cheng, B., Ciotti, B., ... Zhang, J. (2005). NASA supercomputer improves prospects for ocean climate research. *Eos, Transactions American Geophysical Union*, *86*(9), 89–96. doi: https://doi.org/10.1029/2005EO090002

Mentges, A., Deutsch, C., Feenders, C., Lennartz, S. T., Blasius, B., & Dittmar, T. (2020). Microbial physiology governs the oceanic distribution of dissolved organic carbon in a scenario of equal degradability. *Frontiers in Marine Science*, *7*. doi: https://doi.org/10.3389/fmars.2020.549784

Mentges, A., Feenders, C., Deutsch, C., Blasius, B., & Dittmar, T. (2019). Long-term stability of marine dissolved organic carbon emerges from a neutral network of compounds and microbes. *Scientific reports*, *9*(1), 1–13. doi: https://doi.org/10.1038/s41598-019-54290-z

Miller, W. L., & Zepp, R. G. (1995). Photochemical production of dissolved inorganic carbon from terrestrial organic matter: Significance to the oceanic organic carbon cycle. *Geophysical Research Letters*, *22*(4), 417–420. doi: https://doi.org/10.1029/94GL03344

Mol, J., Thomas, H., Myers, P. G., Hu, X., & Mucci, A. (2018). Inorganic carbon fluxes on the Mackenzie Shelf of the Beaufort Sea. *Biogeosciences*, *15*(4), 1011–1027. doi: https://doi.org/10.5194/bg-15-1011-2018

Monod, J. (1942). *Recherches sur la croissance des cultures bactériennes* (Unpublished doctoral dissertation).

Moran, M. A., Sheldon Jr, W. M., & Zepp, R. G. (2000). Carbon loss and optical property changes during long-term photochemical and biological degradation of estuarine dissolved organic matter. *Limnology and Oceanography*, *45*(6), 1254–1264. doi: https://doi.org/10.4319/lo.2000.45.6.1254

Morley, J. K. (2012). *Observations of flow distributions and river breakup in the Mackenzie Delta, NWT* (Master's thesis, University of Alberta). doi: https://doi.org/10.7939/R3N02H

Mucci, A., Lansard, B., Miller, L. A., & Papakyriakou, T. N. (2010). CO_2 fluxes across the air–sea interface in the southeastern Beaufort Sea: Ice-free period. *Journal of Geophysical Research: Oceans*, *115*. doi: https://doi.org/10.1029/2009JC005330

Mulligan, R. P., & Perrie, W. (2019). Circulation and structure of the Mackenzie River plume in the coastal Arctic Ocean. *Continental Shelf Research*, *177*, 59–68. doi: https://doi.org/10.1016/j.csr.2019.03.006

Mulligan, R. P., Perrie, W., & Solomon, S. (2010). Dynamics of the Mackenzie River plume on the inner Beaufort shelf during an open water period in summer. *Estuarine, Coastal and Shelf Science*, *89*(3), 214–220. doi: https://doi.org/10.1016/j.ecss.2010.06.010

Musolff, A., Schmidt, C., Selle, B., & Fleckenstein, J. H. (2015). Catchment controls on solute export. *Advances in Water Resources*, *86*, 133–146. doi: https://doi.org/10.1016/j.advwatres.2015.09.026

Nash, J. E., & Sutcliffe, J. V. (1970). River flow forecasting through conceptual models part I – A discussion of principles. *Journal of hydrology*, *10*(3), 282–290. doi: https://doi.org/10.1016/0022-1694(70)90255-6

Neumann, T., Koponen, S., Attila, J., Brockmann, C., Kallio, K., Kervinen, M., ... Ylöstalo, P. (2021). Optical model for the Baltic Sea with an explicit CDOM state variable: a case study with Model ERGOM (version 1.2). *Geoscientific Model Development*, *14*(8), 5049–5062. doi: https://doi.org/10.5194/gmd-14-5049-2021

Nghiem, S., Hall, D., Rigor, I., Li, P., & Neumann, G. (2014). Effects of Mackenzie River discharge and bathymetry on sea ice in the Beaufort Sea. *Geophysical Research Letters*, *41*(3), 873–879. doi: https://doi.org/10.1002/2013GL058956

Nguyen, A. T., Pillar, H., Ocaña, V., Bigdeli, A., Smith, T. A., & Heimbach, P. (2021). The Arctic Subpolar Gyre sTate Estimate: Description and Assessment of a Data-constrained, Dynamically Consistent Ocean-Sea Ice Estimate for 2002–2017. *Journal of Advances in Modeling Earth Systems*, *13*(5). doi: https://doi.org/10.1029/2020MS002398

Nielsen, D. M., Pieper, P., Barkhordarian, A., Overduin, P., Ilyina, T., Brovkin, V., ... Dobrynin, M. (2022). Increase in Arctic coastal erosion and its sensitivity to warming in the twenty-first century. *Nature Climate Change*, *12*(3), 263–270. doi: https://doi.org/10.1038/s41558-022-01281-0

Nill, L., Ullmann, T., Kneisel, C., Sobiech-Wolf, J., & Baumhauer, R. (2019). Assessing spatiotemporal variations of Landsat land surface temperature and multispectral indices in the Arctic Mackenzie Delta Region between 1985 and 2018. *Remote Sensing*, *11*(19). doi: https://doi.org/10.3390/rs11192329

Normandin, C., Frappart, F., Lubac, B., Bélanger, S., Marieu, V., Blarel, F., ... Guiastrennec-Faugas, L. (2018). Quantification of surface water volume changes in the Mackenzie Delta using satellite multi-mission data. *Hydrology and Earth System Sciences*, *22*(2), 1543–1561. doi: https://doi.org/10.5194/hess-22-1543-2018

Nurser, A., & Bacon, S. (2014). The rossby radius in the Arctic Ocean. *Ocean Science*, *10*(6), 967–975. doi: https://doi.org/10.5194/os-10-967-2014

Odériz, I., Mori, N., Shimura, T., Webb, A., Silva, R., & Mortlock, T. (2022). Transitional wave climate regions on continental and polar coasts in a warming world. *Nature Climate Change*, *12*, 662—671. doi: https://doi.org/10.1038/s41558-022-01389-3

Olson, D. M., Dinerstein, E., Wikramanayake, E. D., Burgess, N. D., Powell, G. V., Underwood, E. C., ... Kassem, K. R. (2001). Terrestrial Ecoregions of the World: A New Map of Life on Earth: A new global map of terrestrial ecoregions provides an innovative tool for conserving biodiversity. *BioScience*, *51*(11), 933–938. doi: https://doi.org/10.1641/0006-3568(2001)051[0933:TEOTWA]2.0.CO;2

Opsahl, S., Benner, R., & Amon, R. M. (1999). Major flux of terrigenous dissolved organic matter through the Arctic Ocean. *Limnology and Oceanography*, *44*(8), 2017–2023. doi: https://doi.org/10.4319/lo.1999.44.8.2017

Ortega-Retuerta, E., Jeffrey, W., Babin, M., Bélanger, S., Benner, R., Marie, D., ... Joux, F. (2012). Carbon fluxes in the Canadian Arctic: patterns and drivers of bacterial abundance, production and respiration on the Beaufort Sea margin. *Biogeosciences*, *9*(9), 3679–3692. doi: https://doi.org/10.5194/bg-9-3679-2012

Østerhus, S., Woodgate, R., Valdimarsson, H., Turrell, B., De Steur, L., Quadfasel, D., ... Berw, B. (2019). Arctic Mediterranean exchanges: A consistent volume budget and trends in transports from two decades of observations. *Ocean Science*, *15*(2), 379–399. doi: https://doi.org/10.5194/os-15-379-2019,2019

Ouyang, Z., Li, Y., Qi, D., Zhong, W., Murata, A., Nishino, S., ... Cai, W.-J. (2021). The changing CO_2 sink in the western Arctic Ocean from 1994 to 2019. *Global Biogeochemical Cycles*, *36*(1). doi: https://doi.org/10.1029/2021GB007032

Overeem, I., Nienhuis, J. H., & Piliouras, A. (2022). Ice-dominated Arctic deltas. *Nature Reviews Earth & Environment*, *3*(4), 225–1240. doi: https://doi.org/10.1038/s43017-022-00268-x

Park, H., Watanabe, E., Kim, Y., Polyakov, I., Oshima, K., Zhang, X., ... Yang, D. (2020). Increasing riverine heat influx triggers Arctic sea ice decline and oceanic and atmospheric warming. *Science advances*, *6*(45), eabc4699. doi: https://doi.org/10.1126/sciadv.abc4699

Pefanis, V., Losa, S. N., Losch, M., Janout, M. A., & Bracher, A. (2020). Amplified Arctic surface warming and sea ice loss due to phytoplankton and colored dissolved material. *Geophysical Research Letters*, *47*(21). doi: https://doi.org/10.1029/2020GL088795

Pickart, R. S. (2004). Shelfbreak circulation in the Alaskan Beaufort Sea: Mean structure and variability. *Journal of Geophysical Research: Oceans*, *109*(C4). doi: https://doi.org/10.1029/2003JC001912

Pisaric, M. F., Thienpont, J. R., Kokelj, S. V., Nesbitt, H., Lantz, T. C., Solomon, S., & Smol, J. P. (2011). Impacts of a recent storm surge on an Arctic delta ecosystem examined in the context of the last millennium. *Proceedings of the National Academy of Sciences*, *108*(22), 8960–8965. doi: https://doi.org/10.1073/pnas.1018527108

Randelhoff, A., Lacour, L., Marec, C., Leymarie, E., Lagunas, J., Xing, X., ... Babin, M. (2020). Arctic mid-winter phytoplankton growth revealed by autonomous profilers. *Science advances*, *6*(39). doi: https://doi.org/10.1126/sciadv.abc2678

Rantanen, M., Karpechko, A. Y., Lipponen, A., Nordling, K., Hyvärinen, O., Ruosteenoja, K., ... Laaksonen, A. (2022). The Arctic has warmed nearly four times faster than the globe since 1979. *Communications Earth & Environment*, *3*(1), 1–10. doi: https://doi.org/10.1038/s43247-022-00498-3

Rawlins, M. A., Connolly, C. T., & McClelland, J. W. (2021). Modeling terrestrial dissolved organic carbon loading to western Arctic rivers. *Journal of Geophysical Research: Biogeosciences*, *126*(10). doi: https://doi.org/10.1029/2021JG006420

Raymond, P. A., McClelland, J., Holmes, R., Zhulidov, A., Mull, K., Peterson, B., ... Gurtovaya, T. (2007). Flux and age of dissolved organic carbon exported to the Arctic Ocean: A carbon isotopic study of the five largest arctic rivers. *Global Biogeochemical Cycles*, *21*(4). doi: https://doi.org/10.1029/2007GB002934

Raynolds, M. K., Walker, D. A., Balser, A., Bay, C., Campbell, M., Cherosov, M. M., ... Troeva, E. (2019). A raster version of the Circumpolar Arctic Vegetation Map (CAVM). *Remote Sensing of Environment*, *232*, 111297. doi: https://doi.org/10.1016/j.rse.2019.111297

Redi, M. H. (1982). Oceanic isopycnal mixing by coordinate rotation. *Journal of Physical Oceanography*, *12*(10), 1154–1158. doi: https://doi.org/10.1175/1520-0485(1982)012<1154:OIMBCR>2.0.CO;2

Riedel, T., & Dittmar, T. (2014). A method detection limit for the analysis of natural organic matter via Fourier transform ion cyclotron resonance mass spectrometry. *Analytical chemistry*, *86*(16), 8376–8382. doi: https://doi.org/10.1021/ac501946m

Roobaert, A., Laruelle, G. G., Landschützer, P., Gruber, N., Chou, L., & Regnier, P. (2019). The spatiotemporal dynamics of the sources and sinks of CO_2 in the global coastal ocean. *Global Biogeochemical Cycles*, *33*(12), 1693–1714. doi: https://doi.org/10.1029/2019GB006239

Rosenberg, D., & Barton, D. (2013). *The ecology of river systems* (Vol. 60; B. R. Davies &

K. F. Walker, Eds.). Springer Science & Business Media.

Roshan, S., & DeVries, T. (2017). Efficient dissolved organic carbon production and export in the oligotrophic ocean. *Nature communications*, *8*(1), 1–8. doi: https://doi.org/10.1038/s41467-017-02227-3

Runkel, R. L., Crawford, C. G., & Cohn, T. A. (2004). *Load Estimator (LOADEST): A FORTRAN program for estimating constituent loads in streams and rivers* (Tech. Rep.). U.S. Geological Survey (USGS).

Saito, K., Walsh, J. E., Bring, A., Brown, R., Shiklomanov, A., & Yang, D. (2021). Future trajectory of Arctic system evolution. In *Arctic hydrology, permafrost and ecosystems* (pp. 893–914). Springer. doi: https://doi.org/10.1007/978-3-030-50930-9_30

Schuur, E. A., Abbott, B. W., Commane, R., Ernakovich, J., Euskirchen, E., Hugelius, G., ... Turetsky, M. (2022). Permafrost and Climate change: Carbon Cycle Feedbacks from the Warming Arctic. *Annual Review of Environment and Resources*, *47*, 343–371. doi: https://doi.org/10.1146/annurev-environ-012220011847

Schuur, E. A., McGuire, A. D., Schädel, C., Grosse, G., Harden, J. W., Hayes, D. J., ... Vonk, J. E. (2015). Climate change and the permafrost carbon feedback. *Nature*, *520*(7546), 171–179. doi: https://doi.org/10.1038/nature14338

Schwab, M. S., Hilton, R. G., Raymond, P. A., Haghipour, N., Amos, E., Tank, S. E., ... Eglinton, T. I. (2020). An abrupt aging of dissolved organic carbon in large Arctic rivers. *Geophysical research letters*, *47*(23). doi: https://doi.org/10.1029/2020GL088823

Searcy, C., Dean, K., & Stringer, W. (1996). A river-coastal sea ice interaction model: Mackenzie River Delta. *Journal of Geophysical Research: Oceans*, *101*, 8885–8894. doi: https://doi.org/10.1029/96JC00120

Serreze, M. C., Barrett, A. P., Slater, A. G., Woodgate, R. A., Aagaard, K., Lammers, R. B., ... Lee, C. M. (2006). The large-scale freshwater cycle of the Arctic. *Journal of Geophysical Research: Oceans*, *111*. doi: https://doi.org/10.1029/2005JC003424

Shen, Y., Fichot, C., & Benner, R. (2012). Dissolved organic matter composition and bioavailability reflect ecosystem productivity in the Western Arctic Ocean. *Biogeosciences*, *9*(12), 4993–5005. doi: https://doi.org/10.5194/bgd-9-9571-2012

Shiklomanov, A., Holmes, R., McClelland, J., Tank, S., & Spencer, R. (2021). *ArcticGRO Discharge Dataset* (Tech. Rep.). Version 2021-05-27, available at: https://arcticgreatrivers.org/data/.

Sholkovitz, E. (1976). Flocculation of dissolved organic and inorganic matter during the mixing of river water and seawater. *Geochimica et Cosmochimica Acta*, *40*(7), 831–845. doi: https://doi.org/10.1016/0016-7037(76)90035-1

Shrestha, R. R., Prowse, T. D., & Tso, L. (2019). Modelling historical variability of phosphorus and organic carbon fluxes to the Mackenzie River, Canada. *Hydrology Research*, *50*(5), 1424–1439. doi: https://doi.org/10.2166/nh.2019.161

Slater, A. G., & Lawrence, D. M. (2013). Diagnosing present and future permafrost from climate models. *Journal of Climate*, *26*(15), 5608–5623. doi: https://doi.org/10.1175/JCLI-D-12-00341.1

Soppa, M. A., Pefanis, V., Hellmann, S., Losa, S. N., Hölemann, J., Martynov, F., ... Bracher, A. (2019). Assessing the influence of water constituents on the radiative heating of Laptev Sea shelf waters. *Frontiers in Marine Science*, *6*. doi: https://doi.org/10.3389/fmars.2019.00221

Spencer, R. G., Mann, P. J., Dittmar, T., Eglinton, T. I., McIntyre, C., Holmes, R. M., ... Stubbins, A. (2015). Detecting the signature of permafrost thaw in Arctic rivers. *Geophysical Research Letters*, *42*(8), 2830–2835. doi: https://doi.org/10.1002/2015GL063498

Stammer, D., Wunsch, C., Giering, R., Eckert, C., Heimbach, P., Marotzke, J., ... Marshall, J.

(2002). Global ocean circulation during 1992–1997, estimated from ocean observations and a general circulation model. *Journal of Geophysical Research: Oceans*, *107*(C9). doi: https://doi.org/10.1029/2001JC000888

Stedmon, C., Amon, R. M., Rinehart, A., & Walker, S. (2011). The supply and characteristics of colored dissolved organic matter (CDOM) in the Arctic Ocean: Pan Arctic trends and differences. *Marine Chemistry*, *124*(1-4), 108–118. doi: https://doi.org/10.1016/j.marchem.2010.12.007

Steele, M., Bliss, A., Peng, G., Meier, W., & Dickinson, S. (2019). Arctic Sea Ice Seasonal Change and Melt/Freeze Climate Indicators from Satellite Data, Version 1. *Boulder, Colorado USA. NASA National Snow and Ice Data Center Distributed Active Archive Center*. doi: https://doi.org/10.5067/KINANQKEZI4T

Sverdrup, H. U., Johnson, M. W., & Fleming. (1942). *The Oceans: Their physics, chemistry, and general biology* (Vol. 1087). Prentice-Hall New York.

Tank, S. E., Lesack, L. F., Gareis, J. A., Osburn, C. L., & Hesslein, R. H. (2011). Multiple tracers demonstrate distinct sources of dissolved organic matter to lakes of the Mackenzie Delta, western Canadian Arctic. *Limnology and Oceanography*, *56*(4), 1297–1309. doi: https://doi.org/10.4319/lo.2011.56.4.1297

Tank, S. E., Raymond, P. A., Striegl, R. G., McClelland, J. W., Holmes, R. M., Fiske, G. J., & Peterson, B. J. (2012). A land-to-ocean perspective on the magnitude, source and implication of DIC flux from major Arctic rivers to the Arctic Ocean. *Global Biogeochemical Cycles*, *26*(4). doi: https://doi.org/10.1029/2011GB004192

Tank, S. E., Striegl, R. G., McClelland, J. W., & Kokelj, S. V. (2016). Multi-decadal increases in dissolved organic carbon and alkalinity flux from the Mackenzie drainage basin to the Arctic Ocean. *Environmental Research Letters*, *11*(5). doi: https://doi.org/10.1088/1748-9326/11/5/054015

Tanski, G., Bröder, L., Wagner, D., Knoblauch, C., Lantuit, H., Beer, C., ... Vonk, J. E. (2021). Permafrost carbon and CO_2 pathways differ at contrasting coastal erosion sites in the Canadian Arctic. *Frontiers in Earth Science*, 207. doi: https://doi.org/10.3389/feart.2021.630493

Tanski, G., Couture, N., Lantuit, H., Eulenburg, A., & Fritz, M. (2016). Eroding permafrost coasts release low amounts of dissolved organic carbon (DOC) from ground ice into the nearshore zone of the Arctic Ocean. *Global Biogeochemical Cycles*, *30*(7), 1054–1068. doi: https://doi.org/10.1002/2015GB005337

Tarnocai, C., Canadell, J., Schuur, E. A., Kuhry, P., Mazhitova, G., & Zimov, S. (2009). Soil organic carbon pools in the northern circumpolar permafrost region. *Global biogeochemical cycles*, *23*(2). doi: https://doi.org/10.1029/2008GB003327

Terhaar, J., Lauerwald, R., Regnier, P., Gruber, N., & Bopp, L. (2021a). Around one third of current Arctic Ocean primary production sustained by rivers and coastal erosion. *Nature Communications*, *12*(1), 1–10. doi: https://doi.org/10.1038/s41467-020-20470-z

Terhaar, J., Lauerwald, R., Regnier, P., Gruber, N., & Bopp, L. (2021b). Around one third of current arctic ocean primary production sustained by rivers and coastal erosion. *Nature Communications*, *12*(1), 169.

Terhaar, J., Orr, J., Ethé, C., Regnier, P., & Bopp, L. (2019). Simulated Arctic Ocean response to doubling of riverine carbon and nutrient delivery. *Global Biogeochemical Cycles*, *33*(8), 1048–1070. doi: https://doi.org/10.1029/2019GB006200

Timmermans, M.-L., & Labe, Z. (2021). Sea Surface Temperature. *Arctic Report Card 2021*, 41–45. doi: https://doi.org/10.25923/2y8r-0e49

Tokuda, D., Kim, H., Yamazaki, D., & Oki, T. (2019). Development of a global river water temperature model considering fluvial dynamics and seasonal freeze-thaw cycle. *Water*

Resources Research, *55*(2), 1366–1383. doi: https://doi.org/10.1029/2018WR023083

Torres-Valdés, S., Tsubouchi, T., Bacon, S., Naveira-Garabato, A. C., Sanders, R., McLaughlin, F. A., ... Whitledge, T. E. (2013). Export of nutrients from the Arctic Ocean. *Journal of Geophysical Research: Oceans*, *118*(4), 1625–1644. doi: https://doi.org/10.1002/jgrc.20063

Tuerena, R. E., Mahaffey, C., Henley, S. F., De La Vega, C., Norman, L., Brand, T., ... März, C. (2022). Nutrient pathways and their susceptibility to past and future change in the Eurasian Arctic Ocean. *Ambio*, *51*(2), 355–369. doi: https://doi.org/10.1007/s13280-021-01673-0

Tumel, N. (2002). *Permafrost. The physical geography of Northern Eurasia* (M. Shahgedanova, Ed.). Oxford Univ. Press.

Vaqué, D., Lara, E., Arrieta, J. M., Holding, J., Sà, E. L., Hendriks, I. E., ... Duarte, C. M. (2019). Warming and CO_2 enhance arctic heterotrophic microbial activity. *Frontiers in microbiology*, *10*, 494. doi: https://doi.org/10.3389/fmicb.2019.00494

Vetrov, A., & Romankevich, E. (2019). Distribution and fluxes of dissolved organic carbon in the Arctic Ocean. *Polar Research*. doi: https://doi.org/10.33265/polar.v38.3500

Vincent, W. F., Lemay, M., & Allard, M. (2017). Arctic permafrost landscapes in transition: towards an integrated Earth system approach. *Arctic Science*, *3*(2), 39–64. doi: https://doi.org/10.1139/as-2016-0027

Vörösmarty, C., Fekete, B. M., Meybeck, M., & Lammers, R. B. (2000). Global system of rivers: Its role in organizing continental land mass and defining land-to-ocean linkages. *Global Biogeochemical Cycles*, *14*(2), 599–621. doi: https://doi.org/10.1029/1999GB900092

Wagner, S., Schubotz, F., Kaiser, K., Hallmann, C., Waska, H., Rossel, P. E., ... Galy, V. (2020). Soothsaying DOM: a current perspective on the future of oceanic dissolved organic carbon. *Frontiers in marine science*, *7*, 341. doi: https://doi.org/10.3389/fmars.2020.00341

Wanninkhof, R. (1992). Relationship between wind speed and gas exchange over the ocean. *Journal of Geophysical Research: Oceans*, *97*(C5), 7373–7382. doi: https://doi.org/10.1029/92JC00188

Watson, A. J., Schuster, U., Shutler, J. D., Holding, T., Ashton, I. G., Landschützer, P., ... Goddijn-Murphy, L. (2020). Revised estimates of ocean-atmosphere CO_2 flux are consistent with ocean carbon inventory. *Nature communications*, *11*(1), 1–6. doi: https://doi.org/10.1038/s41467-020-18203-3

Weiss, R. (1974). Carbon dioxide in water and seawater: the solubility of a non-ideal gas. *Marine chemistry*, *2*(3), 203–215. doi: https://doi.org/10.1016/0304-4203(74)90015-2

Weiss, R., & Price, B. (1980). Nitrous oxide solubility in water and seawater. *Marine chemistry*, *8*(4), 347–359. doi: https://doi.org/10.1016/0304-4203(80)90024-9

Wickland, K. P., Aiken, G. R., Butler, K., Dornblaser, M. M., Spencer, R., & Striegl, R. G. (2012). Biodegradability of dissolved organic carbon in the Yukon River and its tributaries: Seasonality and importance of inorganic nitrogen. *Global Biogeochemical Cycles*, *26*(4). doi: https://doi.org/10.1029/2012GB004342

Wunsch, C., & Heimbach, P. (2007). Practical global oceanic state estimation. *Physica D: Nonlinear Phenomena*, *230*(1-2), 197–208. doi: https://doi.org/10.1016/j.physd.2006.09.040

Wunsch, C., Heimbach, P., Ponte, R. M., Fukumori, I., & MEMBERS, E.-G. C. (2009). The global general circulation of the ocean estimated by the ECCO-Consortium. *Oceanography*, *22*(2), 88–103. doi: https://doi.org/10.5670/oceanog.2009.41

Yasunaka, S., Siswanto, E., Olsen, A., Hoppema, M., Watanabe, E., Fransson, A., ... Mathis, J. T. (2018). Arctic Ocean CO_2 uptake: an improved multiyear estimate of the air–sea CO_2 flux incorporating chlorophyll a concentrations. *Biogeosciences*, *15*(6), 1643–1661. doi: https://doi.org/10.5194/bg-15-1643-2018

Zakem, E. J., Al-Haj, A., Church, M. J., van Dijken, G. L., Dutkiewicz, S., Foster, S. Q., ... Follows, M. J. (2018). Ecological control of nitrite in the upper ocean. *Nature communications*, *9*(1), 1–13. doi: https://doi.org/10.1038/s41467-018-03553-w

Zakem, E. J., Cael, B., & Levine, N. M. (2021). A unified theory for organic matter accumulation. *Proceedings of the National Academy of Sciences*, *118*(6). doi: https://doi.org/10.1073/pnas.2016896118

Zark, M., Christoffers, J., & Dittmar, T. (2017). Molecular properties of deep-sea dissolved organic matter are predictable by the central limit theorem: Evidence from tandem FT-ICR-MS. *Marine Chemistry*, *191*, 9–15. doi: https://doi.org/10.1016/j.marchem.2017.02.005

Zhang, H., Menemenlis, D., & Fenty, I. (2018). *ECCO LLC270 ocean-ice state estimate* (Tech. Rep.). Jet Propulsion Laboratory, California Institute of Technology.

Zhang, J., Hibler, W., Steele, M., & Rothrock, D. (1998). Arctic ice–ocean modeling with and without climate restoring. *Journal of Physical Oceanography*, *28*(2), 191–217. doi: https://doi.org/10.1175/1520-0485(1998)028<0191:AIOMWA>2.0.CO;2

APPENDIX

Chapter 1: General Introduction

Table A.1: State variables simulated in ED-SBS with their units and description. Crosses indicate the presence of the state variable in ED-SBS Baseline and Arctic-specific configurations

State Variable	Units	Description	Baseline	Arctic
DIC	mmol C m^{-3}	dissolved inorganic carbon	X	X
NO_3	mmol N m^{-3}	nitrate	X	X
NO_2	mmol N m^{-3}	nitrite	X	X
NH_4	mmol N m^{-3}	ammonia	X	X
PO_4	mmol P m^{-3}	phosphate	X	X
FeT	mmol Fe m^{-3}	total dissolved iron	X	X
SiO_2	mmol Si m^{-3}	inorganic silica	X	X
DOC	mmol C m^{-3}	dissolved organic carbon	X	
DOCsl	mmol C m^{-3}	semi-labile dissolved organic carbon		X
DOCsr	mmol C m^{-3}	semi-refractory dissolved organic carbon		X
DON	mmol N m^{-3}	dissolved organic nitrogen	X	X
DOP	mmol P m^{-3}	dissolved organic phosphorus	X	X
DOFe	mmol Fe m^{-3}	dissolved organic iron	X	X
POC	mmol C m^{-3}	particulate organic carbon	X	X
PON	mmol N m^{-3}	particulate organic nitrogen	X	X
POP	mmol P m^{-3}	particulate organic phosphorus	X	X
POFe	mmol Fe m^{-3}	particulate organic iron	X	X
POSi	mmol Si m^{-3}	particulate organic silica	X	X
PIC	mmol C m^{-3}	particulate inorganic carbon	X	X
Alk	meq m^{-3}	alkalinity	X	X
O_2	mmol O_2 m^{-3}	oxygen	X	X
c_1	mmol C m^{-3}	diatoms	X	X
c_2	mmol C m^{-3}	large eukaryotes	X	X
c_3	mmol C m^{-3}	*Synechococcus*	X	
c_4	mmol C m^{-3}	low-light adapted *Prochlorococcus*	X	
c_5	mmol C m^{-3}	high-light adapted *Prochlorococcus*	X	
c_6	mmol C m^{-3}	small zooplankton	X	X
c_7	mmol C m^{-3}	large zooplankton	X	X
chl_1	mg Chl m^{-3}	diatoms chlorphyll-a	X	X
chl_2	mg Chl m^{-3}	large eukaryotes chlorphyll-a	X	X
chl_3	mg Chl m^{-3}	*Synechococcus* chlorphyll-a	X	
chl_4	mg Chl m^{-3}	low-light adapted *Prochlorococcus* chlorphyll-a	X	
chl_5	mg Chl m^{-3}	high-light adapted *Prochlorococcus* chlorphyll-a	X	

Chapter 3: Merging satellite and in situ data to assess the flux of terrestrial dissolved organic carbon from the Mackenzie River to the coastal Beaufort Sea

Table A.2: Regression model equations available in the LOADEST estimator to retrieve the load (L) of a river constituent from discharge (Q) and decimal time (dtime).

Model Number	Regression model ($\ln L =$)
1	$a_0 + a_1 \ln Q$
2	$a_0 + a_1 \ln Q + a_2 \ln Q^2$
3	$a_0 + a_1 \ln Q + a_5 dtime$
4	$a_0 + a_1 \ln Q + a_3 \sin 2\pi dtime + a_4 \cos 2\pi dtime$
5	$a_0 + a_1 \ln Q + a_2 \ln Q^2 + a_6 dtime^2$
6	$a_0 + a_1 \ln Q + a_2 \ln Q^2 + a_3 \sin 2\pi dtime + a_4 \cos 2\pi dtime$
7	$a_0 + a_1 \ln Q + a_3 \sin 2\pi dtime + a_4 \cos 2\pi dtime + a_5 dtime$
8	$a_0 + a_1 \ln Q + a_2 \ln Q^2 + a_3 \sin 2\pi dtime + a_4 \cos 2\pi dtime + a_5 dtime$
9	$a_0 + a_1 \ln Q + a_2 \ln Q^2 + a_3 \sin 2\pi dtime + a_4 \cos 2\pi dtime + a_5 dtime + a_6 dtime^2$

Table A.3: Constants ($\pm$ standard deviation) of the regression models.

Estimate (tDOC$_{est}$)	a_0	a_1	a_2
tDOC$_{est_ref}$	14.82 ($\pm$0.04)	1.17 ($\pm$0.03)	0.26 ($\pm$0.07)
tDOC$_{est_sat}$ (Shallow Bay)	13.78 ($\pm$0.02)	1.16 ($\pm$0.02)	0.09 ($\pm$0.03)
tDOC$_{est_sat}$ (Beluga Bay)	14.02 ($\pm$0.01)	1.14 ($\pm$0.01)	0.02 ($\pm$0.02)
tDOC$_{est_sat}$ (Kugmallit Bay)	13.86 ($\pm$0.02)	1.15 ($\pm$0.02)	0.02 ($\pm$0.03)

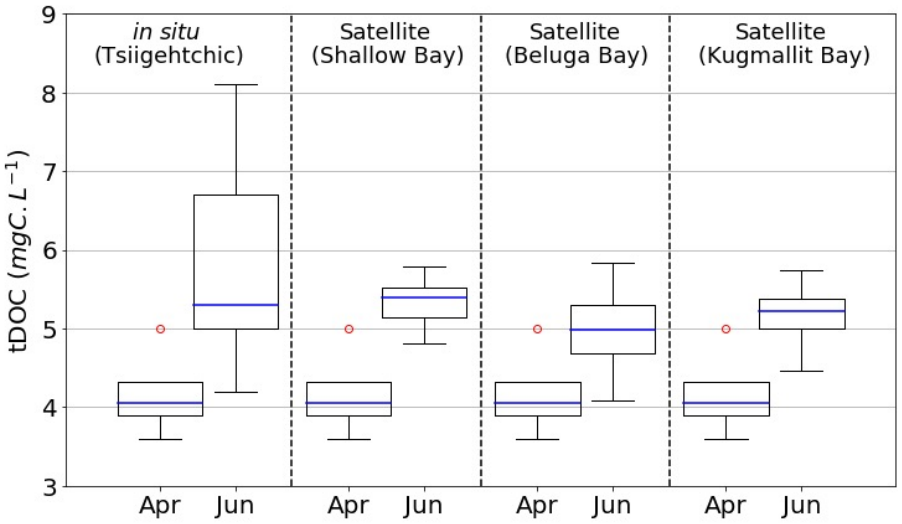

Figure A.1: *In situ* and remotely-sensed tDOC concentrations (mgC L^{-1}) in April and June. The blue line shows the median, the box encloses the 25^{th} and 75^{th} percentiles, the whiskers delimit the 5^{th} and 95^{th} percentiles, and the circles represent the outliers.

Chapter 4: Biogeochemical river runoff drives intense Arctic Ocean outgassing

Text A1. ECCO-Darwin Regional Simulation Ocean and sea-ice dynamics were simulated with the Massachusetts Institute of Technology (MIT) general circulation model (MITgcm, Marshall et al., 1997). MITgcm was coupled online with the MIT Darwin ecosystem model (Follows et al., 2006; Dutkiewicz et al., 2009; Follows & Dutkiewicz, 2011; Dutkiewicz et al., 2015). The model assimilates physical ocean observations using the adjoint method according to the Estimating the Circulation and Climate of the Ocean (ECCO) consortium efforts (Wunsch et al., 2009). The assimilation of biogeochemical observations and optimization of the initial conditions for the Darwin biogeochemical and ecological parameters uses a Green's Functions approach (Menemenlis, Fukumori, & Lee, 2005). The regional configuration of the Southern Beaufort Sea (SBS) ECCO-Darwin model (ED-SBS) was extracted from the ECCO LLC270 configuration (H. Zhang et al., 2018). ED-SBS model has an averaged 12km horizontal spacing and 44 evenly-spaced vertical levels. ED-SBS was integrated from January 1992 to December 2019, with a time step of 1200 sec; only the last 19 years (2000–2019) were analyzed to mitigate spin up. The Darwin ecosystem model was modified from Carroll et al. (2020) to account for the specific environment of the SBS. It has two phytoplankton (diatoms and large eukaryotes) and two zooplankton (small and large). In order to maintain a sufficient stock of phytoplankton biomass in winter, we set a minimal threshold at 0.05 mmolC m^{-3} to the phytoplankton biomass based on high-frequency observations (Randelhoff et al., 2020). ED-SBS simulates two distinct DOC tracers fields representative of molecules retrieved in Arctic coastal water and both forced by riverine discharge of terrestrial DOC (tDOC) according to a specific ratio (Text S2). The semi-labile (DOC_{sl}) compartment includes molecules with rapid turnover rates (weeks to month) while the semi-refractory (DOC_{sr}) includes molecules already reworked with longer lifetime (decades) (Lønborg et al., 2020; Dittmar et al., 2021). Initial and boundary conditions for DOC_{sl} were obtained from the DOC tracer in Carroll et al. (2020). DOC_{sr} boundary conditions conditions were set to 50μM at all horizontal and vertical wet grid cells to represent the more recalcitrant matter present in the waters. This value was based on an offset observed between the global ECCO-Darwin simulation and *in situ* DOC observations.

Text A2. River Forcing Mackenzie River discharge data from January 1992 to December 2019 was derived from the Arctic Great Rivers Observatory (ArcticGRO) dataset (Shiklomanov et al., 2021). Freshwater discharge was sampled daily at the Tsiigehtchic station (67.45°N, 133.74°W), roughly 200 km upstream from the Mackenzie Delta. A quadratic method was used to interpolate 285 missing points (total of 10958). Terrestrial DIC (tDIC) concentrations in the Mackenzie River were estimated by using a nonlinear regression model based on the U.S. Geological Survey LOADEST estimator (Runkel et al., 2004). The model associates *in situ* tDIC measurements sampled from 2003–2010 with time-coincident daily freshwater discharge data (Tank et al., 2012) through a chemodynamic relationship. We applied this model to estimate the daily tDIC concentrations and load from 1992–2019 using the ArcticGRO discharge dataset. We derived daily terrestrial alkalinity (tAlk) in the Mackenzie River using a Alk:tDIC ratio of 0.93 (Tank et al., 2012). We estimated daily tDOC concentrations and load from 1992–2019 at three main delta outlets using the LOADEST estimator according to the methods described in Bertin et al. (2022). Based on a recent study (F. Joux, unpublished data; see Lizotte et al., 2022) that estimated the fraction of tDOC being bioavailable in the SBS, we assumed that DOC_{sr} and DOC_{sl} received each 50% of the total tDOC input. Both DOC pools are degraded at a constant rate $\lambda = 1/\tau$ (s^{-1}) modulated by seawater temperature, where τ is the turnover time. DOC_{sr} and DOC_{sl} turnover times were set to τ=10 years (Manizza et al., 2009) and τ=1 month (Spencer et al., 2015; Holmes et al., 2008), respectively. We used the GlobalNEWS2 climatology (Mayorga et al., 2010) to derive the riverine tDON, tDOP and tDSi load. Annual loads were combined with the ArcticGRO freshwater discharge dataset to generate climatological times series of riverine load from 1992–2019.

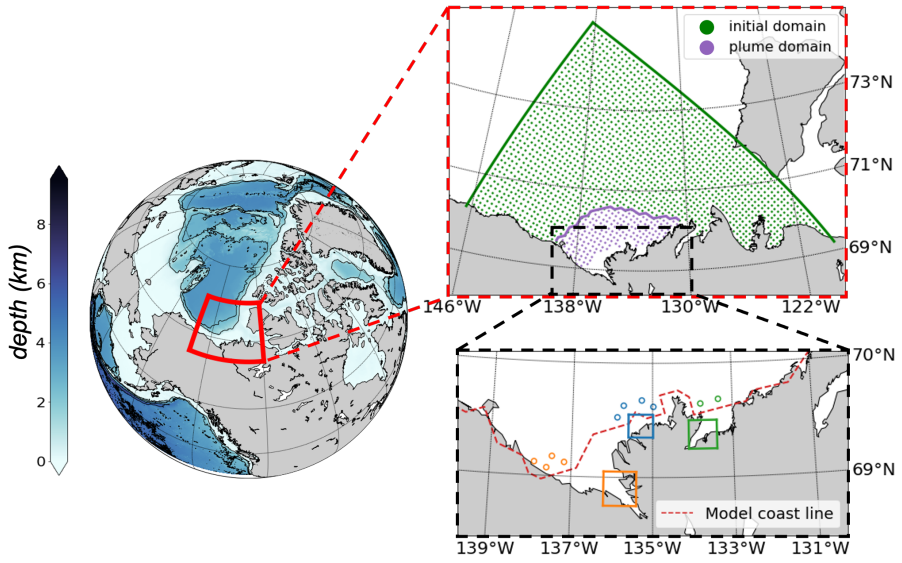

Figure A.2: Location and bathymetry of the Southeastern Beaufort Sea (left panel) with the full numerical domain and plume-influenced region (upper right). The colored circles (lower right panel) are the grid cells at which river forcing is applied: Shallow Bay (orange), Beluga Bay (blue), and Kugmallit Bay (green). The red dashed line represents the coastline of the numerical domain.

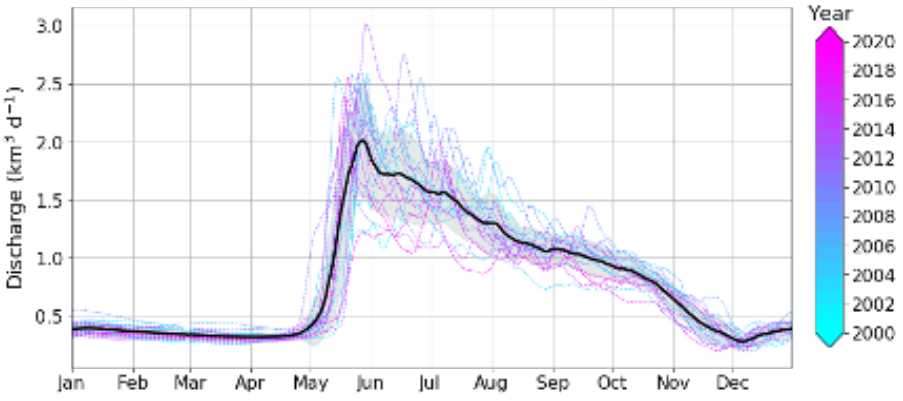

Figure A.3: Mackenzie River discharge (km^3 d^{-1}) from 2000 to 2019 measured by the Arctic Great River Observatory (AGRO; Shiklomanov et al., 2021). The black solid line shows the average discharge and the shaded area indicates the standard deviation.

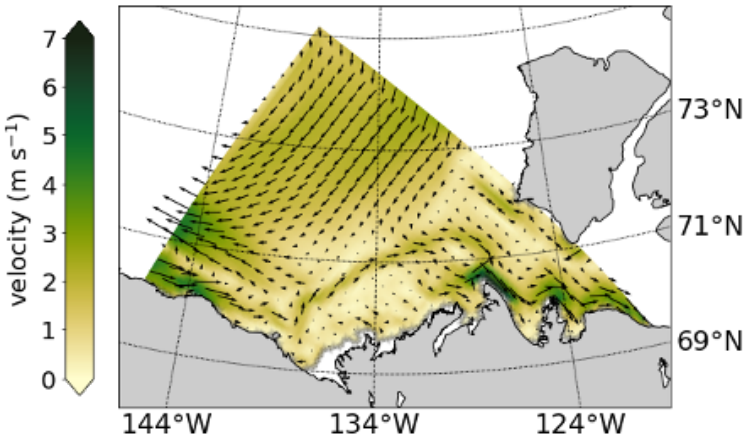

Figure A.4: July to September mean surface velocity field simulated over the 2000–2019 period

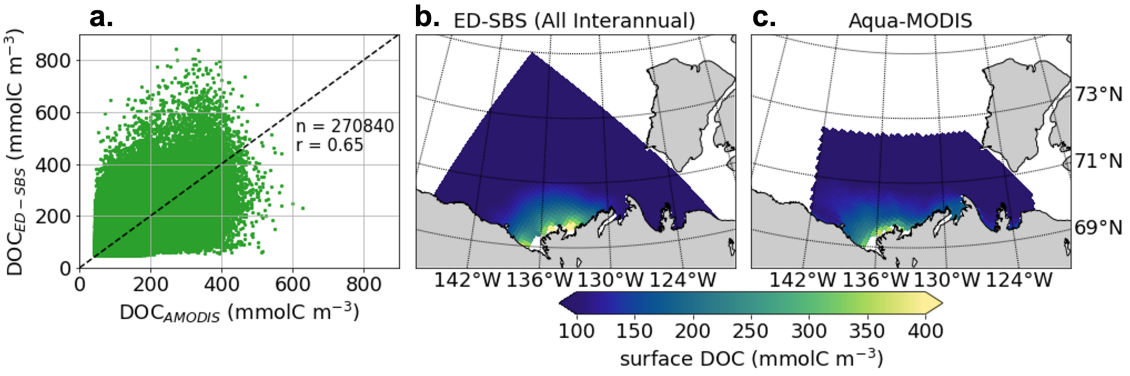

Figure A.5: (a) Scatter plot of surface DOC concentrations (mmolC m^{-3}) simulated by ED-SBS ("All Interannual") and retrieved from space by the Aqua-MODIS sensor from 2003 to 2017 (Matsuoka et al., 2017). Mean surface DOC concentrations (b) simulated by ED-SBS ("All Interannual") and (c) derived from satellite data.

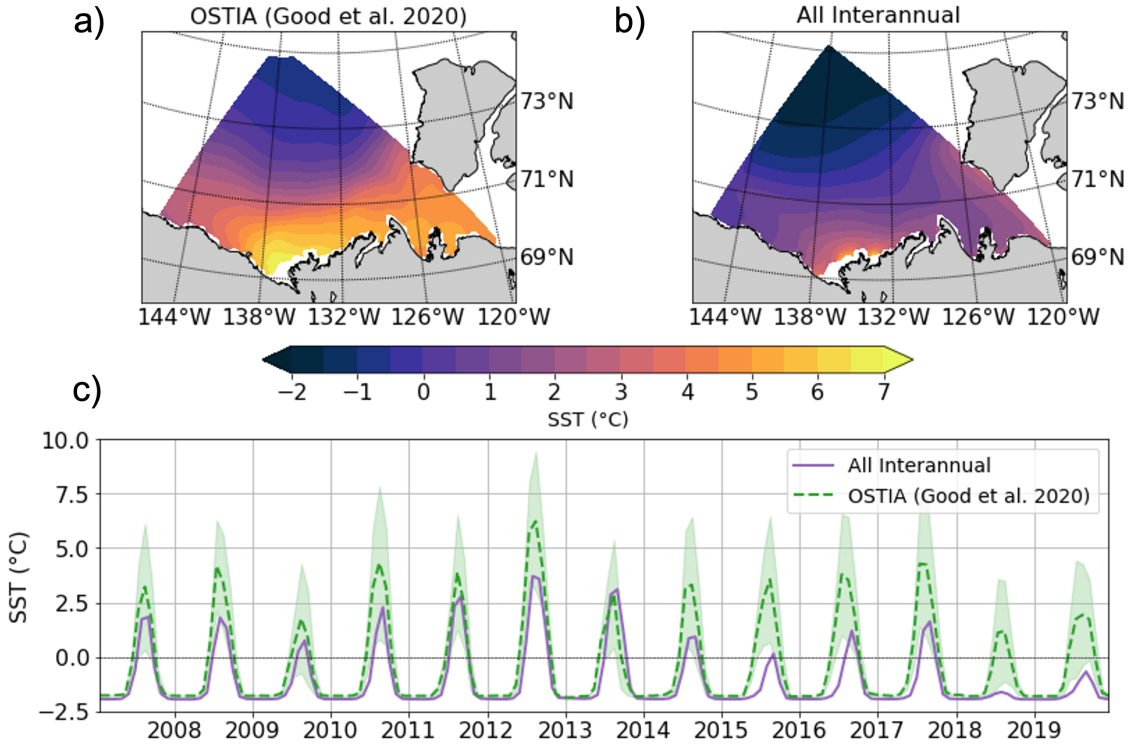

Figure A.6: July and September mean SST (a) derived from Operational Sea Surface Temperature and Sea Ice Analysis (OSTIA; Good et al., 2020) and (b) simulated in the "All Interannual" run. Panel (c) shows the mean SST (solid lines) and standard deviation (shaded area) for OSTIA (green) and the model (purple).

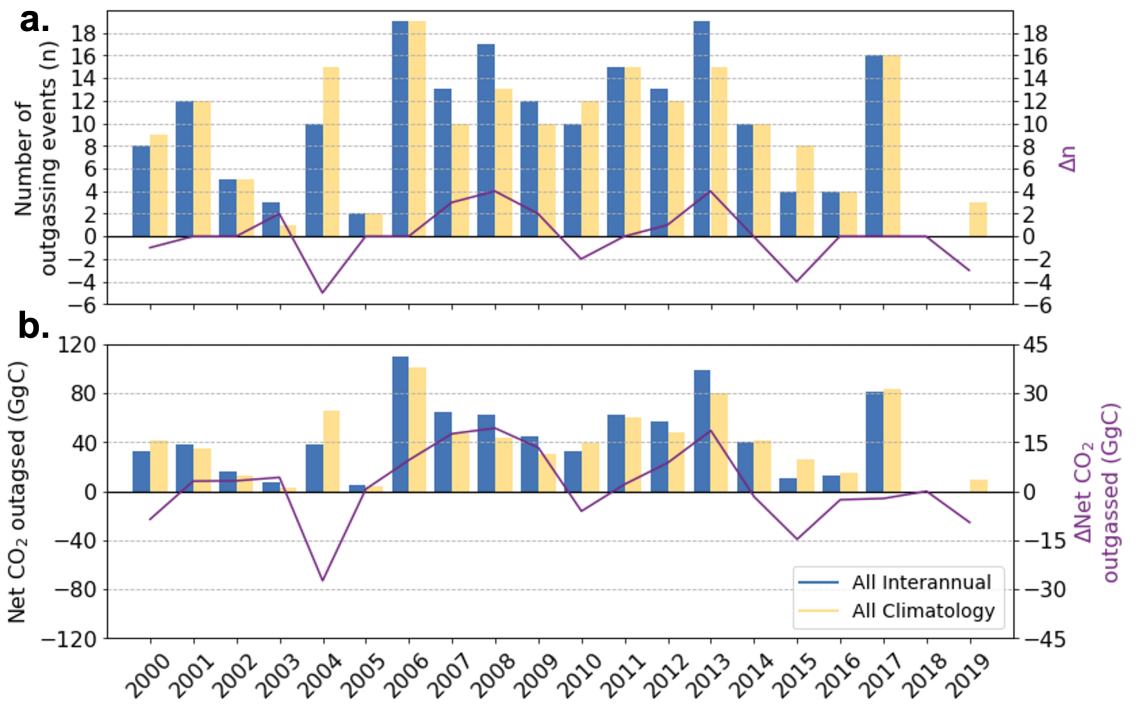

Figure A.7: (a) Number of outgassing events (n) and (b) total CO_2 outgassed (GgC) during these events simulated in the "All interannual" (in blue) and "All climatology" (in yellow) runs. The purple solid line represents the difference between the "All interannual" and "All climatology" runs.

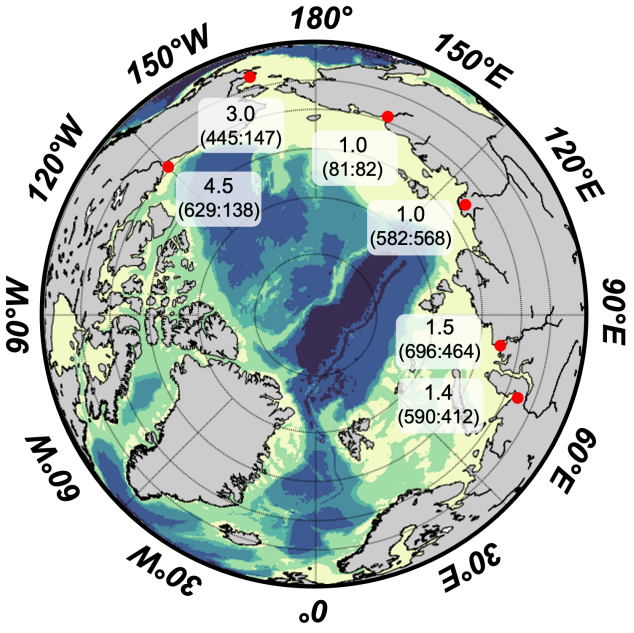

Figure A.8: tDIC:tDOC ratio estimated for the six major Pan-Arctic rivers (Mackenzie, Yukon, Kolyma, Lena, Yenisey and Ob'; Holmes et al., 2012; Tank et al., 2012)

Table A.4: Riverine annual flux of tDOC, tDIC, and tAlk, tDON, tDOP, and tDSi (Gg yr^{-1}, as C, N, P and Si) prescribed in the "All Interannual" run (mean $\pm$ std (min-max)), in the "All Climatology" run and estimated in previous studies

	This Study		Previous estimates
	Interannual	Climatology	
tDOC	1,410 $\pm$ 160 (1,080–1,660)	1,410	1,377-1,575[c,d]
tDIC	6,070 $\pm$ 450 (5,170–6,760)	6,080	5,781-6,290[b,e]
tAlk	5,650 $\pm$ 420 (4,810–6,290)	5,650	5,830[e]
tDON	X	80.5	31-50.8[a,b,c,d]
tDOP	X	4.3	1[a]
tDSi	X	712	464-1,060[a,b,c,d]

[a]Computed from AGRO data (2003-2017; Holmes et al. (2021))
[b]Terhaar et al. (2021b), computed from AGRO data (1999-2008)
[c]Le Fouest et al. (2013)
[d]Holmes et al. (2012), computed from AGRO data (1999-2008)
[e]Tank et al. (2012), computed from AGRO data (2000-2009)

Table A.5: SBS model runs and riverine forcing. Circles indicate interannual riverine forcing while triangles indicate climatological forcing.

Run	Freshwater	Temperature	tDIC-tAlk	tDOC	tDON-tDOP-tDSi
Q+Temp	o	o	-	-	-
All Interannual	o	o	o	o	△
All Climatology	△	o	△	△	△
No tDIC-tAlk	o	o	-	o	o
No tDOC	o	o	o	-	o
No Nutrients	o	o	o	o	-
No river	-	-	-	-	-
Q	o	-	-	-	-

Table A.6: Number of outgassing events and total net CO_2 outgassed by the event in All Interannual and All Climatology runs

	Event Number		Net outgassing (GgC)	
	All Interannual	All Climatology	All Interannual	All Climatology
July	22	19	87	66
August	68	10	320	326
September	93	66	378	366
October	9	9	30	29
Total	192	191	815	787

frontiers in Earth Science

ORIGINAL RESEARCH
published: 21 February 2022
doi: 10.3389/feart.2022.694062

Merging Satellite and *in situ* Data to Assess the Flux of Terrestrial Dissolved Organic Carbon From the Mackenzie River to the Coastal Beaufort Sea

Clément Bertin[1]*, *Atsushi Matsuoka*[2,3], *Antoine Mangin*[4], *Marcel Babin*[2] and *Vincent Le Fouest*[1]

[1]LIttoral ENvironnement et Sociétés (LIENSs)—UMR 7266, La Rochelle, France, [2]Takuvik Joint International Laboratory, CNRS, Québec, QC, Canada, [3]Institute for the Study of Earth, Oceans, and Space, University of New Hampshire, Durham, NH, United States, [4]ACRI-ST, Sophia Antipolis, France

In response to global warming, the Arctic is undergoing rapid and unprecedented changes that alter the land-to-sea forcing in large Arctic rivers. Improving our knowledge of terrestrial dissolved organic carbon (tDOC) flux to the coastal Arctic Ocean (AO) is thus critical and timely as these changes strongly alter the biogeochemical cycles on AO shelves. In this study, we merged riverine *in situ* tDOC concentrations with satellite ocean-color estimates retrieved at the land-marine interface of the Mackenzie Delta to make a first assessment of the tDOC export from its main outlets to the shelf. We combined tDOC and river discharge data to develop a regression model that simulated tDOC concentrations and fluxes from daily to interannual (2003–2017) time scales. We then compared the simulated satellite-derived estimates to those simulated by the model constrained by *in situ* tDOC data only. As the satellite tDOC estimates reflect the delta effect in terms of tDOC enrichment and removal, our results inform us of how much tDOC can potentially leave the delta to reach the ocean (1.44 ± 0.14 $TgC.yr^{-1}$). The chemodynamic relationships and the model suggest contrasting patterns between Shallow Bay and the two easternmost delta outlets, which can be explained by the variability in their geomorphological settings. At the seasonal scale and for all outlets, the satellite-derived tDOC export departs from the estimate based on *in situ* tDOC data only. During the river freshet in May, the satellite-derived tDOC export is, on average, ~15% (Shallow Bay) to ~20% (Beluga Bay) lower than the in situ-derived estimate. This difference was the highest (–60%) in 2005 and exceeds 30% over most of the last decade, and can be explained by qualitative and quantitative differences between the $tDOC_{in\ situ}$ and $tDOC_{sat}$ datasets in a period when the freshet is highly variable. In contrast, in summer and fall, the satellite-derived tDOC export is higher than the in situ-derived estimate. The temporal difference between the satellite and in situ-derived export estimates suggests that predicting seasonal tDOC concentrations and fluxes from remote Arctic deltas to the coastal AO remains a challenge for assessing their impact on already changing carbon fluxes.

Keywords: terrestrial DOC, land-to-sea interface, permafrost, Mackenzie delta, space remote sensing

OPEN ACCESS

Edited by:
Louise Farquharson, University of Alaska Fairbanks, United States

Reviewed by:
Eurico D'Sa, Louisiana State University, United States
Benjamin M. Jones, University of Alaska Fairbanks, United States

***Correspondence:**
Clément Bertin
clement.bertin1@univ-lr.fr

Specialty section:
This article was submitted to Biogeoscience, a section of the journal Frontiers in Earth Science

Received: *12 April 2021*
Accepted: *12 January 2022*
Published: *21 February 2022*

Citation:
Bertin C, Matsuoka A, Mangin A, Babin M and Le Fouest V (2022) Merging Satellite and in situ Data to Assess the Flux of Terrestrial Dissolved Organic Carbon From the Mackenzie River to the Coastal Beaufort Sea. Front. Earth Sci. 10:694062. doi: 10.3389/feart.2022.694062

Geophysical Research Letters

RESEARCH LETTER
10.1029/2022GL102377

Biogeochemical River Runoff Drives Intense Coastal Arctic Ocean CO_2 Outgassing

C. Bertin[1], D. Carroll[2,3], D. Menemenlis[3], S. Dutkiewicz[4], H. Zhang[3], A. Matsuoka[5], S. Tank[6], M. Manizza[7], C. E. Miller[3], M. Babin[8], A. Mangin[9], and V. Le Fouest[1]

[1]LIttoral ENvironnement et Sociétés (LIENSs) – UMR 7266, Bâtiment ILE, La Rochelle, France, [2]Moss Landing Marine Laboratories, San José State University, Moss Landing, CA, USA, [3]Jet Propulsion Laboratory, California Institute of Technology, Pasadena, CA, USA, [4]Department of Earth Atmospheric and Planetary Sciences, Massachusetts Institute of Technology, Cambridge, MA, USA, [5]Institute for the Study of Earth, Oceans, and Space, University of New Hampshire, Durham, NH, USA, [6]Department of Biological Sciences, University of Alberta, Edmonton, AB, Canada, [7]Geosciences Research Division, Scripps Institution of Oceanography, University of California San Diego, La Jolla, CA, USA, [8]Takuvik Joint International Laboratory, Université Laval and CNRS, Québec, QC, Canada, [9]ACRI-ST, Sophia Antipolis, France

Key Points:

- Mackenzie River biogeochemical discharge decreases the southeastern Beaufort Sea carbon sink
- Terrestrial dissolved inorganic carbon (DIC) is the primary driver of outgassing events in the SBS, followed by terrestrial DOC
- Interannual variability in river discharge modulates localized air-sea CO_2 flux

Supporting Information:

Supporting Information may be found in the online version of this article.

Correspondence to:

C. Bertin,
clement.bertin1@univ-lr.fr

Citation:

Bertin, C., Carroll, D., Menemenlis, D., Dutkiewicz, S., Zhang, H., Matsuoka, A., et al. (2023). Biogeochemical river runoff drives intense coastal Arctic Ocean CO_2 outgassing. *Geophysical Research Letters*, *50*, e2022GL102377. https://doi.org/10.1029/2022GL102377

Received 9 DEC 2022
Accepted 9 MAR 2023

Author Contributions:

Conceptualization: D. Carroll, D. Menemenlis, S. Dutkiewicz, H. Zhang, V. Le Fouest
Formal analysis: D. Carroll, D. Menemenlis, S. Dutkiewicz, M. Manizza, V. Le Fouest
Funding acquisition: C. E. Miller, M. Babin, A. Mangin, V. Le Fouest
Investigation: V. Le Fouest
Methodology: D. Carroll, D. Menemenlis, S. Dutkiewicz, H. Zhang, V. Le Fouest
Resources: A. Matsuoka, S. Tank
Software: H. Zhang

Abstract Arctic warming alters land-to-sea fluxes of nutrients and organic matter, which impact air-sea carbon exchange. Here we use an ocean-biogeochemical model of the southeastern Beaufort Sea (SBS) to investigate the role of Mackenzie River biogeochemical discharge in modulating air-sea CO_2 fluxes during 2000–2019. The contribution of six biogeochemical discharge constituents leads to a net CO_2 outgassing of 0.13 TgC yr^{-1}, with a decrease in the coastal SBS carbon sink of 0.23 and 0.4 TgC yr^{-1} due to riverine dissolved organic and inorganic carbon, respectively. Years with high (low) discharge promote more CO_2 outgassing (uptake) from the river plume. These results demonstrate that the Mackenzie River modulates the capacity of the SBS to act as a sink or source of atmospheric CO_2. Our work suggests that accurate model representation of land-to-sea biogeochemical coupling can be critical for assessing present-day Arctic coastal ocean response to the rapidly changing environment.

Plain Language Summary We modeled the discharge of freshwater and six biogeochemical constituents from the Mackenzie River into the southeastern Beaufort Sea to study their impact on ocean-atmosphere carbon dioxide (CO_2) fluxes during 2000–2019. We find that biogeochemical constituents from river runoff promote CO_2 outgassing to the atmosphere in the river plume region. Dissolved inorganic carbon is the main contributor to this phenomenon, with river discharge events driving pulses of intense CO_2 outgassing during ice-free periods. Our results show that the capacity of the SBS to act as an atmospheric CO_2 sink or source is strongly related to interannual variability in biogeochemical river discharge. Our results highlight the increased coupling of Arctic land-ocean biogeochemical systems under rapid environmental changes.

1. Introduction

The Arctic Ocean (AO) is estimated to be a carbon sink of roughly 118 to 180 TgC yr^{-1} (Arrigo et al., 2010; Manizza et al., 2019; Yasunaka et al., 2018). Its net contribution to global CO_2 uptake is massive relative to its surface area (Bates & Mathis, 2009). However, whether the coastal periphery, which occupies approximately 50% of the AO (e.g., Carmack et al., 2006), acts as a net atmospheric CO_2 source or sink, remains poorly understood (Forest et al., 2014; Roobaert et al., 2019). For example, warming-induced changes in land-to-sea fluxes of freshwater associated with biogeochemical variables (Mann et al., 2022; Tank et al., 2012, 2016) can drive CO_2 outgassing rather than CO_2 uptake (Lacroix et al., 2021; Roobaert et al., 2019). An improved understanding of the effect of freshwater-biogeochemical discharge from Arctic rivers is therefore critical for accurately estimating AO air-sea CO_2 exchange.

Arctic rivers transport 11% of global freshwater to the world's ocean (McClelland et al., 2012) and contribute half of the net freshwater input to the AO (Brown et al., 2020). Additionally, these rivers transport significant amounts of inorganic nutrients and organic matter into the coastal zone (Dittmar & Kattner, 2003; Holmes et al., 2012; Juhls et al., 2020; Le Fouest et al., 2013; Rawlins et al., 2021), with part of the organic matter signal originating from thawing of northern permafrost and peatlands (Hugelius et al., 2014; Schuur et al., 2015). While riverine inorganic nutrients promote phytoplankton growth and enhance nearshore CO_2 uptake, fluxes of terrestrial

Merging remotely-sensed and *in situ* data to assess the riverine flux of dissolved organic carbon from the Mackenzie River to the Beaufort Sea

C. Bertin[1], A. Matsuoka[2], A. Mangin[3], M. Babin[2], V. Le Fouest[1]

ARCTIC CHANGE 2020

Background. There is growing evidence that permafrost thaws and influences biogeochemistry in Arctic coastal waters (Lantuit et al. 2012, Schuur et al. 2015). We need to quantify the daily land-to-sea flux of riverine dissolved organic carbon (tDOC) to infer on the ecosystem response at the synoptic to seasonal scale, which determines the physical-biological coupling in Arctic coastal seas. Here we assess the potential of using remotely-sensed tDOC estimates to quantify daily tDOC fluxes from the Mackenzie River to the shelf.

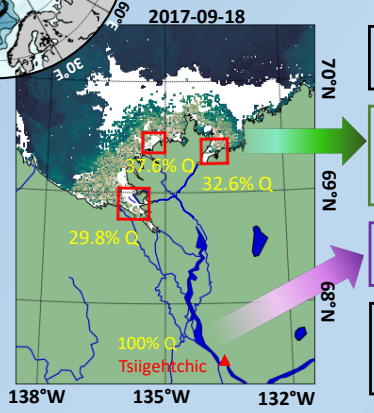

Daily discharge (Q)

Satellite tDOC retrieved in 3 bays (defined according to Morley, 2012)

In situ tDOC samples

Daily discharge coincident with tDOC data

Merge

3 merged datasets

1 *in situ* dataset

LOADEST regression model coefficients

a_0, a_1, a_2

$$\ln(L) = a_0 + a_1 \ln Q + a_2 \ln Q^2$$

Simulated daily tDOC flux (L) & concentration

4 estimates (2003-2017) :

- **1 "Reference"** : Based on *in situ* data (Tsiigehtchic)
- **3 "Satellite"** : Based on merged *in situ* and remote sensing data

Effect of satellite data on simulated tDOC concentrations (Table 1)

Adding satellite data in the LOADEST model :

- Increased the number of data during ice-free conditions
- Decreased the data dispersion (simulated *vs* observations)
- Improved the model prediction efficiency
- Maintain a high correlation between the model and the observations

Table 1: Simulated tDOC comparison metrics (*in situ versus in situ* + satellite)

	"REFERENCE"	"SATELLITE"					
		SHALLOW BAY		BELUGA BAY		KUGMALLIT BAY	
N	66	108	+	220	+	144	+
r	0.81	0.85	+	0.74	–	0.79	≃
NSE	0.44	0.53	+	0.30	–	0.38	–
URMSE	0.82	0.49	+	0.49	+	0.54	+
MPE	12.74	5.35	+	6.02	+	6.34	+

(N: number of data; r: correlation coefficient; NSE: Nash-Sutcliffe Efficiency; URMSE: unbiased root mean square error; MPE: model predictive percentage error)

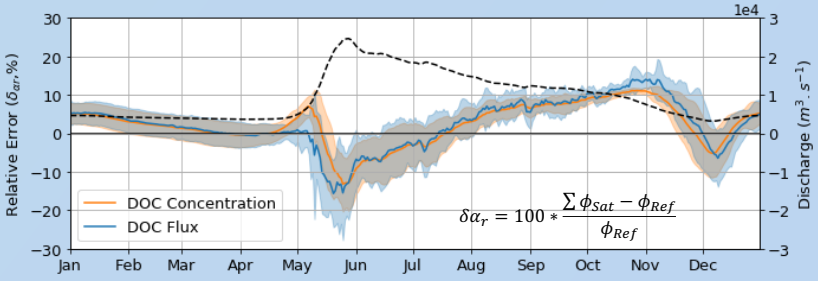

Fig. 1: Relative error between the « Satellite » *versus* « Reference » tDOC estimates

Seasonal shift in the simulated tDOC concentration and flux (Fig. 1)

With tDOC satellite data:

- Simulated tDOC concentration and flux lower in May-June but higher in summer-fall
- Simulated tDOC flux 15% lower, in average, during the seasonal peak of discharge

Take home message

Merging remotely-sensed and *in situ* tDOC concentrations :

1. Provides simulated tDOC concentrations and fluxes at the 3 main outlets of the Mackenzie delta
2. Leads to simulated tDOC estimates closer to observations than with *in situ* tDOC data only
3. Induces a seasonal shift in the simulated tDOC flux

Such a seasonal shift may result into contrasted biogeochemical responses in the coastal Arctic that will further need to be assessed.

References

Lantuit, H., Overduin, P. P., Couture, N., Wetterich, S., Aré, F., Atkinson, D., et al. (2012). The Arctic Coastal Dynamics Database: A New Classification Scheme and Statistics on Arctic Permafrost Coastlines. *Estuaries and Coasts* 35, 383–400. doi:10.1007/s12237-010-9362-6.

Morley, J. K. (2012). Observations of Flow Distributions and River Breakup in the Mackenzie Delta, NWT. doi:10.7939/R3N02H.

Schuur, E. A. G., McGuire, A. D., Schädel, C., Grosse, G., Harden, J. W., Hayes, D. J., et al. (2015). Climate change and the permafrost carbon feedback. *Nature* 520, 171–179. doi:10.1038/nature14338.

[1] Littoral, Environnement et Sociétés (LIENSs), Université de La Rochelle, UMR 7266, CNRS-ULR, 1700 La Rochelle, France
[2] Takuvik Joint International Laboratory, Département de Biologie, Université Laval, 1045, avenue de la Médecine, Québec, QC G1V 0A6, Canada
[3] ACRI-ST, 260, route du Pin Montard — B.P. 234, 06904 Sophia Antipolis Cedex, France

Quantifying the impact of terrestrial dissolved organic carbon (tDOC) on Beaufort Sea coastal air-sea CO_2 fluxes over seasonal to interannual timescales

Clément Bertin[1], Dustin Carroll[2,3], Dimitris Menemenlis[3], Stephanie Dutkiewicz[4], Manfredi Manizza[5], Hong Zhang[3], Charles Miller[3], Atsushi Matsuoka[6], Marcel Babin[7], Antoine Mangin[8], Vincent Le Fouest[1]

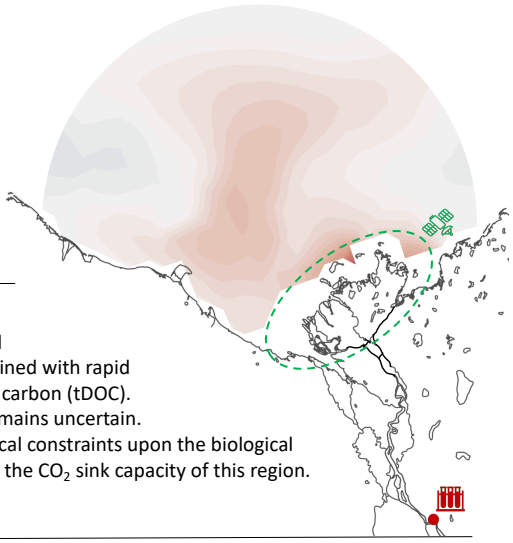

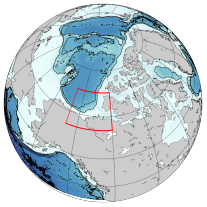

Background. In response to climate change, the Arctic is undergoing historically unprecedented changes in both its watersheds and coastal waters. Accelerating riverine freshwater flux[1], combined with rapid permafrost thaw[2], can drive an increase in the land-to-sea flux of terrigenous dissolved organic carbon (tDOC). However, the response of air-sea CO_2 fluxes near river deltas, and hence coastal ecosystems, remains uncertain. Given the strong regional and seasonal differences[3] a better understanding of the biogeochemical constraints upon the biological communities at these space and temporal scales is now required to infer on future evolution of the CO_2 sink capacity of this region.

Land

Assessing the riverine tDOC flux to the coast using satellite data

- Satellite data resolve the different delta outlets: gain in spatial and temporal resolution to compute the tDOC flux[4].
- By merging *in situ* and satellite tDOC, we estimate the daily to interannual riverine tDOC flux to the coast.

With or without satellite data: from the interannual to seasonal scale

- The simulated annual tDOC flux (1.47 ± 0.18 TgC.yr $^{-1}$) using satellite data is consistent with *in situ* tDOC only (< 5 % difference, Fig. 1).
- With satellite data: seasonal shift of the tDOC flux (Fig. 2):
  Freshet → lower by up to 20 %
  Sea Ice minimum (summer) → higher by up to 15%
- With satellite data, more tDOC is exported to the sea during sea ice minimum period.

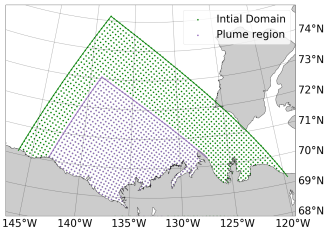

Simulating the coastal Beaufort Sea

- ECCO-Darwin regional simulation extracted from global model[6] (Fig. 3)
- Mackenzie River input of discharge, temperature and 6 biogeochemical tracers

Figure 3. Southeastern Beaufort Sea domain (green and purple) modeled. The purple domain represents the plume region.

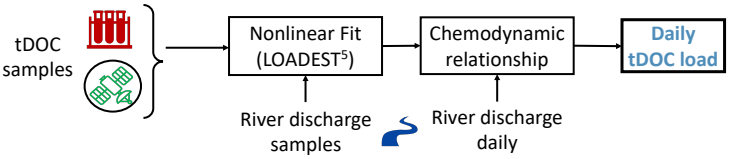

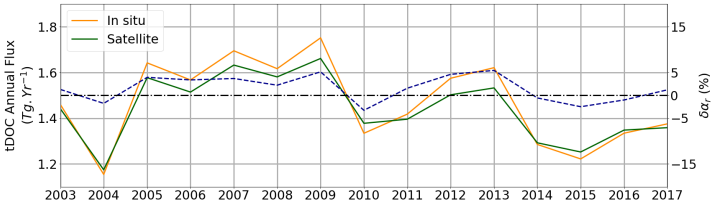

Figure 1. Simulated annual tDOC flux (TgC.yr^{-1}) estimated from the "In situ" dataset (orange line) and the "Satellite" dataset (green line). The dashed blue line represents the error of the "Satellite" estimate relative to the "Reference" estimate (δ_{ar} ,%) (from Bertin et al. 2022)

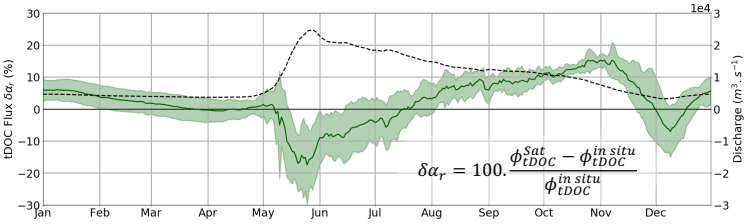

Figure 2. Error of the simulated daily tDOC flux estimated from the "Satellite" dataset relative to the "In situ" estimate (δ_{ar} , %) averaged over the 2003–2017 period. The shaded area represents the mean ± SD. The black dashed line corresponds to the daily freshwater river discharge averaged over the 2003–2017 period (from Bertin et al. 2022).

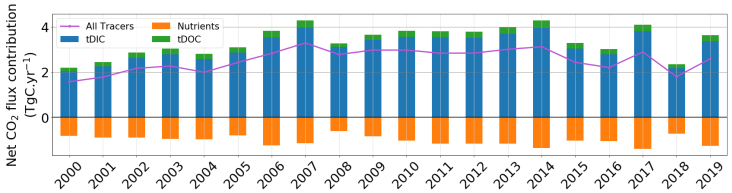

Figure 4. Simulated contribution of tDIC (blue), tDOC (green) and nutrients (DON/DOP/DSi, orange) to CO_2 fluxes (TgC.yr^{-1}) in the plume region. The purple line indicates the overall contribution of the biogeochemical plume.

Contribution of the riverine biogeochemical tracers to the CO_2 fluxes

- Nutrients (DON/DOP/DSi) promote ocean pumping with 1.03 ± 0.21 TgC.yr $^{-1}$ captured by enhancing the primary production (Fig. 4).
- tDIC & tDOC exports both contribute to 3.13 ± 0.59 and 0.24 ± 0.09 TgC.yr $^{-1}$ ventilated, respectively (Fig. 4).
- tDIC plays a major role: 3 times and 13 times higher than nutrients and tDOC, respectively.

Sea

Take home message

- Using satellite data translates into a seasonal shift in the riverine tDOC flux to the ocean: important to force ocean-biogeochemical models.
- In the plume area, tDIC plays a major role in controlling CO_2 fluxes and cannot be missed in modelling studies.
- tDOC appears to play a minor role, but its dynamics is very dependent on the representation of its remineralization: improvements must be done this way to get more realistic and accurate parametrization in predictive models.

References

1. Ahmed, R., Prowse, T., Dibike, Y., Bonsal, B., & O'Neil, H. (2020). Recent trends in freshwate influx to the arctic ocean from four major arctic-draining rivers. Water, 12(4), 1189. doi: https://doi.org/10.3390/w12041189

2. Schuur, E. A., McGuire, A. D., Schädel, C., Grosse, G., Harden, J. W., Hayes, D. J., ... & Vonk, J. E. (2015). Climate change and the permafrost carbon feedback. *Nature*, *520*(7546), 171-179. doi: https://doi.org/10.1038/nature14338

3. Brown, K. A., Holding, J. M., & Carmack, E. C. (2020). Understanding regional and seasonal variability is key to gaining a pan-arctic perspective on arctic ocean freshening. Frontiers in Marine Science, 606. doi: https://doi.org/10.3389/fmars.2020.00606

4. Matsuoka, A., Boss, E., Babin, M., Karp-Boss, L., Hafez, M., Chekalyuk, A., ... & Bricaud, A. (2017). Pan-Arctic optical characteristics of colored dissolved organic matter: Tracing dissolved organic carbon in changing Arctic waters using satellite ocean color data. *Remote sensing of Environment*, *200*, 89-101. https://doi.org/10.1016/j.rse.2017.08.009

5. Runkel, R. L., Crawford, C. G., Cohn, T. A., & US GS, L. E. (2004). A FORTRAN program for estimating constituent loads in streams and rivers. US Department of the Interior. *US Geological Survey*.

6. Carroll, D., Menemenlis, D., Adkins, J. F., Bowman, K. W., Brix, H., Dutkiewicz, S., ... & Zhang, H. (2020). The ECCO-Darwin data-assimilative global ocean biogeochemistry model: Estimates of seasonal to multidecadal surface ocean pCO2 and air-sea CO2 flux. *Journal of Advances in Modeling Earth Systems*, *12*(10), e2019MS001888. doi: https://doi.org/10.1029/2019MS001888

[1]Littoral ENvironnement et Sociétés (UMR 7266), La Rochelle Université, La Rochelle, France
[2]Moss Landing Marine Laboratories, San José State University, Moss Landing, USA
[3]NASA Jet Propulsion Laboratory-California Institute of Technology, Pasadena, USA
[4]Massachusetts Institute of Technology (MIT), Cambridge, USA
[5]Scripps Institution of Oceanography, University of California San Diego, La Jolla, USA
[6]Institute for the Study of Earth, Oceans, and Space, University of New Hampshire, Durham, USA
[7]Takuvik Joint International Laboratory, CNRS, Québec, Canada
[8]ACRI-ST, Sophia Antipolis, France

ELIGIBLE FOR THE ARCTIC FRONTIERS–APECS EARLY CAREER SCIENTIST AWARD

Le rôle du fleuve Mackenzie dans la biogéochimie du carbone des eaux côtières de la mer de Beaufort (Océan Arctique)

Cinq des plus grands fleuves mondiaux sont en Arctique et transportent des quantités importantes de carbone dissous organique (COD) et inorganique (CID) dans l'Océan Arctique (OA). La réponse de l'océan côtier à ces apports est encore incertaine, ce qui est un frein à l'estimation des flux air/mer de CO_2 dans cette région. Dans un contexte de réchauffement climatique et de changement rapide de l'environnement arctique, il est donc important de mieux comprendre l'effet de ces apports de carbone terrigène sur les flux de CO_2 dans les panaches fluviaux. Le modèle couplé océan/glace/biogéochimie ECCO-Darwin est utilisé afin d'étudier la réponse du sud-est de la mer de Beaufort aux apports de carbone dissout du fleuve Mackenzie des échelles synoptiques à interannuelles. Ce modèle régional intègre le tout premier forçage interannuel journalier de COD terrigène provenant du Mackenzie estimé grâce à la fusion de données *in situ* et de données satellites acquises aux trois embouchures principales du delta. Nous observons que la variabilité interannuelle du débit du Mackenzie module localement les flux air/mer de CO_2 dans le panache fluvial côtier. Le CID terrigène contribue deux fois plus que le COD terrigène au dégazage du panache. Avec le dégel du pergélisol, les incertitudes sur la dégradation du COD terrigène dans les panaches fluviaux sont nombreuses. La variabilité des flux air/mer de CO_2 liée à la dégradation bactérienne est estimée à ± 0.39 TgC yr^{-1} en 2009. D'autres processus biophysiques contribuent également à cette variabilité comme la floculation du COD terrigène (+0.14 TgC yr^{-1} absorbé par l'océan) et la stratification verticale induite par le panache (+0.35 TgC yr^{-1} rejeté par l'océan). Ce travail de thèse met en lumière l'importance d'inclure une représentation réaliste du continuum terre/mer dans les modèles régionaux arctiques afin d'améliorer les estimés de flux de carbone dans cet océan changeant et fortement altéré par les modifications de ses bassins versants.

Mots clés : Arctique, interface terre/mer, panaches fluviaux, carbone dissout terrigène, modélisation océan/glace/biogéochimie

The role of the Mackenzie River in the carbon biogeochemistry of the Beaufort Sea coastal waters (Arctic Ocean)

About 10 % of atmospheric carbon dioxide is sequestered in the ocean above 60°N, half of which is in coastal seas where 10 % of the global riverine freshwater volume flows in. Five of the world's largest rivers convey in the Arctic Ocean (AO) huge quantities of dissolved carbon in the organic (DOC) and inorganic (DIC) form. The response of the coastal ocean to this supply is still highly uncertain, which makes the assessment of air-sea CO_2 fluxes challenging in this remote region. It is thus timely to gain a better understanding of the impact of terrestrial carbon released by watersheds on air-sea CO_2 fluxes in Arctic rivers plumes, especially in a context of global warming. In the present PhD thesis, the ECCO-Darwin ocean-sea ice-biogeochemical model is used to investigate the synoptic to interannual response of the Southeastern Beaufort Sea (Western AO) to the Mackenzie River's carbon exports. The model includes the very first daily terrestrial DOC (tDOC) runoff forcing estimated through merging riverine *in situ* measurements and coastal remotely sensed data at three major delta outlets, over the last two decades (2000-2019). We find that interannual variability in river discharge modulates localized air-sea CO_2 flux in the coastal plume with riverine DIC contributing twice as much as riverine DOC to CO_2 outgassing. As current knowledge on tDOC remineralization in Arctic plume regions is still uncertain, the range of air-sea CO_2 flux variability due to microbial remineralization is estimated to ± 0.39 TgC yr^{-1} in 2009. Other biophysical processes also contribute to the high CO_2 flux variability, such as tDOC flocculation (+0.14 TgC yr^{-1} ingassing) and enhanced plume stratification (+0.35 TgC yr^{-1} outgassing). To conclude, the work presented here intends to pave the way toward a better representation of the land-to-ocean continuum (LOAC) in regional Arctic models with the aim to improve the simulated carbon cycle in rapidly changing Arctic watersheds and coastal seas.
Keywords: Arctic, land-to-sea interface, riverine plumes, terrigenous dissolved carbon, ocean-sea ice-biogeochemical modeling

LIENSs - UMRi 7266

2, rue Olympe de Gouges

17000 LA ROCHELLE